INFORMATION TO USERS

This manuscript has been reproduced from the microfilm master. UMI films the text directly from the original or copy submitted. Thus, some thesis and dissertation copies are in typewriter face, while others may be from any type of computer printer.

The quality of this reproduction is dependent upon the quality of the copy submitted. Broken or indistinct print, colored or poor quality illustrations and photographs, print bleedthrough, substandard margins, and improper alignment can adversely affect reproduction.

In the unlikely event that the author did not send UMI a complete manuscript and there are missing pages, these will be noted. Also, if unauthorized copyright material had to be removed, a note will indicate the deletion.

Oversize materials (e.g., maps, drawings, charts) are reproduced by sectioning the original, beginning at the upper left-hand corner and continuing from left to right in equal sections with small overlaps.

Photographs included in the original manuscript have been reproduced xerographically in this copy. Higher quality 6" x 9" black and white photographic prints are available for any photographs or illustrations appearing in this copy for an additional charge. Contact UMI directly to order.

Bell & Howell Information and Learning
300 North Zeeb Road, Ann Arbor, MI 48106-1346 USA
800-521-0600

A Finite Element Method for the Fully-Coupled Magnetohydrodynamics

Nizar Ben Salah

A Thesis
in
The Department
of
Mechanical Engineering

Presented in Partial Fulfillment of the Requirements
for the Degree of Doctor of Philosophy at
Concordia University
Montreal, Quebec, Canada

May 1999

Abstract

A Finite Element Method for the Fully-Coupled Magnetohydrodynamics

Nizar Ben Salah, Ph.D.

Concordia University, 1999

This thesis presents a finite element method for the solution of three-dimensional magnetohydrodynamic flows. The physics of such flows is governed by the Navier-Stokes equations, which are extended to account for the Lorentz forces, and by Maxwell equations from which the magnetic induction equation is obtained. Magnetohydrodynamic problems are, thus, interdisciplinary and coupled in a two-way fashion, since the effect of the velocity field appears in the magnetic transport equations, and the interaction between the electric current and the magnetic field appears in the momentum transport equations. Such a complex problem has to be carefully addressed and we choose to tackle it in a two-step fashion.

In the first step, the magnetic problem is addressed. A conservative stabilized finite element method is proposed, taking into account, and this for the first time, the explicit respect of the free-divergence constraint. The introduction of this equation would normally lead to an over-determined system of equations. The introduction of a new scalar variable circumvents this overdetermination by giving rise to an equivalent system of equations which is not over-determined. This scalar is interpreted as the Lagrange multiplier of the free-divergence constraint on the magnetic field.

In the second step, the fully-coupled problem is tackled. The Navier-Stokes equations are extended to account for the electromagnetic Lorentz forces. Since the simultaneous solution of all the fluid and the magnetic variables would require huge computational requirements, a segregated algorithm is proposed for the solution of the coupled equations. Versions of this algorithm, taking into account the relative intensity of the magnetic diffusion to the magnetic convection, have been developed. It is seen from the numerical tests that updating the magnetic field at each time step iteration is enough for good convergence even for high magnetic Reynolds numbers Re_m.

Numerical results are obtained for both the decoupled magnetic problem and the coupled magnetohydrodynamic problem. The first tests address the stability and the accuracy of the finite element formulations that are developed throughout this thesis, while other tests concern 1D, 2D and 3D typical benchmarks in the MHD context. Results are satisfying showing good agreement with analytical solutions when available, putting into evidence the physical effects of the electromagnetic forces and the physical mechanisms governing the magnetic quantities and underlying the robustness of the developed segregated algorithm.

Remerciements

Cette thèse est le fruit de quatre années de recherche sous la direction des Professeurs Wagdi G. Habashi de l'Université Concordia et Azzeddine Soulaimani de l'École de Technologie Supérieure, Université du Québec. Aussi, je voudrais leur exprimer ma profonde gratitude pour le soutien, l'aide , les suggestions et les précieux conseils, qu'ils m'ont prodigué tout le long de ces quatre années. Qu'ils trouvent ici, mes plus respectueuses et humbles salutations. Ils resteront pour toujours mes professeurs, et pour ce, garderont toujours mon respect et ma gratitude.

Je voudrais aussi remercier le Professeur P. Massé de l'École Nationale Supérieure de Physique de Grenoble (I.N.P.G.) d'avoir accepté d'agir à titre d'examinateur externe sur mon jury de thèse et d'ainsi donner une dimension internationale à ce travail de recherche. Mes remerciements vont aussi aux Professeurs F. Haghighat, G. Guèvremont et Y. Bourgault (Présentement à l'Université d'Ottawa) de l'Université Concordia pour avoir accepté de faire partie de mon jury de thèse et de critiquer ce travail.

Je voudrais aussi exprimer ma gratitude au Professeur Michel Fortin de l'Université Laval pour les discussions et le soutien si généreusement fourni.

Aussi je voudrais saisir l'occasion pour exprimer ma reconnaissance au Professeur Y. Beauchamp directeur de l'enseignement et de la recherche à l'École de Technologie Supérieure, pour m'avoir donné l'occasion d'enseigner au Département de Génie Mécanique à titre de chargé de cours et d'ainsi approfondir mon expérience d'enseignant universitaire.

À mon collègue et ami C. Lepage, un grand merci pour toutes les corrections d'anglais, les discussions sur le contenu de la thèse et les initiations à Latex et Gnuplot.

Mes remerciements vont aussi à Jennifer Habashi du CFD Lab de l'Université Concordia pour les corrections d'anglais ainsi qu'à France Péloquin du Département

de Génie Mécanique de l'École de Technologie Supérieure pour les fichiers post-script et les figures.

Je remercie également tous mes collègues du groupe CFD Lab ainsi que les chercheurs de RealNumerix, avec qui j'ai eu du plaisir à interagir pendant ces quelques années. Ainsi, je voudrais remercier Dr. D. Ait-Ali-Yahia (présentement chez PWC), Dr. G. Baruzzi, Dr. L. Dutto, Dr. D. Stanescu, Dr. V. Kozel, M. Bogstad, Z. Boutanious and M.E. Chenard et leur souhaiter les plus heureuses des continuations dans leur travaux respectives.

Du groupe GRANIT de l'École de Technologie Supérieure, je voudrais particulièrement remercier Dr. Nacer ELkadri (Présentement Professeur à l'Université du Québec), Professeur M. Idrissi (Présentement à l'Université de Tatouane au Maroc) ainsi que Mr. G. Da Ponte et de leur souhaiter les meilleures chances dans la continuité de leurs travaux.

Que ma mère Nagia et mon père Midani trouvent ici ma plus sincère gratitude pour m'avoir rappelé mes objectifs lorsque l'inquiètude, le doute, le stress, l'anxiété et les soubresauts de la vie avaient failli me sortir de mon droit chemin. Pour tout ce qu'ils ont fait pour moi, je remercie mes soeurs Yousra et Balkis et mon frère Sofiene. À mon épouse Rimeh et à mon fils Omar, je présente un grand merci pour les parenthèses de bonheur familial simple, serein et sincère, moments de répit nécessaires pour la réalisation de ce travail. Merci aussi pour les sourires innocents, désintéressés et si généreusement offerts.

À la mémoire de ma mère Nagia Ben Salah.

30-1-1936 / 11-12-1997.

À mon père Midani Ben Salah, qui a toujours su voir plus loin et viser plus haut que moi.

À la Tunisie, mon pays que j'aime tant.

Contents

List of Figures

Nomenclature

English symbols

$\mathbf{A}$ Magnetic vector potential

$\hat{\mathbf{A}}$ Reduced magnetic vector potential

$\mathbf{B}$ Magnetic field

$\mathbf{B}^*$ Non-dimensional magnetic field

B_0 Reference magnetic field

$\{B\}$ Global nodal variables vector for the magnetic problem

$\mathbf{D}$ Electric induction field

$\mathbf{E}$ Electric field

$\{F(U,B)\}$ Right-hand-side vector for the fluid problem

$\{F'(B,U)\}$ Right-hand-side vector for the magnetic problem

$\mathbf{H}$ Magnetic induction field

Ha Hartmann number

I Electric current

Im Imaginary part

J_m Bessel function of first kind of order m

L Reference length

$\mathcal{O}$ Order of

Q Electric charge

$\{R(U,B)\}$ Residual vector for the fluid problem

$\{R'(B,U)\}$ Residual vector for the magnetic problem

Re Reynolds number

$Real$ Real part

Re_m Magnetic Reynolds number

Re_ω Shielding parameter

$\{U\}$ Global nodal variables vector for the fluid problem

e Element index

$\mathbf{f}$ Body forces for the Navier-Stokes equations

$\mathbf{j}$ Electric current density

$\mathbf{j_s}$ Electric current density source

$\mathbf{n}$ Normal vector

p Pressure

p^* Non-dimensional pressure

q Lagrange multiplier for the free-divergence constraint

t Time

t^* Non-dimensional time

$\mathbf{u}$ Velocity vector

$\mathbf{u}^*$ Non-dimensional velocity vector

u_0 Reference velocity

$\mathbf{x}$ Position vector, components (x, y, z) in Cartesian, (r, θ) in cylindrical

$\mathbf{x}^*$ Non-dimensional position vector

Δt Time step

Greek symbols

ϵ Electric permittivity

θ Angular coordinate in the cylindrical system

η Magnetic diffusion coefficient

λ Hydraulic losses

ν Kinematic viscosity

μ Magnetic permeability

$\vec{\xi}$ Position vector in the reference element, components (ξ, η, ζ)

ρ Density

σ Electric conductivity

Ω Computational domain

Ω_e Computational domain at the element level

$\hat{\Omega}_e$ Reference element

Γ Boundary of Ω

Γ_1 Part of the boundary of Ω

Γ_2 Part of the boundary of Ω

Ψ_j Interpolation functions on the reference element

Φ Electric scalar potential

ω Pulsation

Chapter 1

Introduction

In his work entitled "A textbook of magnetohydrodynamics" [1], J.A. Shercliff defines the science of magnetohydrodynamics (MHD) as the study of the motion of electrically conducting fluids under magnetic fields. With paths available for electric charges, electric currents ensue, with two consequences:

1. The induced magnetic field associated with these electric currents perturbs the original magnetic field;

2. The electromagnetic forces due to the interaction of electric currents and magnetic field modify the original motion of the conducting fluid.

The situation is essentially one of coupled interaction between a flow quantity (the velocity field) and a magnetic quantity (the magnetic field), expressed by the label magnetohydrodynamics.

Interest in MHD phenomena has existed ever since the end of the nineteenth century, especially in the astrophysics community where the work of Cowling [2] and Ferraro [3] can be seen as pioneering work establishing the formal theory of MHD on an astrophysical scale. One has to, however, wait until the nineteen forties for the maturing interest in magnetohydrodynamics with the work of Hartmann [4] and Alfven [5], whose contributions are associated with two unique MHD physical features, namely: the Hartmann layer and Alfven waves.

Like many other applied sciences, the postwar boom in technology had positive effects on MHD research, resulting in the emergence of new industrial and scientific applications. For an overview of MHD on astrophysical scales and its main features and issues, one can consult appropriate sections of Berton [6] and the references therein.

At the opposite end of the spectrum, MHD at the industrial levels can be divided in two sub-categories:

- MHD of compressible fluids, mainly encompassing the use of cold or hot ionized plasma.
- MHD of incompressible media, essentially encompassing liquid metals.

Moreover, one can subdivide MHD at the industrial level into two other sub-categories: Ideal (or inviscid) MHD, generally associated with compressible media, and viscous MHD, generally associated with liquid metals and thus with the incompressibility assumption.

The study of MHD phenomena implies the interaction of two disciplines of applied sciences, namely: fluid mechanics and electromagnetism, with the physical coupling between the two fields mathematically expressed through Ohm's law:

$$\mathbf{j} = \sigma(\mathbf{E} + \mathbf{u} \times \mathbf{B}) \tag{1.1}$$

and the expression for the electromagnetic forces:

$$\mathbf{f} = \mathbf{j} \times \mathbf{B} \tag{1.2}$$

The coupling requires the study of the fluid and the electromagnetic problems, making MHD a coupled, complex and interdisciplinary problem.

1.1 Industrial Applications of MHD

Historically, MHD suffered a setback due to the failure of a major application dating to the seventies. During those years, the open cycle energy conversion using cold plasma

$(3000 - 5000K)$ drew a great deal of attention. When this technique failed because of technical reasons (no refractory material lasted long enough at these temperatures), the interest in MHD dropped substantially and the general impression that lasted for a while was that "MHD does not work". Since then, interest has been gradually revived due to the emergence of potential industrial applications of MHD.

1.1.1 Electromagnetic Pumping

The use of centrifugal pumps in the transport of liquid metals poses the problem of material resistance to hot liquids. Electromagnetic pumps, because of the absence of moving parts, are ideal in such situations. A transverse electric current, $\mathbf{J}_y$, interacts with an imposed magnetic field $\mathbf{B}$ (see Figure 1.1) to create a Lorentz force $\mathbf{J}_y\mathbf{B}_x$ equal to:

$$\frac{\partial p}{\partial z} = \mathbf{J}_y\mathbf{B}_x \tag{1.3}$$

according to the momentum equation (if one neglects viscosity and convection). In order to obtain the pressure along the duct, one integrates the above expression and obtains:

$$P = \int_L \mathbf{J}_y\mathbf{B}_x dz \tag{1.4}$$

Inefficiencies in an MHD pump are attributed to hydraulic losses due to viscosity, and to electric losses due to the electric Joule heating effect. The hydraulic losses, λ, can be written, in laminar MHD flow, as

$$\lambda = \frac{32Ha}{Re} \tag{1.5}$$

and in turbulent flow as

$$\frac{1}{\sqrt{\lambda}} = 2.0\ log_{10}\ (Re\sqrt{\lambda}) - 0.8 + F\left(\frac{Ha^2}{Re^*}\right) \tag{1.6}$$

with Re and Ha being the usual Reynolds and Hartmann numbers, Re^* being the friction Reynolds number defined as:

$$Re^* = \sqrt{\frac{\lambda}{8}}\frac{Re}{4} \tag{1.7}$$

and where F is a function obtained experimentally (Berton[6]).

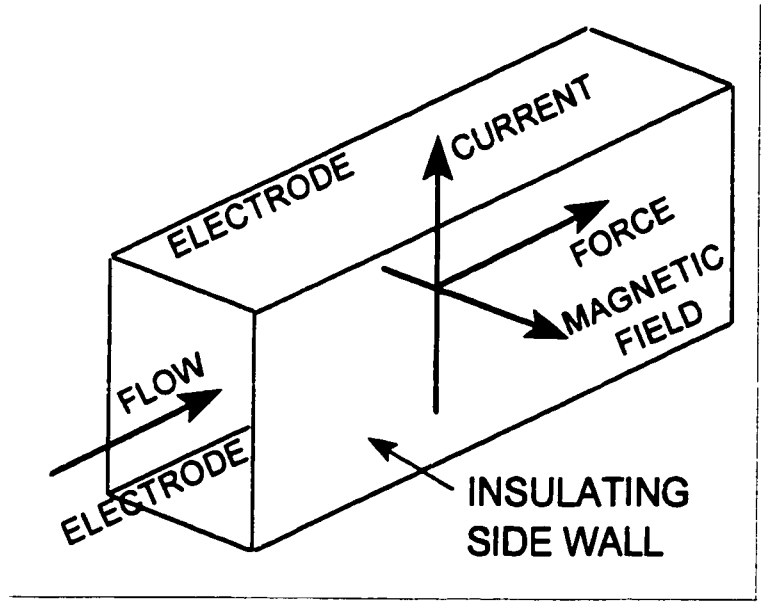

Figure 1.1: Principles of electromagnetic pumping.

1.1.2 Electricity Generation

In this process, the mechanical energy of a moving fluid, typically a liquid metal or a plasma polluted by metallic vapors, is changed into electrical energy. When an electrically conducting fluid is flowing in a duct with a velocity **u**, under two poles of a magnet, an induced current is produced, according to Ohm's law (1.1), and is collected at electrodes (see Figure 1.2). The fluid plays the role of a rotor and the duct the role of a stator. One advantage of this type of electricity production is the absence of any mechanical turning parts.

Electricity can be generated with an open cycle system or with a closed cycle system. The latter process is adopted for space vehicle systems since there is a need for recycling the rotor fluid. The primary energy for the open cycle devices is provided by a heat generator. For the closed cycle devices, heat is provided from a nuclear reactor or solar captors. Finally, MHD generators can be classified into four main categories according to their form and to the conducting fluid they use:

- Linear generators (Plasma)
- Circular generators (Plasma)

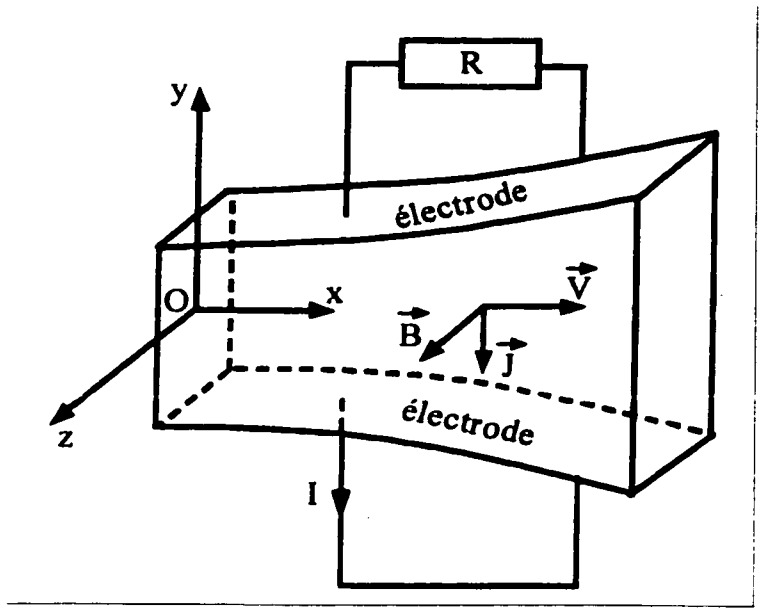

Figure 1.2: Principles of MHD electricity generation.

- Liquid metal generators (Liquid metal)
- Induction generators

Nowadays, the most significant contributions to MHD electricity generation have occurred in the US in the program MHD, Proof of Concept (POF), which ended in 1993. The continuation of the program is still under question. The Japanese have developed the concept of a circular generator (Program FUJI) and Russia has been exploiting a semi-industrial prototype (U25). Other countries such as China, Australia and Italy also have significant research programs.

1.1.3 MHD Propulsion

The basic idea of MHD propulsion emerges from the fact that electromagnetic forces are developed whenever there is an electric current circulating in the presence of a magnetic field (see Figure 1.3).

The DC electric linear engine can be seen as the solid counterpart of a MHD propulsion device. The propulsion agent is injected between two electrodes circulating an electric current. In typical MHD propulsion devices, this electric current is radial,

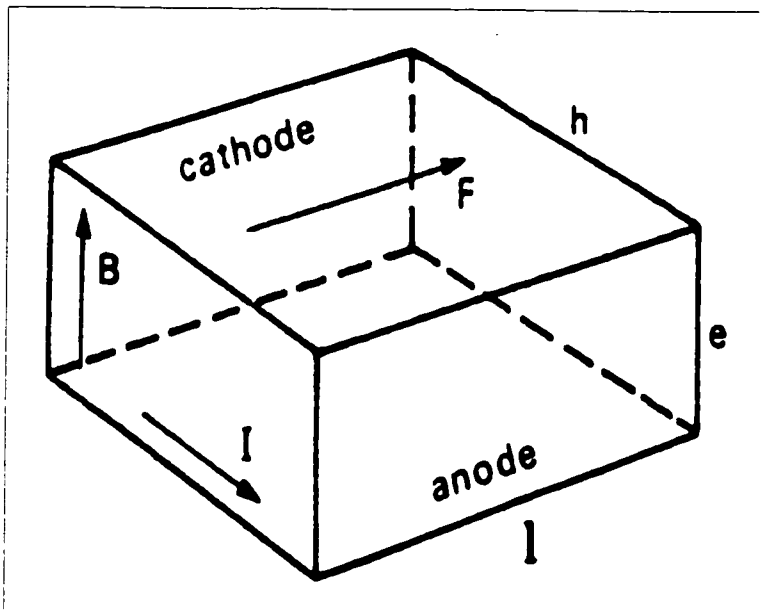

Figure 1.3: Principles of MHD propulsion.

thus inducing a tangential magnetic field $\mathbf{B}_\theta$ according to:

$$\mu_0 \mathbf{J}_r = -\frac{\partial \mathbf{B}_\theta}{\partial z} \tag{1.8}$$

The coupling between this magnetic field $\mathbf{B}_\theta$ and $\mathbf{J}_r$ produces the axial Lorentz force:

$$\mathbf{F}_z = \mathbf{J}_r \mathbf{B}_\theta \tag{1.9}$$

This force accelerates the propulsion agent outside of the propulsion device and causes the nozzle to accelerate in the opposite direction. While being less developed than chemical or electric propulsion, MHD propulsion has recently gained a great deal of attention. The MHD propulsion devices are able to operate with high power levels ranging from 4 to $10MW$. Under these conditions, the electric current density is of the order 20 to 30 kA, final velocities of up to 30 km/s and mass flow rates of nearly 5 g/s can be reached. The thrust developed is around 150 N. Efficiency coefficients for the typical Magneto-Plasma-Dynamic thrusters are around 0.3 to 0.4, heading towards 0.5.

MHD propulsion can be divided into three main categories according to the propellant used. As its name states, Magneto-Plasma-Dynamics (MPD) uses hot plasma

gases ($3000K$) as propellants. Typical gases are argon (Ar) or nitrogen (N). The great advantage of such devices is their low propellant consumption. For the same efficiency, a MHD thruster will need 3 to 10 times less propellant than a chemical thruster. The main disadvantage of such devices is the erosion of electrodes and isolating surfaces due to the high temperature of the plasma.

The second category of MHD propulsion devices uses liquid metals as propellant. The devices operate at low temperatures ($400K$), thus electrodes erosion is not as important as in MPD thrusters. Most metals used are mercury (Hg), potassium (K), calcium (Ca), tin (Sn) and zinc (Zn). Typical characteristics are 500 kW, 8 kA and 10 N in terms of power, current density and thrust.

MHD Naval Propulsion The operating principle of MHD propulsion holds for naval propulsion, where the Lorentz forces are used to propel ships and submarines. One obvious way to do so is to use electrodes delivering a direct current density $\mathbf{j}$, which interacts with a magnetic field, thus creating forces according to $\mathbf{j} \times \mathbf{B}$. This technique is called "conduction MHD naval propulsion". Another way of generating the necessary propulsive forces is by the so-called "induction technique". In this case, there is no need for electrodes and one avoids the electrolysis process of the sea water they cause. An alternative electric current generates an alternative magnetic field which induces currents closing their lines in the flow.

Already, the Japanese Yamato-1 prototype is a proof of the feasibility of a viable MHD propulsion (Motora *et al.* [8]). The major challenge for the MHD naval propulsion is to overcome the poor electric conductivity of sea water. Supraconductor magnets are certainly "the way to the future" for the MHD sea propulsion.

1.1.4 Metallurgical MHD Applications

Whether solid or liquid, metals present the great advantage of having very high electric conductivities (σ of order $O(10^6)\Omega^{-1}m^{-1}$) and the electromagnetic forces that they can generate are very important. These forces can set the liquid in motion, as in

electromagnetic stirring, make it levitate, assume a certain shape, or pulverize. The basic assumption common to all MHD applications in metallurgy is that the magnetic Reynolds number is very small (Re_m of order $O(10^{-1})$). This assumption implies that the electromotive field $\mathbf{u} \times \mathbf{B}$ is negligible when compared to the electric field $\mathbf{E}$, and Ohm's law then reduces to the form:

$$\mathbf{j} = \sigma \mathbf{E} \tag{1.10}$$

One can then speak of weak electromagnetic-fluid coupling.

Electromagnetic Stirring The fundamental mechanism under which any electromagnetic stirring device (Figure 1.4) works is the following:

- An alternative electric current creates a vector potential $\mathbf{A}$ which in itself produces a magnetic field $\mathbf{B}$.
- Electric currents $\mathbf{j}$ are induced according to Ohm's law.
- Lorentz forces are generated within the liquid metal.

These forces are responsible for the liquid movement within the crucible. These movements are used for the stirring of alloys during their fusion process.

Aluminum Electrolysis In a typical aluminum reduction cell, a direct current enters the cell via the anode, whose lower surfaces are immersed in a molten salt electrolyte. This molten salt, known as cryolite, is a mixture of sodium and aluminum fluorides, together with minor constituents. The cryolite acts as solvent for the aluminum oxide fed to the cell, and beneath the cryolite is a pool of molten aluminum. The reduction of aluminum ions to metal occurs at the interface between the two liquids thus increasing the aluminum pool. The pool is partially siphoned at regular intervals. The current passes through the aluminum to the cathode.

A typical modern cell would carry 100-200,000 Amperes, contain ten to twenty anodes, operate at 960 Celcius and be 3 by 8 meters in its horizontal dimensions. Cells are arranged in lines of several tens known as potlines, and a typical plant

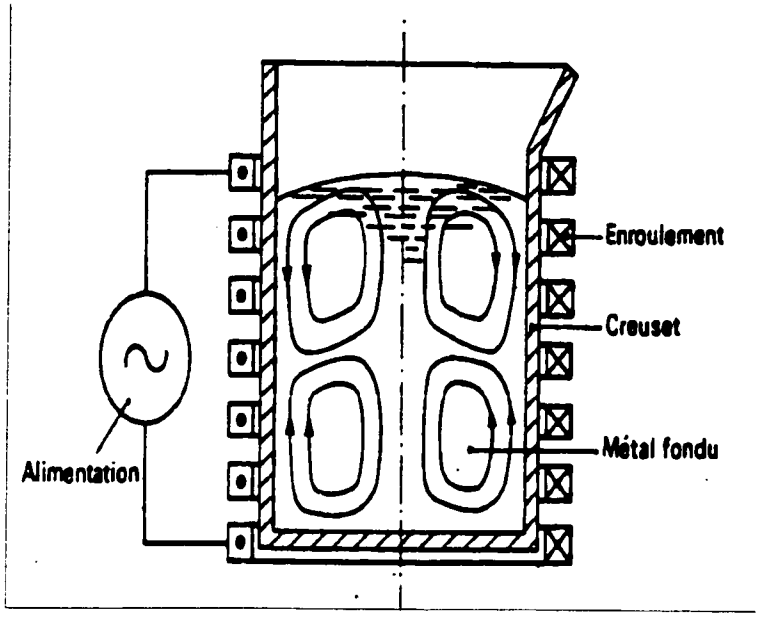

Figure 1.4: Principles of electromagnetic stirring (From Berton [6]).

might contain several potlines usually running parallel to each other and few meters apart.

1.1.5 Fundamental MHD Research

MHD research is present in many domains; while certainly not exhaustive, the following list represents four domains with good prospects for the coming years:

- Solidification process under a magnetic field: Here, the aim is to magnetically control the natural convection present in any solidification process in order to obtain homogeneous crystal growth.
- Cooling of thermo-nuclear fusion reactors.
- Study of the magnetic control of turbulence.
- Study of the dynamo effect for astrophysical scales of MHD.

For more details or for an overview on the applications of MHD cited above, see Berton [6] or Alemany [7] and the references therein.

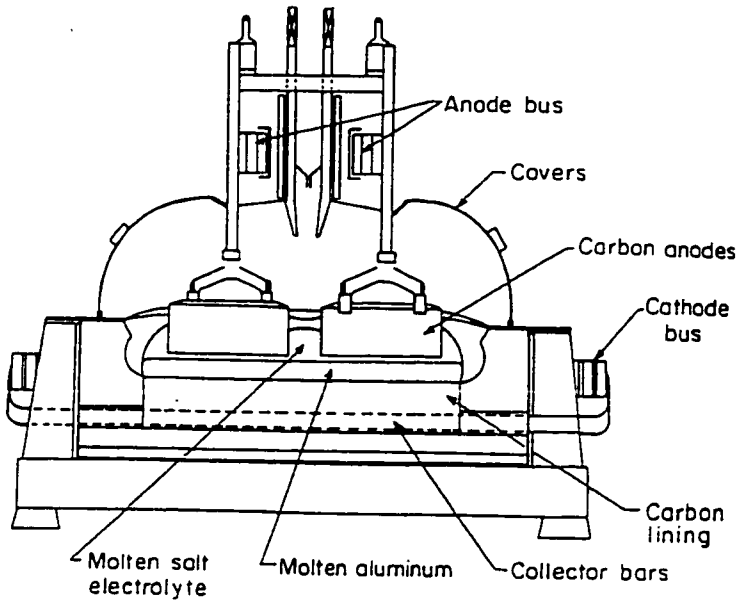

Figure 1.5: Typical aluminum reduction cell (From Lympany *et al.* [29]).

1.2 Literature Review

Despite the great development of computer resources and numerical methods in the two last decades, MHD research is still today mainly analytical or experimental in nature. For proof of this, one can simply look at the proportion of numerical research activities over all the MHD research. For example, in the seventies (1970-1979), Compendex EI database records 1970 journal articles with the keyword "mhd or magnetohydrodynamic*". If the keyword restriction "numeric*" is added, then the number of records is reduced to 219 articles. The same pattern is repeated during the eighties and the nineties with, respectively, 501 articles out of 3473, and 561 articles out of 3046 articles. However, the absolute number of numerical articles has been increasing since the seventies and there are many indications that this trend is to be maintained.

Presenting a general view of the numerical activities in MHD is a very hard task for two reasons. First, MHD is an interdisciplinary domain, and in our opinion, this has prevented the emergence of unified and well-established numerical test cases, as is the case for the CFD community for example. The second reason is that MHD covers

a very large spectrum of applications, making the issues and features of each domain very different from the others. However, and as presented previously, MHD can be subdivided into two sub-categories: compressible (Plasma) MHD and incompressible (Liquid metal) MHD.

For the mathematical modeling of compressible, inviscid MHD problems, one can consult Roe and Balsara [9], where the authors examine the eigenstructure of the equations governing one-dimensional ideal MHD, with the aim of constructing high-resolution computational algorithms. Another key reference on the subject is Powell [10], which describes approaches for Cartesian grid generation, for gasdynamics and magnetohydrodynamic flow solvers that work well on adaptive Cartesian grids. The above short list of articles is only a starting point for any reader interested in the numerical modeling of inviscid compressible MHD flows.

On the other side of the spectrum, numerical modeling of liquid metal MHD flows has attracted the interest of many researchers. This modeling was done essentially in the framework of the development of a fusion reactor liquid metal coolant and the revival of liquid metal MHD electricity generation. These MHD problems have been studied extensively by the method of asymptotic expansions (see Walker [11] for a review of the results of these studies). Asymptotic analysis is based on the assumption that the liquid metal flow is essentially dominated by electromagnetic and pressure forces, thus neglecting inertia and friction viscous forces.

The obvious restrictions inherent in these asymptotic methods have been partially overcome by the development of semi-numerical methods (Hua and Walker [12], Cuevas *et al.* [13]). However, these methods are still not able to describe the velocity profiles near the boundaries. Nevertheless, the details of the flow are worth exploring and this can be done only by means of a fully numerical approach. Yet, only a small number of articles present mostly one-dimensional or two-dimensional analysis. Ramos and Winowich [14] proposed a primitive variable finite element formulation, a stream function-vorticity finite difference method and a primitive variable difference scheme of the control volume type. Regarding electromagnetic quantities, they solved for the electric potential, while the imposed magnetic field is supposed to

remain unchanged.

Scandiuzzi and Schrefler [15] presented a finite element method for solving cross-sections MHD flows. They treated arbitrarily conducting walls and solved for the only non-zero component of the velocity and the magnetic field. For the boundary conditions on the magnetic field, they developed the following relation:

$$\frac{dB}{dn} + C\,B = 0 \tag{1.11}$$

where C is the ratio of the fluid to the wall conductivities.

Three-dimensional simulations of MHD incompressible flows are more rare. From the 561 numerical MHD articles (published during the nineties), only 56 have the keyword "3D or three dimension*". Here, we would like to refer to some articles where the authors used three-dimensional MHD models to solve for various numerical tests. Sterl [16] presented a finite difference method for MHD flows in rectangular ducts. He decoupled the magnetic field problem from the fluid one by considering the limit that no perturbation is induced for the magnetic field. He solved for the velocity field and the electric scalar potential with $\mathbf{B}$ considered constant in the equations and presented results for a 2D MHD rectangular duct and the 3D effects of the developing entry. Starting from Walker's work, Sterl generalized the boundary conditions that have to be assigned for the potential ϕ in order to account for varying relative conductivity ratio.

Seungsoo and Dulikravich [17] also proposed a finite difference method in the general non-orthogonal curvilinear boundary-conforming coordinate system. The algorithm is based on an explicit Runge-Kutta time-stepping scheme. The model they developed takes into account the velocity, the magnetic and the temperature fields. They presented results for the Hartmann-Poiseuille flow, the 3D Hartmann flow and a 2D Benard cell problem under a magnetic field. They put into evidence the magnetic weakening of the thermally induced vortices and the eventual damping of buoyancy movement when the Hartmann number is high ($Ha = 10,\ Gr = 3000$).

Dulikravich *et al.* [18] solved for the three-dimensional laminar viscous flow undergoing solidification or melting under the influence of arbitrarily oriented externally

applied magnetic field. The algorithm used is the same as in [17], with the difference that the magnetic field is decoupled from the velocity and the temperature fields ($Re_m \ll 1$) and that the energy model accounts for a temperature dependence of the physical properties. One can also consult Sazhin and Makhlouf [19] which presents another finite difference method for the 3D MHD equations.

Regarding the methods used for solving the MHD equations, the finite element method has not been used as often as the finite difference or the finite volume methods. In her theoretical article [20], Peterson proposed finite element approximations of steady incompressible flows of electrically conducting fluids by considering the special case of undisturbed external magnetic field. She chose to retain the velocity and the electric potential as the variables and proposed a weak variational formulation. She proved the stability and the continuity of linear forms and the existence and uniqueness of the solution. Notably, she proved that the scalar ϕ has to be chosen in the same functional sub-space as the velocity field. For another kind of finite element approximations, one can consult Gardner and Gardner [21], where the authors presented a two-dimensional bi-cubic B-spline finite element method for the MHD channel flow.

Solving for the magnetic field $\mathbf{B}$ would normally result in an over-determined system of equations. This can be overcome by dropping the free-divergence equation and the terms implying this same divergence within the magnetic induction equation. The resulting vectorial equation is a diffusion-convection "Helmholtz" like equation. While this is done in all the previously cited references, we would like to underline that doing so would result in only the implicit respect of one of the fundamental Maxwell equations. On the other hand, instead of choosing the magnetic field $\mathbf{B}$ as the main electromagnetic quantity, many authors choose to solve for the vector potential $\mathbf{A}$, mostly used in the context of pure electromagnetism ([22],[23],[24] and [25]). For a general overview of the vector potential methods and some of their electromagnetic applications, see Biro *et al.* [26].

In the context of MHD, these vector potential methods have also been popular and intensively used especially for metallurgical applications. Fautrelle [27] used a vector

potential formulation to solve the magnetic part of electromagnetic stirring problems. He treated it as a pure electromagnetic problem by dropping the motion effects in the Maxwell equations. Mestel [28] examined, both analytically and numerically, the process of levitation melting of metals. Lympany *et al.* [29] presented numerical results for the MHD effects in aluminum reduction cells. Assuming a steady two-dimensional phenomenon, they solved for the scalar potential ϕ and deduced the magnetic field using the Biot-Savart law.

Besson *et al.* [30] developed a two-dimensional steady state finite element method for solving both the MHD and the free surface problems associated with electromagnetic casting (EMC). They represented the outside potential by an integral equation, so their method could be described as a FEM/BEM one. More recently, Conraths [31] described the magnetic field by an electric vector potential and a magnetic scalar potential for modeling an inductive heating device for thin moving metal strips.

In [32], Masse *et al.* presented the leading conclusions of 10 years of numerical modeling in MHD using the vector potential formulation. The description given is quite impressive; however, an obvious drawback is the non uniformity of the numerical approach: a finite volume method for the fluid problem, a finite element method for the magnetic problem in the conducting domain and an integral method for the non conducting domain. For an overview of the vector potential methods in MHD, one can consult Trophime [33]. While this literature survey is by no means exhaustive, it illustrates the general use of vector potential formulations, indicates their great deal of popularity and wide use in the literature.

The leading idea to vector potential methods is that since it has to be solenoidal, then the magnetic field derives from a vector potential. Introducing this vector potential would then implicitly respect the free-divergence constraint on the magnetic field. However, as stated previously, this would result in only an implicit respect of the free-divergence condition on the magnetic field. To the best of our knowledge, only Oki and Tanahashi ([34],[35]) have developed numerical schemes which explicitly satisfy the solenoidal condition of the magnetic field. They introduced a variable called hydro-magnetic cross helicity $G = \mathbf{u} \cdot \mathbf{B}$ and retained the free-divergence equation

within their system of equations. They presented results for the natural convection of a thermo-electrically conducting fluid under a magnetic field. In [36] and partially in [37], Ben Salah *et al.* have also explicitly respected the free-divergence condition by including it directly in the system of equations while getting rid of the overdetermination of the system.

In the remainder of the chapter, an outline of the proposed research is provided and the main steps of this research are discussed, followed by a summary of the contributions and the achievements of the thesis.

1.3 Outline of Proposed Research

The primary goal of the thesis is to develop a robust and cost-effective magneto-hydrodynamic algorithm that combines a Navier-Stokes flow solver and a magnetic solver for the solution of three-dimensional MHD equations. Robustness is achieved by the solution of the two systems of equations in a fully-coupled fashion. In order to achieve this goal, the following questions, among many others, are addressed:

- What is the appropriate way to approach such a coupled multi-disciplinary problem?
- What is the proper way to formulate the magnetic aspects of the problem?
- To what extent does the fluid movement change the magnetic behavior? Similarily, to what extent does the magnetic field change the fluid movement?
- What type or class of solvers should be used for each system of equations?

To acquire a basic understanding of MHD phenomena and to simplify a rather difficult problem, we first consider a decoupled approach for which the fluid and the magnetic problems are considered separately. More precisely, we investigate the magnetic aspects of MHD flows with the velocity field given as input data. This step appears to be essential, not only because of the reasons cited above, but also because it makes it possible to focus the efforts on an adequate formulation of the

magnetic aspects of the problem. It will be seen in the second chapter that there are alternative formulations of MHD problems; the choice between them is mainly guided by the physical nature of the problem. Furthermore, it will be seen that any formulation of the magnetic aspects of an MHD flow should explicitly respect local magnetic conservation.

Next, the focus will turn to the selection of the coupling algorithm. Since the problem is a multi-disciplinary one, involving at the nodal level eight variables, one can expect to deal with huge computational requirements if the two problems are considered in a simultaneous fashion. In the proposed implicit algorithm, the two systems are solved in a segregated way, but with the two solvers exchanging information in a tight two-way fashion. This solution strategy is based on a GMRES-like algorithm for the fluid solver, associated with an ILUT right preconditioning. In this algorithm, the exchange of information can be performed at each GMRES direction when a new fluid solution is computed, at each Newton iteration, or at each time step. Since the algorithm is essentially a segregated one, the magnetic problem thus becomes a linear problem allowing the use of a simple solver. It will also be seen that for low magnetic Reynolds numbers, a classical segregated algorithm is suitable for very efficient convergence. This is permitted because the physical coupling is stronger one way than the other. On one hand, the influence of the magnetic field on the velocity is very strong; increasing or decreasing the magnetic field induces a dramatic change in the velocity field, while on the other hand the magnetic field is not very much influenced by the velocity field behavior.

The major thesis developments and contributions are now listed and are detailed in the chapters of this thesis:

- A thorough review of the magnetic equations for the MHD flows, stressing the need for an explicit respect of the local magnetic conservation;

- The development and implementation of a magnetic finite element solver for the 3D MHD equations, with the magnetic field as the main variable;

- The development and implementation of a magnetic finite element solver for the 3D MHD equations, with the vector potential as the main variable;

- Extension of an unsteady 3D Navier-Stokes incompressible finite element solver to account for the electromagnetic Lorenz body forces;

- Development of an MHD (fluid-magnetic) coupling algorithm. Two versions of this algorithm are available: one for high and the other for low magnetic Reynolds numbers;

- Implementation of a coupling structure with sequential calls for fluid or magnetic solvers;

- Application in the context of MHD of state-of-the-art iterative methods and preconditionings such as Non-Linear GMRES and ILUT.

1.4 Overview of the Thesis

The remainder of the thesis is organized in five chapters. In chapter 2, the governing equations of MHD flows are presented and reviewed. Starting from the Maxwell equations, the magnetic induction equation is introduced. Then, the "Helmholtz" formulation of the magnetic induction and the vector potential formulation are presented and briefly commented upon. Following, the conservative formulation is developed. This formulation takes into account the explicit respect of the free-divergence constraint on the magnetic field by the numerical scheme. The introduction of a Lagrange multiplier within the system of equations circumvents the overdetermination of the system, while giving rise to equivalent equations if appropriate boundary conditions are prescribed. The Navier-Stokes equations, taking into account the electromagnetic forces, are then presented. The non-dimensional form of the equations is obtained. The cases of weak and strong MHD couplings, where the magnetic Reynolds number Re_m plays a key role, are discussed.

In chapter 3, the variational formulations of the different systems of equations that are used throughout this thesis are presented. The Galerkin weak form of the $\mathbf{B}, q$ formulation is obtained, giving rise to a mixed finite element formulation. A stabilization technique is introduced to circumvent the usual Brezzi-Babuska stability condition and to allow equal interpolation for all the variables. A penalty factor is then introduced in order to force the magnetic divergence towards zero. For the vector potential formulation, the Galerkin weak form allows for the use of equal interpolation for all variables. Thus, no stabilization technique is required for such formulations. The Navier-Stokes equations are stabilized through a Galerkin Least-Squares term.

In chapter 4, the solution strategy for the decoupled formulations $\mathbf{B}, q$ and $\mathbf{A}, \phi$ and the coupled formulation $\mathbf{B}, q, \mathbf{u}, p$ is presented. The strategy for the coupled problem is based on a non linear GMRES algorithm associated with an ILUT preconditioning. Three versions of the algorithm, each offering a different level of coupling tightness, are available: with the magnetic field updated at each time step, each Newton iteration or each GMRES iteration.

In chapter 5, numerical tests for assessing the accuracy and stability of the different finite element methods are carried out. Results are also presented for test cases. These tests concern the three formulations: $\mathbf{B}, q$, $\mathbf{A}, \phi$ and the coupled formulation $\mathbf{B}, q, \mathbf{u}, p$. In the last chapter, the conclusions of this work and prospects for eventual future work are presented.

Chapter 2

The Governing Equations

2.1 Introduction

In this chapter the basic equations leading to the formulation of MHD flow problems are reviewed. First, the Maxwell equations are recalled and the so-called magnetic induction equation is obtained after some algebra on Maxwell's equations and Ohm's law.

The classical "Helmholtz" formulation is then introduced. It is particularly shown that the magnetic conservation equation is no longer implicit within this formulation and the respect of this conservation condition by the magnetic field is stressed. The classical alternative formulation consisting of introducing the vector potential and its associated scalar one is then reviewed. Following this, the conservative formulation is developed and presented. This formulation takes into account, for the first time, the local respect of the magnetic field conservation. It is seen that the respect of this constraint would normally lead to an over-determined system of equations. We would show that this system is, however, equivalent to a non-over-determined system. To perform that, a Lagrange multiplier of the magnetic conservation constraint is introduced within the magnetic induction equation. This multiplier is shown to be a dummy scalar variable that does not affect the equations while forcing the magnetic divergence towards zero.

Once these electromagnetic aspects of MHD flows are discussed, an extension of the Navier-Stokes equations taking into account the electromagnetic Lorentz forces

is presented. The non-dimensional form of equations puts into evidence the relative importance of different terms of equations. The cases of weak and of strong MHD couplings, where the magnetic Reynolds number plays a fundamental role are discussed. It is seen that in the context of this thesis both these two cases are retained and studied.

2.2 The Maxwell Equations

The Maxwell equations reflect the general laws of physics for electromagnetic phenomena. In their integral form, they can be written as:

$$\oint \mathbf{H} \cdot \mathbf{d}l = \int_A \mathbf{j} \cdot \mathbf{d}A + \int_A \frac{\partial \mathbf{D}}{\partial t} \cdot \mathbf{d}A \tag{2.1}$$

$$\oint \mathbf{E} \cdot \mathbf{d}l = -\int_A \frac{\partial \mathbf{B}}{\partial t} \cdot \mathbf{d}A \tag{2.2}$$

$$\int_A \mathbf{B} \cdot \mathbf{d}A = 0 \tag{2.3}$$

$$\int_V q \, dV = \int_A \mathbf{D} \cdot \mathbf{d}A \tag{2.4}$$

The differential form for the Maxwell equations can then be obtained from equations (2.1)-(2.4), as:

$$\nabla \times \mathbf{H} = \mathbf{j} + \frac{\partial \mathbf{D}}{\partial \mathbf{t}} \tag{2.5}$$

$$\nabla \times \mathbf{E} = -\frac{\partial \mathbf{B}}{\partial \mathbf{t}} \tag{2.6}$$

$$\nabla \cdot \mathbf{B} = 0 \tag{2.7}$$

$$\nabla \cdot \mathbf{D} = q \tag{2.8}$$

In the above set of equations, **B**, **H**, **E**, **D**, **j** and q are, respectively, the magnetic field, the magnetic induction field, the electric field, the electric induction field, the electric current density and the electric charge density. Equations (2.5)-(2.8) are valid for any observer regardless of his motion, so long as all the quantities are measured

in a frame of reference moving with the observer. Equations (2.5) and (2.6) are, respectively, the Maxwell forms of the Ampère and Faraday laws.

Usually, two constitutive laws are associated with equations (2.5) and (2.8), which relate between them the magnetic quantities and the electric quantities. They namely relate the vector $\mathbf{D}$ to $\mathbf{E}$, and $\mathbf{B}$ to $\mathbf{H}$. These constitutive laws are written as:

$$\mathbf{D} = \epsilon \mathbf{E} \tag{2.9}$$

$$\mathbf{B} = \mu \mathbf{H} \tag{2.10}$$

where ϵ and μ are, respectively, the permittivity and the magnetic permeability. Thus equations (2.5)-(2.8) can be rewritten as:

$$\nabla \times (\frac{\mathbf{B}}{\mu}) = \mathbf{j} + \frac{\partial(\epsilon \mathbf{E})}{\partial \mathbf{t}} \tag{2.11}$$

$$\nabla \times \mathbf{E} = -\frac{\partial \mathbf{B}}{\partial \mathbf{t}} \tag{2.12}$$

$$\nabla \cdot \mathbf{B} = 0 \tag{2.13}$$

$$\nabla \cdot (\epsilon \mathbf{E}) = q \tag{2.14}$$

2.2.1 The Principle of Conservation of Electric Charge

The principle of conservation of the electric charge (P.C.E.C.), which is the electromagnetic equivalent of the conservation of mass, can be stated as follows: *The total electric charge Q of a given quantity of matter is conserved.* Thus, the particular derivative of the total charge Q must be zero, which can be written as:

$$\frac{dQ}{dt} = \int_V \left(\frac{\partial q}{\partial t} + \nabla \cdot \mathbf{j} \right) dV = 0 \tag{2.15}$$

For the integral (2.15) to be zero, regardless of the integration domain, the integrand must be null:

$$\frac{\partial q}{\partial t} + \nabla \cdot \mathbf{j} = 0 \tag{2.16}$$

2.2.2 Ohm's Law

Ohm's law can be written for an isotropic medium at rest, as:

$$\mathbf{j} = \sigma \mathbf{E} \tag{2.17}$$

For a moving medium equation (2.17) is still valid if it is written in a reference frame moving with the medium. Retaining the prime symbol for the quantities as seen by an observer attached to that reference frame, one can write:

$$\mathbf{j}' = \sigma \mathbf{E}' \tag{2.18}$$

The Lorentz transforms, which could be written for the electric current and the electric field as:

$$\mathbf{j}' = \mathbf{j} - q\mathbf{u} \tag{2.19}$$

$$\mathbf{E}' = \mathbf{E} + \mathbf{u} \times \mathbf{B} \tag{2.20}$$

lead to an expression of Ohm's law with respect to a fixed frame of reference:

$$\mathbf{j} = q\mathbf{u} + \sigma(\mathbf{E} + \mathbf{u} \times \mathbf{B}) \tag{2.21}$$

where σ is the scalar electric conductivity and $\mathbf{u}$ is the velocity vector.

2.2.3 The MHD Assumptions, Magnetic Induction Equation

MHD deals with media that are conducting enough to consider that the charge relaxation time is much shorter than the transit time for electromagnetic phenomena. One can then neglect the displacement current $\partial \mathbf{D}/\partial t$ when compared to $\mathbf{j}$ and to $\nabla \times \mathbf{H}$, and the time variation of the charge density $\partial q/\partial t$, when compared to the electric current density $\mathbf{j}$. Thus, equation (2.14) decouples from the rest of the equations, and becomes useful only for an *a posteriori* computation of the charge density q. Furthermore, in the MHD context one can reasonably assume that the convection of electric charge $q\mathbf{u}$ is negligible when compared to its conduction proportional to σ and that the permittivity ϵ and the magnetic permeability μ can be considered

constants and equal to those of free space. Thus equations governing electromagnetic phenomena under the MHD assumptions become:

$$\nabla \times \mathbf{B} = \mu \mathbf{j} \tag{2.22}$$

$$\nabla \times \mathbf{E} = -\frac{\partial \mathbf{B}}{\partial t} \tag{2.23}$$

$$\nabla \cdot \mathbf{B} = 0 \tag{2.24}$$

$$\nabla \cdot \mathbf{j} = 0 \tag{2.25}$$

$$\mathbf{j} = \sigma(\mathbf{E} + \mathbf{u} \times \mathbf{B}) \tag{2.26}$$

Since μ is a constant then by virtue of (2.22) the divergence of the electric current density $\mathbf{j}$ is zero, equation (2.25) then becomes superfluous. Making use of (2.26), the system of equations becomes:

$$\nabla \times \mathbf{B} = \mu\sigma(\mathbf{E} + \mathbf{u} \times \mathbf{B}) \tag{2.27}$$

$$\nabla \times \mathbf{E} = -\frac{\partial \mathbf{B}}{\partial t} \tag{2.28}$$

$$\nabla \cdot \mathbf{B} = 0 \tag{2.29}$$

The new system is constituted of seven equations with six unknowns, and hence is over-determined. In order to remove this ambiguity, it is classical to take the curl of Ohm's law (2.27), term by term, to obtain:

$$\nabla \times (\nabla \times \mathbf{B}) = \nabla \times \mu\sigma(\mathbf{E} + \mathbf{u} \times \mathbf{B}) \tag{2.30}$$

Then, assuming the conductivity to be constant which is a classical assumption in the MHD context and making use of Faraday's law (2.28), one obtains:

$$\nabla \times (\nabla \times \mathbf{B}) = \mu\sigma\left(-\frac{\partial \mathbf{B}}{\partial t} + \nabla \times (\mathbf{u} \times \mathbf{B})\right) \tag{2.31}$$

which can be rearranged into:

$$\frac{\partial \mathbf{B}}{\partial t} - \nabla \times (\mathbf{u} \times \mathbf{B}) + \eta \nabla \times (\nabla \times \mathbf{B}) = 0 \tag{2.32}$$

where $\eta = 1/\mu\sigma$, is the magnetic diffusivity coefficient. Once equations (2.29) and (2.32) are solved for the magnetic field $\mathbf{B}$, the electric field can be deduced from the following equation:

$$\mathbf{E} = \eta(\nabla \times \mathbf{B}) - \mathbf{u} \times \mathbf{B} \tag{2.33}$$

and the electric current density $\mathbf{j}$ calculated from equation (2.26).

Equation (2.32) is the well-known form of the magnetic induction equation. It consists of a diffusive second order curl-curl term, a convective first order curl term and a hyperbolic in time first order term. It brings the advantage of directly relating the main hydrodynamic quantity, the velocity field, to the main electromagnetic one, the magnetic field, without any interference. Here, it should be pointed out that the magnetic free-divergence constraint (2.29) is implicit in equation (2.32). Indeed, if the divergence of equation (2.32) is taken, term by term, one obtains the following condition on the divergence of $\mathbf{B}$:

$$\frac{\partial(\nabla \cdot \mathbf{B})}{\partial t} = 0 \tag{2.34}$$

Equation (2.34) stipulates that the divergence of $\mathbf{B}$ remains constant over time and thus zero if it is initially null. However, it is well-known that, in general, the construction of such an initial divergence-free field is not an easy task. Moreover, although the local conservation of the magnetic field is included in (2.32), this property might not hold exactly for a discrete version developed for a numerical solution of the partial differential equations. Thus the resulting system of equations must consist of both equations (2.29) and (2.32).

2.3 The "Helmholtz" Formulation

As stated in the introduction, this formulation is widely used in the literature. The starting point of this formulation is the system of equations (2.29) and (2.32), then using the vector identity stating that:

$$\nabla \times (\nabla \times \mathbf{B}) = -\nabla^2 \mathbf{B} + \nabla(\nabla \cdot \mathbf{B}) \tag{2.35}$$

the magnetic induction equation (2.32) could be rewritten as:

$$\frac{\partial \mathbf{B}}{\partial t} - \nabla \times (\mathbf{u} \times \mathbf{B}) - \eta \nabla^2 \mathbf{B} + \eta \nabla (\nabla \cdot \mathbf{B}) = 0 \tag{2.36}$$

Making use of equation (2.29) in order to obtain the following "Helmholtz" equation:

$$\frac{\partial \mathbf{B}}{\partial t} - \nabla \times (\mathbf{u} \times \mathbf{B}) - \eta \nabla^2 \mathbf{B} = 0 \tag{2.37}$$

and hence reducing the MHD system of equations (2.29) and (2.32) to equation (2.37) with the appropriate set of boundary conditions. It should be noted that circumventing the constraint (2.29) by solving equation (2.37) results in a much simpler system to solve. However, equation (2.37) does not state anymore that the divergence of $\mathbf{B}$ remains constant over time. It only states that:

$$\frac{\partial (\nabla \cdot \mathbf{B})}{\partial t} = \nabla \cdot (\eta \nabla^2 \mathbf{B}) \tag{2.38}$$

One can expect this divergence to play a non-negligible role in the discrete form of the weak problem associated with the continuous strong problem (2.37).

Remark 1: We would like here to point out an analogy with the Stokes problem for an incompressible fluid with constant viscosity. The Stokes problem is written as:

$$-\nabla \cdot \ (2\eta\gamma(\mathbf{u})) + \nabla \mathbf{p} = \mathbf{f} \tag{2.39}$$

$$\nabla \cdot \mathbf{u} = 0 \tag{2.40}$$

with η, in this case being the dynamic viscosity coefficient and $\gamma(\mathbf{u})$ being the symmetric part of the velocity gradient tensor. If one derives from (2.39) and (2.40), the equations for the special case of constant viscosity η, then by making use of equation (2.40), one gets:

$$-\eta \nabla^2 \mathbf{u} + \nabla \mathbf{p} = \mathbf{f} \tag{2.41}$$

Although equation (2.40) has been used in order to derive (2.41), it is well-known that one has to keep the divergence-free constraint (2.40) within the system of equations while developing any numerical solution of the Stokes problem. The pressure p

plays the role of a Lagrange multiplier in order to enforce the velocity divergence-free condition. This analogy is also valid for the Navier-Stokes equations. The magnetic continuity equation (2.29) is the electromagnetic equivalent of the hydrodynamic continuity equation (2.40) and deserves some attention.

2.4 The Vector Potential Formulation

Alternatively to the above introduction of the magnetic induction equation which relates the magnetic and the velocity fields $\mathbf{B}$ and $\mathbf{u}$, one can introduce a vector potential formulation. From equation (2.24), it is seen that the magnetic field results from a vector potential $\mathbf{A}$:

$$\nabla \times \mathbf{A} = \mathbf{B} \tag{2.42}$$

then, equation (2.24) is automatically satisfied. Noting that the electric field is defined as:

$$\mathbf{E} = -\nabla\phi - \frac{\partial \mathbf{A}}{\partial \mathbf{t}} \tag{2.43}$$

where ϕ is the scalar electric potential, one can write Ohm's law (2.26) in terms of the vector potential $\mathbf{A}$ and the scalar potential ϕ as:

$$\frac{\partial \mathbf{A}}{\partial t} - \mathbf{u} \times (\nabla \times \mathbf{A}) + \frac{1}{\mu\sigma}\nabla \times (\nabla \times \mathbf{A}) + \nabla\phi = 0 \tag{2.44}$$

This equation, known as the vector potential equation, involves that the time evolution of the vector potential is determined by the diffusion and the convection of the vector magnetic potential and by the scalar electric potential gradient. This equation holds for any eddy current conducting domain (Figure 2.1). Here, it should be pointed out that by convention the conductivity σ is null within inductors. By definition, the current density is null outside the inductors. So, in non-conducting regions free of eddy currents, which may contain source currents $\mathbf{j_s}$, the vector potential equation is written:

$$\nabla \times (\nabla \times \mathbf{A}) = \mathbf{j_s} \tag{2.45}$$

The fact that equation (2.44) defines only the curl of $\mathbf{A}$ implies that the vector potential is defined up to the gradient of an arbitrary scalar function. Actually, if

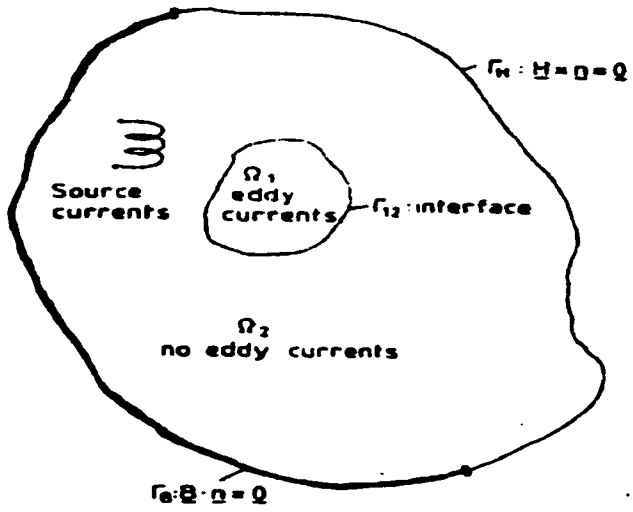

Figure 2.1: Regions, boundary conditions and interface in typical eddy current problem (From Biro and Preis [25]).

$(\mathbf{A}, \phi)$ is a solution of (2.44) and if $f = f(t, \mathbf{x})$ is a scalar function that is differentiable both in time and space, then the new couple $(\mathbf{A}', \phi')$, such that:

$$\mathbf{A}' = \mathbf{A} + \nabla f \tag{2.46}$$

$$\phi' = \phi - \frac{\partial f}{\partial t} \tag{2.47}$$

is also a solution of equation (2.44). Hence the solution of equation (2.44) is not unique. In order to insure the uniqueness of the solution, gauging the vector potential is needed. Such a procedure consists of defining the divergence of $\mathbf{A}$ in addition to its curl. The most used gauge is the Coulomb one defined as:

$$\nabla \cdot \mathbf{A} = 0 \tag{2.48}$$

This gauge could be whether imposed explicitly by adding equation (2.48) to equation (2.44) or as suggested by Biro and Preiss [26], and Bossavit et al [38], by adding a penalty term to the vector potential equation (2.44):

$$\frac{\partial \mathbf{A}}{\partial t} - \mathbf{u} \times (\nabla \times \mathbf{A}) + \frac{1}{\mu\sigma} \nabla \times (\nabla \times \mathbf{A}) - \nabla \left(\frac{1}{\mu\sigma} \nabla \cdot \mathbf{A} \right) + \nabla \phi = 0 \tag{2.49}$$

In case of constant magnetic diffusivity, as under the MHD assumptions, and when the conductivity is constant, this results in the Laplacian operator replacing the curl-curl

operator:

$$\frac{\partial \mathbf{A}}{\partial t} - \mathbf{u} \times (\nabla \times \mathbf{A}) - \frac{1}{\mu\sigma}\nabla^2 \mathbf{A} + \nabla\phi = 0 \tag{2.50}$$

The conservation of the electric current is implicit in the vector potential equation (2.44). Actually, if the divergence of equation (2.44) is taken term by term, then:

$$\nabla \cdot \left(\frac{\partial \mathbf{A}}{\partial t} - \mathbf{u} \times \mathbf{B} + \nabla\phi \right) = 0 \tag{2.51}$$

However, this same conservation condition does not anymore follow from the modified vector potential equation (2.50). The electric current conservation has, then, to be prescribed as:

$$\nabla \cdot \left(-\frac{\partial \mathbf{A}}{\partial t} - \nabla\phi + \mathbf{u} \times (\nabla \times \mathbf{A}) \right) = 0 \tag{2.52}$$

Thus using the $(\mathbf{A}, \phi)$ formulation would result in the system of equations (2.50) and (2.52). Many other formulations using different magnetic, electric, vector or scalar potentials exist in the literature. For a general description, one can consult Trophime [33] and the references therein.

2.4.1 The Reduced Vector Potential

It is possible as stated by Emson and Simkin [39], to define a new vector potential $\hat{\mathbf{A}}$ by the following equation:

$$\hat{\mathbf{A}} = \mathbf{A} + \int_t \nabla\phi \, dt \tag{2.53}$$

Then starting from the vector potential equation (2.44), one can obtain:

$$\frac{\partial \hat{\mathbf{A}}}{\partial t} - \mathbf{u} \times (\nabla \times \hat{\mathbf{A}}) + \frac{1}{\mu\sigma}\nabla \times (\nabla \times \hat{\mathbf{A}}) = 0 \tag{2.54}$$

Emson noted that equation (2.54) has a unique solution with an implied gauge of:

$$\nabla \cdot \hat{\mathbf{A}} = 0 \tag{2.55}$$

which was therefore not imposed. The same remark made in section (2.2.3) regarding the divergence of the magnetic field $\mathbf{B}$ could be made for the divergence of the reduced vector potential $\hat{\mathbf{A}}$. As an alternative to Emson's method, one could follow the same procedure regarding the vector potential formulation by adding a penalty term to

equation (2.54) in order to impose the divergence-free condition (2.55). This would yield the following reduced vector potential equation:

$$\frac{\partial \hat{\mathbf{A}}}{\partial t} - \mathbf{u} \times (\nabla \times \hat{\mathbf{A}}) + \frac{1}{\mu\sigma} \nabla \times (\nabla \times \hat{\mathbf{A}}) - \nabla \left(\eta \, \nabla \cdot \hat{\mathbf{A}} \right) = 0 \tag{2.56}$$

which again in the case of constant diffusivity would result in the Laplacian operator replacing the curl-curl operator as:

$$\frac{\partial \hat{\mathbf{A}}}{\partial t} - \mathbf{u} \times (\nabla \times \hat{\mathbf{A}}) - \frac{1}{\mu\sigma} \nabla^2 \hat{\mathbf{A}} = 0 \tag{2.57}$$

2.5 The Conservative Formulation

In order to introduce this family of formulations, let us recall the "Helmholtz" formulation. The idea leading to this formulation is that the system composed of equations (2.32) and (2.29) is over-specified and leads to more equations than unknowns. For example in the three-dimensional case and if the velocity field is assumed known, the system of equations composed by equations (2.32) and (2.29), leads to four linear equations with three unknowns. In Jiang et al. [40], the authors showed that an equivalent situation exists in the pure electromagnetic context. They demonstrated that the first order div-curl Maxwell's system of equations (2.5)-(2.7) is not an over-determined one. They showed that by introducing two dummy scalar variables, they end up with an equivalent system of eight equations with eight unknowns. They underlined the dangers of circumventing the "over-specification" of system (2.5)-(2.7) by dropping the free divergence equation (2.7). These dangers are related to the ellipticity of the system, the non-uniqueness of the solution and the ensuing spurious numerical solutions that may appear.

Using the same technique, we shall show that the second order system of equations (2.29) and (2.32) is not an over-specified one. Let Ω be a bounded, simply connected, convex and open domain which is included in R^3, with a piecewise smooth boundary Γ, the union of Γ_1 and Γ_2, with $\mathbf{n}$ the unit normal outward vector. Let equations (2.29) and (2.32) hold in the domain Ω and be associated with appropriate boundary conditions on Γ. Adding the gradient of a scalar variable to equation (2.32), one gets

the new following equation:

$$\frac{\partial \mathbf{B}}{\partial t} - \nabla \times (\mathbf{u} \times \mathbf{B}) + \eta \nabla \times (\nabla \times \mathbf{B}) + \nabla q = 0 \quad in\ \Omega \tag{2.58}$$

Let the homogeneous Dirichlet condition

$$q = 0 \tag{2.59}$$

holds on the boundary Γ. Taking the divergence of equation (2.58) and using equation (2.29), one gets:

$$\Delta q = 0 \quad in\ \Omega \tag{2.60}$$

As equation (2.60) is subjected to the boundary condition (2.59), this leads to the unique physical solution $q = 0$ over all the domain Ω. Thus the scalar q is really a dummy variable (which in theory should be null) and the system of equations (2.29) and (2.58) is equivalent to the system (2.29) and (2.32). The new system of equations has in the three-dimensional case, four equations with four unknowns and is no longer over-determined. By analogy to the Stokes and the Navier-Stokes equations, q is interpreted as a Lagrange multiplier used to enforce the divergence-free condition (2.29).

Remark 2: Equation (2.58) could be rewritten in many equivalent forms. Particularly, after making use of the vector identity (2.35), one gets the following equivalent equation:

$$\frac{\partial \mathbf{B}}{\partial t} - \nabla \times (\mathbf{u} \times \mathbf{B}) - \eta \nabla^2 \mathbf{B} + \eta \nabla (\nabla \cdot \mathbf{B}) + \nabla q = 0 \quad in\ \Omega \tag{2.61}$$

In the rest of this thesis, when we refer to the $(\mathbf{B}, q)$ formulation, we would be referring to the system of equations (2.29) and (2.61).

Remark 3: It is easily predictable that the non-explicit respect of the constraint (2.29) could lead to inaccurate numerical solutions. In order to show this, suppose one discards the divergence-free equation and retains only equation (2.32). Let for

simplicity the velocity field be equal to zero and assume the problem to be steady. From (2.32), one obtains:

$$\nabla \times (\nabla \times \mathbf{B}) = 0 \quad in\ \Omega \tag{2.62}$$

with the most probable boundary conditions

$$\mathbf{n} \cdot \mathbf{B} = 0 \quad on\ \Gamma_1 \tag{2.63}$$

$$\mathbf{n} \times \mathbf{B} = 0 \quad on\ \Gamma_2 \tag{2.64}$$

The solution of equation (2.62), subject to the boundary conditions (2.63)-(2.64), is not unique. It admits a kernel composed of the gradient of scalar variables satisfying the conditions (2.63)-(2.64). Any numerical method for problem (2.62)-(2.64) will fail to provide a unique solution. The constraint (2.29) should thus be taken into account and it behaves like a gauge condition filtering the divergence-free solution. The respect of this condition reduces the kernel of spurious solutions to a unique null scalar function.

Indeed, according to the unity partition theorem (Brezis [41]), there exist scalar functions ϕ that are C^∞, satisfying $\partial\phi/\partial n = 0$ on Γ_1, $\mathbf{n} \times \nabla\phi = 0$ on Γ_2 and ϕ non-null in a part of Ω. Thus if $\mathbf{B_0}$ is a particular solution of (2.62)-(2.64) then any vector $\mathbf{B} = \mathbf{B_0} + \nabla\phi$ is also a solution. But if the vector solution has to satisfy the divergence-free condition, then $\Delta\phi = 0$ in Ω. As $\partial\phi/\partial n = 0$ on Γ_1 and $\mathbf{n} \times \nabla\phi = 0$ on Γ_2, then ϕ is equal to a constant in Ω. Since ϕ is prescribed zero over part of the domain, then $\phi = 0$ over all the domain Ω.

2.6 The Navier-Stokes Equations

The continuity equation, which expresses the mass conservation, is written for an incompressible fluid as

$$\nabla \cdot \mathbf{u} = 0 \tag{2.65}$$

The conservation of the momentum for an incompressible flow is written, in differential form as:

$$\frac{\partial \mathbf{u}}{\partial t} + (\mathbf{u} \cdot \nabla)\mathbf{u} - \nu\nabla^2\mathbf{u} + \frac{1}{\rho}\nabla\mathbf{p} = \mathbf{f} \tag{2.66}$$

where p, ρ, ν and $\mathbf{f}$ are, respectively, the pressure, the density, the kinematic viscosity and the body force field. For MHD problems, the body force term is $\mathbf{f} = \mathbf{j} \times \mathbf{B}$, and represents the Lorentz (Laplace) forces due to the interaction between the current density and the magnetic field. Replacing the current density by its expression given by (2.22) gives:

$$\frac{\partial \mathbf{u}}{\partial t} + (\mathbf{u} \cdot \nabla)\mathbf{u} - \nu \nabla^2 \mathbf{u} + \frac{1}{\rho}\nabla p - \frac{1}{\mu\rho}(\nabla \times \mathbf{B}) \times \mathbf{B} = 0 \tag{2.67}$$

The body forces $\mathbf{f}$ could also be decomposed as:

$$\mathbf{f} = \mathbf{j} \times \mathbf{B} = -\nabla\left(\frac{\mathbf{B}^2}{2\mu}\right) + (\mathbf{B} \cdot \nabla)\frac{\mathbf{B}}{\mu} \tag{2.68}$$

The physical interpretation of this decomposition is evident. The Lorentz forces are decomposed into a gradient term which is naturally irrotational and another rotational term. The gradient term $-\nabla\left(\frac{\mathbf{B}^2}{2\mu}\right)$ is a magnetic pressure term. The rotational term $(\mathbf{B} \cdot \nabla)\frac{\mathbf{B}}{\mu}$ is the force that would generate movements within the fluid.

2.7 Magnetohydrodynamic Coupling

The induction equation (2.32), the magnetic conservation (2.29) along with the modified Navier-Stokes equation (2.67) and the mass conservation equation (2.65), represent the governing equations that should, ideally, be resolved in order to describe properly any MHD phenomenon. These equations are fully-coupled, since a two-way coupling exists between the fluid and the electromagnetic fields. On one hand, the influence of the magnetic field on the velocity field is through the term $\mathbf{j} \times \mathbf{B}$ which is added to the usual Navier-Stokes equations. On the other hand the influence of the velocity field on the magnetic field exists through the term $\nabla \times (\mathbf{u} \times \mathbf{B})$ in the magnetic induction equation, which originally appears in Ohm's law as $\mathbf{u} \times \mathbf{B}$. In order to assess the relative influence of the terms through which the coupling is exerted, one has to obtain the non-dimensional form of equations (2.32) and (2.67). This can be obtained by dividing each of the variables by a scaling value chosen appropriately:

$$\mathbf{u}^* = \frac{\mathbf{u}}{u_0}, \quad t^* = \frac{t\,u_0}{L}, \quad p^* = \frac{p}{\rho {u_0}^2}, \quad \mathbf{B}^* = \frac{\mathbf{B}}{B_0}, \quad \mathbf{x}^* = \frac{\mathbf{x}}{L} \tag{2.69}$$

The Navier-Stokes and the induction equations could then be written in the following non-dimensional form:

$$\frac{\partial \mathbf{u}^*}{\partial t} + (\mathbf{u}^* \cdot \nabla)\mathbf{u}^* - \frac{1}{Re}\nabla^2 \mathbf{u}^* + \nabla p^* - \frac{Ha^2}{Re\, Re_m}(\nabla \times \mathbf{B}^*) \times \mathbf{B}^* = 0 \tag{2.70}$$

$$\nabla \cdot \mathbf{u}^* = 0 \tag{2.71}$$

$$\frac{\partial \mathbf{B}^*}{\partial t^*} - \nabla \times (\mathbf{u}^* \times \mathbf{B}^*) + \frac{1}{Re_m}\nabla \times (\nabla \times \mathbf{B}^*) + \nabla q^* = 0 \tag{2.72}$$

$$\nabla \cdot \mathbf{B}^* = 0 \tag{2.73}$$

where the magnetic Reynolds number Re_m and the Hartmann number Ha are defined as follows

$$Re_m = \mu\sigma u_0 L \quad , \; Ha = B_0 L\left(\frac{\sigma}{\rho\nu}\right)^{1/2} \tag{2.74}$$

Equations (2.70) and (2.72) give the relative importance of each term in the equations. For instance, equation (2.72) tells that the ratio of the convection of the magnetic field by the velocity, to the diffusion of the magnetic field proportional to the magnetic diffusion η, is the non-dimensional magnetic Reynolds number Re_m. High values of Re_m indicate that the convection of the magnetic field is the dominant mechanism by which the magnetic field is transported. Low values of Re_m indicate that the diffusion of the magnetic field is the dominant mechanism. This number could be seen as the analog of the hydrodynamic Reynolds number Re defined as:

$$Re = \frac{u_0 L}{\nu} \tag{2.75}$$

Equation (2.70) puts into evidence that same hydrodynamic Reynolds number Re, which is classical in the pure fluid context. However a new non-dimensional parameter appears in front of the electromagnetic forces, namely $\frac{Ha^2}{Re\, Re_m}$. While the Reynolds number measures the relative importance of the diffusion of the velocity field, proportional to the kinematic viscosity ν, to its convection, the new non-dimensional group measures the relative importance of the Lorentz forces to the convective forces. A High value for $\frac{Ha^2}{Re\, Re_m}$, would indicate that the electromagnetic forces are dominant compared to the convective one, and low values would indicate that these same forces can be neglected when compared to the convective one.

2.7.1 Industrial Applications and Non-Dimensional Parameters

At the human level, whether in the laboratory scale or at the industrial scale (except for the MHD surgenerators), magnetic Reynolds numbers Re_m are very low. In such cases, equations (2.70) and (2.72) hint that a certain decoupling is possible between the magnetic phenomena and the hydrodynamic ones. In fact when the convection of the magnetic field by velocity could be neglected compared to its diffusion, the magnetic problem could be decoupled from the fluid one. This decoupling is, however, possible only one way and not the other. Yet the fluid problem can strongly be affected by the magnetic problem through the term $\frac{Ha^2}{Re\ Re_m}$. A low Re_m is by no way an indication that Lorentz forces can be neglected compared to the diffusive or the convective forces. In such a case, one is dealing with a weak MHD coupling. Weak meaning that the coupling is stronger one way than the other (small influence of the velocity field on the magnetic one but strong influence of the magnetic field on the velocity one). Yet, even when Re_m is small, one can be in presence of a strong MHD coupling.

Suppose one is in the presence of inductive fields. Suppose furthermore that one is interested in the quasi-steady regime ($\frac{\partial}{\partial t} = i\omega$) with ω being the pulsation of the source currents, then a new non-dimensional parameter could be defined as:

$$R_\omega = \mu\sigma\omega L^2 \tag{2.76}$$

This parameter, called the shielding or the screen parameter which is a measure of the diffusion time ($\mu\sigma L^2$) to the period $\frac{1}{\omega}$, would then appear in the non-dimensional form of equations as:

$$R_\omega \frac{\partial \mathbf{B}^*}{\partial t^*} - Re_m \nabla \times (\mathbf{u}^* \times \mathbf{B}^*) + \nabla \times (\nabla \times \mathbf{B}^*) = 0 \tag{2.77}$$

equation (2.77) states that in order to be able to neglect the term $\nabla \times (\mathbf{u}^* \times \mathbf{B}^*)$, the term $\frac{Re_m}{R_\omega}$ should be small compared to unity. When $\frac{Re_m}{R_\omega} > 1$, then the magnetic convection term could not be neglected anymore. Thus, one would be in the case of low Re_m but with a strong coupling still needed between the fluid and the magnetic

equations! This is the case, for example, with inductive MHD propulsion. For more details, see Trophime [33].

While in this thesis, we would exclude any study of inductive systems or quasi-steady regimes, we would, however, for generality, keep the possibility of both low and high magnetic Reynolds numbers. We would then be able to develop the appropriate algorithms for each of the two cases, weak MHD coupling and strong MHD coupling. These algorithms could then eventually be applied for the solution of the coupled problem with or without inductive fields and in different possible regimes.

2.8 Boundary Conditions

Boundary conditions reflect the general laws applied to an infinitely small surface, which is an interface between two materials and domains (1) and (2). For the fluid quantities, such considerations lead to:

$$\mathbf{u}^{(1)} = \mathbf{u}^{(2)} \tag{2.78}$$

expressing the continuity of the velocity. For the magnetic field, these considerations lead to:

$$\mathbf{B}^{(1)} \cdot \mathbf{n} = \mathbf{B}^{(2)} \cdot \mathbf{n} \tag{2.79}$$

expressing the continuity of the normal components of the magnetic field, and to:

$$\mathbf{H}^{(1)}{}_t = \mathbf{H}^{(2)}{}_t \tag{2.80}$$

expressing the continuity of the tangential component of the magnetic induction field.

When the vector and the scalar potentials are used, then the boundary conditions are:

$$\mathbf{A} \times \mathbf{n} = 0 \qquad \phi = cst \tag{2.81}$$

for the boundaries where $\mathbf{B} \cdot \mathbf{n} = 0$,

$$\mathbf{A} \cdot \mathbf{n} = 0 \qquad \frac{\partial \phi}{\partial \mathbf{n}} = 0 \tag{2.82}$$

for the boundaries where $\mathbf{H} \times \mathbf{n} = 0$, and

$$\mathbf{A} \cdot \mathbf{n} = 0 \tag{2.83}$$

at infinity.

Chapter 3

Variational Formulations and Finite Element Discretization

3.1 Introduction

This chapter describes the finite element methodologies that have been developed throughout this thesis for the magnetic problem, the vector potential formulations and the incompressible Navier-Stokes equations. In the second section, the weak-Galerkin variational form of the conservative formulation $(\mathbf{B}, q)$ of the magnetic problem is introduced. It is seen that this weak form is of mixed type, requiring either the respect or the circumvention of the L.B.B. stability condition. In this thesis, we opt for a stabilized formulation since mixed formulations are known to be prohibitively expensive in three-dimensional cases. This formulation is presented in the third section. In the fourth section, the weak-Galerkin form of the vector potential formulation $(\mathbf{A}, \phi)$ is presented. This variational statement does not need any particular treatment, since the Galerkin method is sufficient to ensure its stability, in this case.

In the fifth section of the chapter, the Navier-Stokes equations are tackled. Again, the weak-Galerkin form of the equations turns out to be of mixed type and stabilization is provided through a Galerkin Least-Squares like term. The advantage of this technique is that it gives rise to a stable formulation, even when the convective terms are dominant.

In finite element methods, the space and the time discretizations performed on the variational formulations yield systems of n equations in n unknowns that have to

be solved , each, with the most appropriate solver. This depending on the nature of the system (linear versus non-linear) and on the nature of the problem (coupled or decoupled).

3.2 The Galerkin Method for the Conservative Formulation

The Galerkin weighted residual formulation for the system of equations (2.29) and (2.61) consists of multiplying the two equations by two test functions $\mathbf{B}^*$ and q^*, respectively, chosen in two appropriate functional spaces. After integrating the resulting equations over the domain Ω, one gets:

$$\int_\Omega \mathbf{B}^* \cdot \left(\frac{\partial \mathbf{B}}{\partial t}\right) d\Omega - \eta \int_\Omega \mathbf{B}^* \cdot \nabla^2 \mathbf{B}\, d\Omega + \eta \int_\Omega \mathbf{B}^* \cdot \nabla(\nabla \cdot \mathbf{B})\, d\Omega$$

$$- \int_\Omega \mathbf{B}^* \cdot \nabla \times (\mathbf{u} \times \mathbf{B})\, d\Omega + \int_\Omega \mathbf{B}^* \cdot \nabla q\, d\Omega = 0 \tag{3.1}$$

$$\int_\Omega q^* (\nabla \cdot \mathbf{B})\, d\Omega = 0 \tag{3.2}$$

for all $\mathbf{B}^*$ and q^*.

Applying the divergence theorem, the weak form of the Galerkin formulation is obtained as:

$$\int_\Omega \mathbf{B}^* \cdot \left(\frac{\partial \mathbf{B}}{\partial t}\right) d\Omega + \eta \int_\Omega \nabla \mathbf{B}^* \cdot \nabla \mathbf{B}\, d\Omega - \int_\Omega \mathbf{B}^* \cdot \nabla \times (\mathbf{u} \times \mathbf{B})\, d\Omega$$

$$+ \int_\Omega \mathbf{B}^* \cdot \nabla q\, d\Omega - \eta \int_\Omega (\nabla \cdot \mathbf{B})\, (\nabla \cdot \mathbf{B}^*)\, d\Omega - \eta \int_\Gamma (\mathbf{n} \cdot \nabla \mathbf{B}) \cdot \mathbf{B}^*\, d\Gamma$$

$$+ \eta \int_\Gamma (\mathbf{n} \cdot \mathbf{B}^*)\, (\nabla \cdot \mathbf{B})\, d\Gamma = 0 \tag{3.3}$$

$$\int_\Omega q^* (\nabla \cdot \mathbf{B})\, d\Omega = 0 \tag{3.4}$$

In the usual manner, the discrete problem associated with the weak form (3.3)-(3.4) can be established as:

$$\int_\Omega \mathbf{B}_\mathbf{h}^* \cdot \left(\frac{\partial \mathbf{B}_\mathbf{h}}{\partial t}\right) d\Omega + \eta \int_\Omega \nabla \mathbf{B}_\mathbf{h}^* \cdot \nabla \mathbf{B}_\mathbf{h}\, d\Omega - \int_\Omega \mathbf{B}_\mathbf{h}^* \cdot \nabla \times (\mathbf{u}_\mathbf{h} \times \mathbf{B}_\mathbf{h})\, d\Omega$$

$$+\int_\Omega \mathbf{B_h^*}\cdot\ \nabla q_h\, d\Omega - \eta\int_\Omega(\nabla\cdot\ \mathbf{B_h})\ (\nabla\cdot\mathbf{B_h^*})\, d\Omega - \eta\int_\Gamma(\mathbf{n}\cdot\ \nabla\mathbf{B_h})\cdot\mathbf{B_h^*}\, d\Gamma$$

$$+\eta\int_\Gamma(\mathbf{n}\cdot\ \mathbf{B_h^*})\ (\nabla\cdot\mathbf{B_h})\, d\Gamma = 0 \tag{3.5}$$

$$\int_\Omega q_h^*\ (\nabla\cdot\mathbf{B_h})\, d\Omega = 0 \tag{3.6}$$

for all $\mathbf{B_h^*}$ and q_h^* belonging to some finite dimensional functional sub-space.

The variational problem formulated by equations (3.5)-(3.6) is of mixed type and presents many similarities to the mixed variational formulation for the Navier-Stokes equations (Brezzi and Fortin [42]). Hence, it requires the respect of the inf-sup stability condition, also called the L.B.B. condition, in order to find a stable numerical solution $(\mathbf{B_h^*},\ \mathbf{q_h^*})$. In practice, the respect of this stability condition implies the use of different approximations for the two variables $(\mathbf{B_h^*},\ \mathbf{q_h^*})$. In three dimensions, elements respecting the L.B.B. condition could prove complicated and expensive with respect to execution time and memory storage. An alternative way of obtaining a stable finite element method for the system (3.5)-(3.6), is by circumventing the L.B.B. condition (Hughes et al. [43]).

3.3 The Stabilized Finite Element Method

Suppose Ω_h=$\cup\Omega_e$, a certain partition of the domain Ω into elements and h the "size" of an element Ω_e. Following Brezzi and Pitkaranta [44], the continuity equation (3.6) is modified as:

$$\int_\Omega q_h^*\ (\nabla\cdot\mathbf{B_h})\, d\Omega + \sum_{\Omega_e\in\Omega_h}\tau_1\int_{\Omega_e}\nabla q_h\cdot\ \nabla q_h^*\, d\Omega = 0 \tag{3.7}$$

where τ_1 is a function of the mesh size h.

This stabilization technique is equivalent to augmenting the continuity equation (2.29) of the strong problem with a Laplacian dissipation term of the scalar q, and has already been used successfully for the Navier-Stokes incompressible and compressible flows (Baruzzi et al. [45]). Hence, the stabilized formulation can be introduced as:

$$\int_\Omega \mathbf{B_h^*}\cdot\ \left(\frac{\partial\mathbf{B_h}}{\partial t}\right)\, d\Omega + \eta\int_\Omega \nabla\mathbf{B_h^*}\ \cdot\ \nabla\mathbf{B_h}\, d\Omega - \int_\Omega \mathbf{B_h^*}\cdot\ \nabla\times(\mathbf{u}\times\mathbf{B_h})\, d\Omega$$

$$+\int_\Omega \mathbf{B}_\mathbf{h}^* \cdot \nabla q_h \, d\Omega - \eta \int_\Omega (\nabla \cdot \mathbf{B}_\mathbf{h}) (\nabla \cdot \mathbf{B}_\mathbf{h}^*) \, d\Omega - \eta \int_\Gamma (\mathbf{n} \cdot \nabla \mathbf{B}_\mathbf{h}) \cdot \mathbf{B}_\mathbf{h}^* \, d\Gamma$$

$$+\eta \int_\Gamma (\mathbf{n} \cdot \mathbf{B}_\mathbf{h}^*) (\nabla \cdot \mathbf{B}_\mathbf{h}) \, d\Gamma = 0 \tag{3.8}$$

$$\int_\Omega q_h^* (\nabla \cdot \mathbf{B}_\mathbf{h}) \, d\Omega + \sum_{\Omega_e \in \Gamma_h} \tau_1 \int_{\Omega_e} \nabla q_h \cdot \nabla q_h^* \, d\Omega = 0 \tag{3.9}$$

This formulation (3.8) and (3.9) creates the necessary coupling between the momentum and the continuity equations. This coupling can be seen as the counterpart to the use of staggered grids in finite difference schemes. Once the stability of the formulation is insured, the volume integral emanating from the $\nabla(\nabla \cdot \mathbf{B})$ term is penalized with a term τ_2, in order to enforce the magnetic divergence towards small values when the convection is dominant (i.e. small values of η). Then, the formulation reads as:

$$\int_\Omega \mathbf{B}_\mathbf{h}^* \cdot \left(\frac{\partial \mathbf{B}_\mathbf{h}}{\partial t} \right) d\Omega + \eta \int_\Omega \nabla \mathbf{B}_\mathbf{h}^* \cdot \nabla \mathbf{B}_\mathbf{h} \, d\Omega - \int_\Omega \mathbf{B}_\mathbf{h}^* \cdot \nabla \times (\mathbf{u} \times \mathbf{B}_\mathbf{h}) \, d\Omega$$

$$+\int_\Omega \mathbf{B}_\mathbf{h}^* \cdot \nabla q_h \, d\Omega + (\tau_2 - \eta) \int_\Omega (\nabla \cdot \mathbf{B}_\mathbf{h}) (\nabla \cdot \mathbf{B}_\mathbf{h}^*) \, d\Omega - \eta \int_\Gamma (\mathbf{n} \cdot \nabla \mathbf{B}_\mathbf{h}) \cdot \mathbf{B}_\mathbf{h}^* \, d\Gamma$$

$$+\eta \int_\Gamma (\mathbf{n} \cdot \mathbf{B}_\mathbf{h}^*) (\nabla \cdot \mathbf{B}_\mathbf{h}) \, d\Gamma = 0 \tag{3.10}$$

$$\int_\Omega q_h^* (\nabla \cdot \mathbf{B}_\mathbf{h}) \, d\Omega + \sum_{\Omega_e \in \Gamma_h} \tau_1 \int_{\Omega_e} \nabla q_h \cdot \nabla q_h^* \, d\Omega = 0 \tag{3.11}$$

The stabilized method defined by (3.10)-(3.11) allows for the use of equal interpolation for the two variables ($\mathbf{B}_\mathbf{h}^*$, $\mathbf{q}_\mathbf{h}^*$), thus facilitating the implementation and permitting the use of elements less costly in terms of calculations.

3.4 Galerkin Method for the Vector Potential Formulation

The Galerkin weighted residual formulation for the system of equations (2.50) and (2.52) is obtained by multiplying the two equations by two test functions $\mathbf{A}^*$ and ϕ^*, respectively, chosen in two appropriate functional spaces. After integrating the resulting equations over the whole domain Ω, one gets:

$$\int_\Omega \mathbf{A}^* \cdot \left(\frac{\partial \mathbf{A}}{\partial t} \right) d\Omega - \eta \int_\Omega \mathbf{A}^* \cdot \nabla^2 \mathbf{A} \, d\Omega$$

$$-\int_\Omega \mathbf{A}^* \cdot \mathbf{u} \times (\nabla \times \mathbf{A})\, d\Omega + \int_\Omega \mathbf{A}^* \cdot \nabla\phi\, d\Omega = 0 \tag{3.12}$$

$$\int_\Omega \phi^* \nabla \cdot \left(-\frac{\partial \mathbf{A}}{\partial t} + \mathbf{u} \times (\nabla \times \mathbf{A}) - \nabla\phi\right) d\Omega = 0 \tag{3.13}$$

for all $\mathbf{A}^*$ and ϕ^*.

After integration of the second order terms appearing in equations (3.12) and (3.13), the weak form of the Galerkin formulation becomes:

$$\int_\Omega \mathbf{A}^* \cdot \left(\frac{\partial \mathbf{A}}{\partial t}\right) d\Omega + \eta \int_\Omega \nabla \mathbf{A}^* \cdot \nabla \mathbf{A}\, d\Omega + \int_\Omega \mathbf{A}^* \cdot \nabla\phi\, d\Omega$$
$$-\int_\Omega \mathbf{A}^* \cdot \mathbf{u} \times (\nabla \times \mathbf{A})\, d\Omega - \eta \int_\Gamma (\mathbf{n} \cdot \nabla \mathbf{A}) \cdot \mathbf{A}^*\, d\Gamma = 0 \tag{3.14}$$

$$\int_\Omega \left(\frac{\partial \mathbf{A}}{\partial t} - \mathbf{u} \times (\nabla \times \mathbf{A}) + \nabla\phi\right) \cdot \nabla\phi^*\, d\Omega + \int_\Gamma (\mathbf{j} \cdot \mathbf{n}) \cdot \phi^*\, d\Gamma = 0 \tag{3.15}$$

In the usual manner, the discrete problem associated with the weak form (3.14)-(3.15) can be established as:

$$\int_\Omega \mathbf{A}_\mathbf{h}^* \cdot \left(\frac{\partial \mathbf{A}_\mathbf{h}}{\partial t}\right) d\Omega + \eta \int_\Omega \nabla \mathbf{A}_\mathbf{h}^* \cdot \nabla \mathbf{A}_\mathbf{h}\, d\Omega + \int_\Omega \mathbf{A}_\mathbf{h}^* \cdot \nabla\phi_h\, d\Omega$$
$$-\int_\Omega \mathbf{A}_\mathbf{h}^* \cdot \mathbf{u}_\mathbf{h} \times (\nabla \times \mathbf{A}_\mathbf{h})\, d\Omega - \eta \int_\Gamma (\mathbf{n} \cdot \nabla \mathbf{A}_\mathbf{h}) \cdot \mathbf{A}_\mathbf{h}^*\, d\Gamma = 0 \tag{3.16}$$

$$\int_\Omega \left(\frac{\partial \mathbf{A}_\mathbf{h}}{\partial t} - \mathbf{u}_\mathbf{h} \times (\nabla \times \mathbf{A}_\mathbf{h}) + \nabla\phi_h\right) \cdot \nabla\phi_h^*\, d\Omega + \int_\Gamma (\mathbf{j}_\mathbf{h} \cdot \mathbf{n}) \cdot \phi_h^*\, d\Gamma = 0 \tag{3.17}$$

Since both equations (2.50) and (2.52) include second order terms in $\mathbf{A}$ and ϕ, the formulation (3.16) and (3.17) does not need additional stabilizing terms to allow equal interpolation for the variables $(\mathbf{A}, \phi)$.

3.4.1 Galerkin Method for the Reduced Vector Potential Equation

The discrete weak Galerkin form for the reduced vector potential equation (2.57) is presented as:

$$\int_\Omega \hat{\mathbf{A}}_h^* \cdot \left(\frac{\partial \hat{\mathbf{A}}_h}{\partial t} - \mathbf{u}_\mathbf{h} \times (\nabla \times \hat{\mathbf{A}}_h)\right) d\Omega + \eta \int_\Omega \nabla \hat{\mathbf{A}}_h^* \cdot \nabla \hat{\mathbf{A}}_h\, d\Omega$$
$$-\eta \int_\Gamma (\mathbf{n} \cdot \nabla \hat{\mathbf{A}}_h) \cdot \hat{\mathbf{A}}_h^*\, d\Gamma = 0 \tag{3.18}$$

for all $\hat{\mathbf{A}}_h^*$ belonging to some finite dimensional sub-spaces.

3.5 Galerkin Method for the Navier-Stokes Equations

The Galerkin weighted residual formulation for the Navier-Stokes equations (2.65) and (2.67) is obtained by multiplying the two equations by two test functions, $\mathbf{v}$ for the momentum equations and p^* for the continuity equation, respectively, chosen in two appropriate functional spaces. After integrating over the whole domain Ω, one obtains:

$$\int_\Omega \mathbf{v} \cdot \left(\frac{\partial \mathbf{u}}{\partial t} + (\mathbf{u} \cdot \nabla)\mathbf{u} - \nu \nabla^2 \mathbf{u} + \frac{1}{\rho}\nabla p - \frac{1}{\mu}(\nabla \times \mathbf{B}) \times \mathbf{B} \right) d\Omega = 0 \tag{3.19}$$

$$\int_\Omega p^* \, (\nabla \cdot \mathbf{u}) \, d\Omega = 0 \tag{3.20}$$

for all $\mathbf{v}$ and p^*. Integrating by parts the second order term appearing in the integral form of the momentum equations (3.19) gives the weak Galerkin form:

$$\int_\Omega \mathbf{v} \cdot \left(\frac{\partial \mathbf{u}}{\partial t} + (\mathbf{u} \cdot \nabla)\mathbf{u} \right) d\Omega + \nu \int_\Omega \nabla \mathbf{u} \cdot \nabla \mathbf{v} \, d\Omega - \frac{1}{\rho} \int_\Omega p \, \nabla \cdot \mathbf{v} \, d\Omega$$

$$-\frac{1}{\mu} \int_\Omega ((\nabla \times \mathbf{B}) \times \mathbf{B}) \cdot \mathbf{v} \, d\Omega + \frac{1}{\rho} \int_\Gamma p \, \mathbf{v} \cdot \mathbf{n} \, d\Gamma - \nu \int_\Gamma (\nabla \mathbf{u} \cdot \mathbf{n}) \cdot \mathbf{v} \, d\Gamma = 0 \tag{3.21}$$

$$\int_\Omega p^* \, (\nabla \cdot \mathbf{u}) \, d\Omega = 0 \tag{3.22}$$

Again, in the usual manner, the discrete problem associated with the weak Galerkin formulation (3.21) and (3.22) is:

$$\int_\Omega \mathbf{v_h} \cdot \left(\frac{\partial \mathbf{u_h}}{\partial t} + (\mathbf{u_h} \cdot \nabla)\mathbf{u_h} \right) d\Omega + \nu \int_\Omega \nabla \mathbf{u_h} \cdot \nabla \mathbf{v_h} \, d\Omega - \frac{1}{\rho} \int_\Omega p_h \, \nabla \cdot \mathbf{v_h} \, d\Omega$$

$$-\frac{1}{\mu} \int_\Omega ((\nabla \times \mathbf{B_h}) \times \mathbf{B_h}) \cdot \mathbf{v_h} \, d\Omega + \frac{1}{\rho} \int_\Gamma p_h \, \mathbf{v_h} \cdot \mathbf{n} \, d\Gamma - \nu \int_\Gamma (\nabla \mathbf{u_h} \cdot \mathbf{n}) \cdot \mathbf{v_h} \, d\Gamma = 0 \tag{3.23}$$

$$\int_\Omega p_h^* \, (\nabla \cdot \mathbf{u_h}) \, \mathbf{d\Omega} = \mathbf{0} \tag{3.24}$$

for all $\mathbf{v_h}$ and p_h^* belonging to some finite dimensional functional sub-spaces.

3.5.1 Galerkin Least-Squares Formulation

The variational problem formulated by equations (3.23) and (3.24) is of mixed type, and, again, requires circumventing the L.B.B. condition. Moreover, Galerkin formulation like (3.23) and (3.24) is known to generate unstable numerical solutions whenever the convective term $(\mathbf{u}\cdot\nabla)\mathbf{u}$ is dominant. In the context of fluid mechanics, Galerkin Least-Squares formulations ([46]) have been used successfully by many authors, in order to ensure both the stabilization for equal order interpolation and for high Reynolds numbers. In this case, such formulation could be presented in the following compact form as:

$$\int_\Omega \mathbf{v_h}\cdot\left(\frac{\partial \mathbf{u_h}}{\partial t}+(\mathbf{u_h}\cdot\nabla)\mathbf{u_h}\right)d\Omega+\nu\int_\Omega \nabla\mathbf{u_h}\cdot\nabla\mathbf{v_h}\,d\Omega-\frac{1}{\rho}\int_\Omega p_h\,\nabla\cdot\mathbf{v_h}\,d\Omega$$

$$+\sum_{\Omega_e\in\Omega_h}\tau_1\int_{\Omega_e}\left(\frac{\partial \mathbf{u_h}}{\partial t}+(\mathbf{u_h}\cdot\nabla)\mathbf{u_h}-\nu\nabla^2\mathbf{u_h}+\frac{1}{\rho}\nabla p_h\right)\cdot\left((\mathbf{u_h}\cdot\nabla)\mathbf{v_h}+\nu\nabla^2\mathbf{v_h}+\frac{1}{\rho}\nabla p_h^*\right)d\Omega_e$$

$$-\frac{1}{\mu}\int_\Omega((\nabla\times\mathbf{B_h})\times\mathbf{B_h})\cdot\mathbf{v_h}\,d\Omega+\frac{1}{\rho}\int_\Gamma p_h\,\mathbf{v_h}\cdot\mathbf{n}\,d\Gamma-\nu\int_\Gamma(\nabla\mathbf{u_h}\cdot\mathbf{n})\cdot\mathbf{v_h}\,d\Gamma$$

$$+\int_\Omega p_h^*(\nabla\cdot\mathbf{u_h})\,d\Omega=0 \tag{3.25}$$

From the above stabilized formulation (3.25), one can obtain the corresponding momentum equations by choosing $p_h^*=0$, or obtain the corresponding continuity equation for $\mathbf{v_h}=\mathbf{0}$.

Remark 1: If the test and the shape functions are interpolated on a linear basis, then the second order terms appearing in the stabilization terms of (3.25) cancel and the formulation simplifies to:

$$\int_\Omega \mathbf{v_h}\cdot\left(\frac{\partial \mathbf{u_h}}{\partial t}+(\mathbf{u_h}\cdot\nabla)\mathbf{u_h}\right)d\Omega+\nu\int_\Omega \nabla\mathbf{u_h}\cdot\nabla\mathbf{v_h}\,d\Omega-\frac{1}{\rho}\int_\Omega p_h\,\nabla\cdot\mathbf{v_h}\,d\Omega$$

$$+\sum_{\Omega_e\in\Omega_h}\tau_1\int_{\Omega_e}\left(\frac{\partial \mathbf{u_h}}{\partial t}+(\mathbf{u_h}\cdot\nabla)\mathbf{u_h}+\frac{1}{\rho}\nabla p_h\right)\cdot\left((\mathbf{u_h}\cdot\nabla)\mathbf{v_h}+\frac{1}{\rho}\nabla p_h^*\right)d\Omega_e$$

$$+\int_\Omega p_h^*(\nabla\cdot\mathbf{u_h})\,d\Omega$$

$$-\frac{1}{\mu}\int_\Omega((\nabla\times\mathbf{B_h})\times\mathbf{B_h})\cdot\mathbf{v_h}\,d\Omega+\frac{1}{\rho}\int_\Gamma p_h\,\mathbf{v_h}\cdot\mathbf{n}\,d\Gamma-\nu\int_\Gamma(\nabla\mathbf{u_h}\cdot\mathbf{n})\cdot\mathbf{v_h}\,d\Gamma=0 \tag{3.26}$$

3.6 Finite Element Space Discretization

In finite element methods, the domain Ω is decomposed into a finite number of elements, Nel, ($\Omega = \bigcup_{e=1}^{Nel} \Omega_e$). The solution vectors $\mathbf{B_h}$, q_h, $\mathbf{A_h}$, ϕ_h, $\mathbf{u_h}$ and p_h are approximated within each element by the same polynomial shape functions. These approximations lead to the following expressions:

$$\begin{aligned}
\mathbf{B_h} &= \sum_{j=1}^{nnd} \mathbf{B_{h_j}}(t)\ \psi_j(\mathbf{x}) \\
q_h &= \sum_{j=1}^{nnd} q_{h_j}(t)\ \psi_j(\mathbf{x}) \\
\mathbf{A_h} &= \sum_{j=1}^{nnd} \mathbf{A_{h_j}}(t)\ \psi_j(\mathbf{x}) \\
\phi_h &= \sum_{j=1}^{nnd} \phi_{h_j}(t)\ \psi_j(\mathbf{x}) \\
\mathbf{u_h} &= \sum_{j=1}^{nnd} \mathbf{u_{h_j}}(t)\ \psi_j(\mathbf{x}) \\
p_h &= \sum_{j=1}^{nnd} p_{h_j}(t)\ \psi_j(\mathbf{x})
\end{aligned} \tag{3.27}$$

where $\mathbf{B_{h_j}}$, q_{h_j}, $\mathbf{A_{h_j}}$, ϕ_h, $\mathbf{u_{h_j}}$ and p_{h_j} are the values of the approximate solutions at node j, ψ_j is the shape (or the interpolation) function associated with node j and nnd is the total number of nodes per element. Then, from the above expressions, one can derive that:

$$\begin{aligned}
\frac{\partial \mathbf{B_h}}{\partial t} &= \sum_{j=1}^{nnd} \dot{\mathbf{B}}_{h_j}(t)\ \psi_j(\mathbf{x}) \\
\frac{\partial q_h}{\partial t} &= \sum_{j=1}^{nnd} \dot{q}_{h_j}(t)\ \psi_j(\mathbf{x}) \\
\frac{\partial \mathbf{A_h}}{\partial t} &= \sum_{j=1}^{nnd} \dot{\mathbf{A}}_{h_j}(t)\ \psi_j(\mathbf{x}) \\
\frac{\partial \phi_h}{\partial t} &= \sum_{j=1}^{nnd} \dot{\phi}_{h_j}(t)\ \psi_j(\mathbf{x}) \\
\frac{\partial \mathbf{u_h}}{\partial t} &= \sum_{j=1}^{nnd} \dot{\mathbf{u}}_{h_j}(t)\ \psi_j(\mathbf{x})
\end{aligned}$$

$$\frac{\partial p_h}{\partial t} = \sum_{j=1}^{nnd} \dot{p}_{hj}(t)\ \psi_j(\mathbf{x}) \tag{3.28}$$

where $\dot{\mathbf{B}}_{hj}$, $\dot{q}_{hj}$, $\dot{\mathbf{A}}_{hj}$, $\dot{\phi}_{hj}$, $\dot{\mathbf{u}}_{hj}$ and $\dot{p}_{hj}$ are the nodal values of the different time derivatives. Substituting equations (3.27) and (3.28) into the variational formulations (3.10)-(3.11), (3.16)-(3.17), (3.18) and (3.26) gives rise to four coupled systems that can generically be put in the following form:

$$[M]\ \dot{U}\ + [K]\ U = F \tag{3.29}$$

where U represents $\mathbf{B_h}$ and q_h, $\mathbf{A_h}$ and ϕ_h or $\mathbf{u_h}$ and p_h and where $\dot{U}$ represents $\dot{\mathbf{B}}_{hj}$ and $\dot{q}_{hj}$, $\dot{\mathbf{A}}_{hj}$ and $\dot{\phi}_{hj}$ or $\dot{\mathbf{u}}_{hj}$ and $\dot{p}_{hj}$. The coefficients of the matrices $[M]$ and $[K]$ are obtained from the variational formulations that are used for each pair of variables.

3.6.1 Linear Tetrahedral Reference Element

In the present work, the computational domain is subdivided into four-node tetrahedral elements with all the variables interpolated by linear functions. To facilitate the computation of the coefficients of the mass matrix, $[M]$, of the influence matrix, $[K]$, and of the right-hand-side vector F, it is classical to evaluate these coefficients at the element level, after mapping the element to a reference element, $\hat{\Omega}_e$, of fixed simple geometry (Figure 3.1). The interpolation functions are defined over the reference linear tetrahedral as:

$$\begin{aligned} \hat{\psi}_1 &= 1 - \xi - \eta - \zeta \\ \hat{\psi}_2 &= \xi \\ \hat{\psi}_3 &= \eta \\ \hat{\psi}_4 &= \zeta \end{aligned} \tag{3.30}$$

Since the interpolation functions are linear, the integrals in the elementary systems are computed analytically. The elementary systems that are obtained are then assembled in a global system of a form like (3.29).

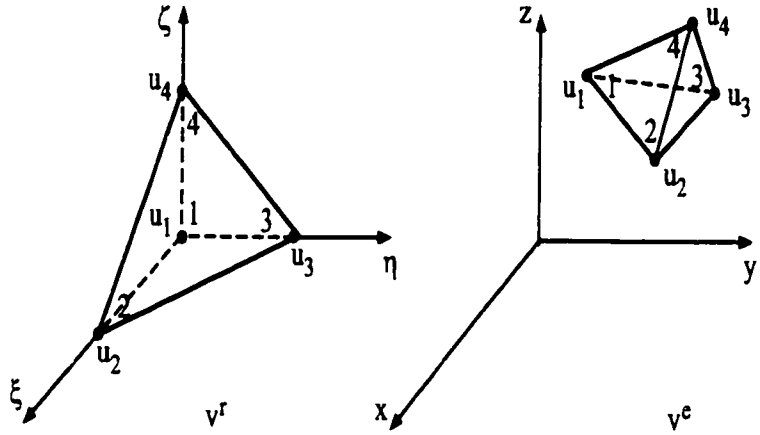

Figure 3.1: Actual linear tetrahedral element in the (x,y,z) global coordinates (right) and the reference element in the (ξ, η, ζ) local coordinates (left)

3.7 Time Discretization

The time derivative vector $\dot{U}$ is evaluated by a finite difference-like expression and substituted into equation (3.29). Using the Gear scheme, the vector $\dot{U}$ is written as:

$$\dot{U} = \frac{3\,U_n - 4\,U_{n-1} + U_{n-2}}{2\,\Delta\,t} \tag{3.31}$$

The Gear scheme is a variable order variant of the implicit Euler scheme, with the order chosen here to be 2. It, however, requires solution vectors at two time steps $n-2$ and $n-1$, in order to be implemented. During the first time step, one can use the first order implicit Euler scheme:

$$\dot{U} = \frac{U_n - U_{n-1}}{\Delta\,t} \tag{3.32}$$

then, from the second time step on, the second order Gear scheme can be appropriately used. Using (3.31) or (3.32) into (3.29) gives a new global system of the following generic form:

$$[K]\;U = F \tag{3.33}$$

The nature of such a system depends mainly on the formulation that is used. The systems emanating from the $(\mathbf{B}, q)$, or the $(\mathbf{A}, \phi)$ formulations are linear ones. The solution of such systems can be handled without major obstacles. When the fluid

problem $(\mathbf{u}, p)$ is coupled with the magnetic one $(\mathbf{B}, q)$, the system obtained is non-linear and presents more challenging problems in its solution. Ways of solving each of these systems are presented and discussed in the following chapter.

Chapter 4

Solution Strategies

4.1 Introduction

As stated in the introduction, a two-step approach has been adopted in order to achieve the goals of the thesis. In the first step, the magnetic problem has been decoupled from the fluid problem, while, in the second step, both problems are coupled. Since the problems to be solved at each step are different, the solution strategy has to adapt to the problem that is solved. For the fluid solver, a GMRES-based algorithm with an ILUT preconditioning is implemented. In the third section, an overview of the solution strategy of the decoupled magnetic problem is presented. This strategy concerns the $(\mathbf{B}, q)$ conservative formulation, the $(\mathbf{A}, \phi)$ or the $\hat{\mathbf{A}}$ formulations.

In the second step, the coupled problem is tackled. First, it should be noticed that the coupling has been developed between the $(\mathbf{B}, q)$ conservative formulation and the Navier-Stokes equations, rather than between the $(\mathbf{A}, \phi)$ or $\hat{\mathbf{A}}$ potential formulations and the Navier-Stokes equations, because of the following reasons:

- The $(\mathbf{A}, \phi)$ or the $\hat{\mathbf{A}}$ formulations are generally associated with inductive systems in which the vector potential $\mathbf{A}$ (called the source generator) results from an alternative source, and is written as:

$$\mathbf{A}(\mathbf{x}, t) \;=\; Real\left(e^{i\omega t}\mathbf{A}(\mathbf{x})\right) \tag{4.1}$$

  Since this kind of quasi-steady regime has been excluded from this work, it is logical to exclude the coupling between the vector potential formulations and the Navier-Stokes equations.

- The use of the $(\mathbf{B}, q)$ conservative formulation in the coupling brings about the main electromagnetic variable, namely the magnetic field $\mathbf{B}$, a physical quantity that can be easily and directly measured.

- The computation of the Lorentz body forces is straightforward when the magnetic field is used. When the vector potential $\mathbf{A}$ is used, the expression of the body forces is somewhat more difficult to express and to implement.

In the fourth section of the present chapter, the solution strategy for the $(\mathbf{B}, q, \mathbf{u}, p)$ coupled problem is presented. This strategy is based on a segregated scheme. Two versions of the algorithm are available: one for a weak MHD coupling and the other for a strong MHD coupling. Both the magnetic and the fluid problems are addressed in the coupled strategy.

The basic difference between the weak and the strong coupling is the frequency of updating the magnetic field during the fluid computations. It will be seen that high magnetic Reynolds numbers require a frequent and robust updating of the magnetic problem, while for low magnetic Reynolds numbers the updating of the magnetic problem could be done less frequently.

4.2 The Fluid Solver

The fluid problem, which can be described in its strong form by equations (2.70)-(2.71), or in its weak form by the variational statement (3.26), can be put in the following generic form:

$$[K(U)]\{U\} = \{F(U,B)\} \tag{4.2}$$

where $[K(U)]$ is the global matrix, $\{U\}$ is the global nodal variables vector and $F(U,B)$ is the global right-hand-side vector. The non linearities in system (4.2) are due to the convective terms of the governing equations and results in a fluid matrix $[K(U)]$ which depends on the velocity itself. In order to solve such a non linear system, one has to linearize it, say by, Newton's method. Defining the residual vector

$\{R(U,B)\}$ as:

$$\{R(U,B)\} = \{F(U,B)\} - [K(U)]\{U\}, \tag{4.3}$$

Newton's method consists of solving a succession of linear systems obtained from the Taylor series development of the expression of the residual vector $\{R(U,B)\}$ around $\{U^i, B^i\}$, the solution vector at the ith iteration. For a given $\{B^i\}$, the residual vector at the $ith+1st$ iteration is written as:

$$\left\{R(U^{i+1},B^i)\right\} = \left\{R(U^i,B^i)\right\} + \left[\frac{\partial R(U^i,B^i)}{\partial U^i}\right]\left\{\Delta U^{i+1}\right\} + \left[\frac{\partial^2 R(U^i,B^i)}{\partial U^{i^2}}\right]\left\{\Delta^2 U^{i+1}\right\} + \ldots \tag{4.4}$$

If one neglects the second and higher-order terms, then:

$$\left\{R(U^{i+1},B^i)\right\} \simeq \left\{R(U^i,B^i)\right\} + \left[\frac{\partial R(U^i,B^i)}{\partial U^i}\right]\left\{\Delta U^{i+1}\right\} \tag{4.5}$$

One is looking for a solution $\{U^{i+1}\}$ in such a way that the residual is null at the $ith+1st$ iteration. Thus, at each iteration, one has to solve:

$$\left[\frac{\partial R(U^i,B^i)}{\partial U^i}\right]\left\{\Delta U^i\right\} = -\left\{R(U^i,B^i)\right\} \tag{4.6}$$

The matrix $\left[\frac{\partial R(U^i,B^i)}{\partial U^i}\right]$ is called the Jacobian matrix of the residual $\{R(U^i,B^i)\}$ and is denoted by:

$$\left[J(U^i)\right] = \left[\frac{\partial R(U^i,B^i)}{\partial U^i}\right] \tag{4.7}$$

Thus, finding $\{U^{i+1}\}$ is equivalent to computing $\{\Delta U^{i+1}\}$ in such a way that:

$$\left[J(U^i)\right]\left\{\Delta U^{i+1}\right\} = -\left\{R(U^i,B^i)\right\} \tag{4.8}$$

Newton's algorithm reads:

Newton-Raphson Algorithm for Fluid Problem

1- Begin: Choose an initial solution $\{U^0\}$ and a convergence criterion ϵ

2- Newton iteration: For i=0, 1,...., nNewton

- 2.1. Solve

$$\left[J(U^i)\right]\left\{\Delta U^{i+1}\right\} = -\left\{R(U^i,B^i)\right\}$$

- 2.2. Update the Solution:

$$\left\{U^{i+1}\right\} = \left\{U^{i}\right\} + \left\{\Delta U^{i+1}\right\}$$

- 2.3. Convergence Test: If $|| \{\Delta U^{i+1}\} ||_2 \leq \epsilon$ Then Stop

3- End of Newton iterations

4- End

Remark 1: A drawback of the Newton method is the computation of the Jacobian matrix at each Newton iteration. Updating the matrix is expensive in terms of the computation and storage. In order to reduce such requirements, one needs a less expensive resoiution method.

Remark 2: Iterative solvers are known not to require an exact computation of the matrix. Rather, they only require exact computations of the residual vector (the right-hand-side). Hence, an iterative solver seems to be a viable method for the solution of the fluid problem.

4.2.1 GMRES Method

Among iterative methods, Krylov-based methods are known to require only the computation of matrix-vector products and thus are appealing since the decomposition of the Jacobian matrix is avoided. For an overview of Krylov-based methods, one can consult Dutto [47]. Among Krylov-based methods, the GMRES method developed by Saad [48] has been applied successfully to non-symmetric matrices.

Let us, for simplicity of notation, rewrite the linear system to be solved at the *ith* Newton iteration as:

$$[A]\{x\} = \{b\}. \tag{4.9}$$

The GMRES method consists, then, of finding an approximate solution of $\{x\}$ which is a vector of K_m, the Krylov subspace of dimension m associated with $\{b\}$ (the initial residual vector) and the matrix $[A]$:

$$K_m = span\left\{\{b\}, [A]\{b\}, ..., [A]^{m-1}\{b\}\right\} \tag{4.10}$$

The approximate solution $\{x\}^m$ is constructed such that:

$$|| \{b\} - [A]\{x\}^m ||_2 = \min_{x \in K_m} || \{b\} - [A]\{x\}^m ||_2 \tag{4.11}$$

Remark 3 It can be shown that if the dimension of the Krylov sub-space m is chosen to be N, the dimension of the Jacobian matrix, then, neglecting the round-off errors, the approximate solution obtained by the GMRES method is the exact solution ([48]). In this case, the GMRES method becomes essentially a direct method. However, it is clear that $m = N$ makes the method too expensive. In practice, $m \ll N$ so the computation requirements remain reasonable.

Remark 4 In the non-linear version of GMRES, the matrix-vector products, required for the computation of the $m-1$ basis vectors of the Krylov sub-space, are performed through the following difference-like expression:

$$[A] \cdot v = \frac{\{R(U^i + \epsilon v, B^i)\} - \{R(U^i, B^i)\}}{\epsilon} \tag{4.12}$$

As with any finite difference scheme, the above product is subject to a truncation error. In the case of (4.12), the truncation error is of order $O(\epsilon)$, stressing the need for the coefficient ϵ to be carefully chosen in such a way to insure both a good approximation of the directional derivative and the numerical stability of the method. Brown [49] gives the necessary conditions on ϵ for a local convergence of the Newton method. In the present work, ϵ is given by the following expression:

$$\epsilon = \epsilon_0 \left(|| \left\{ R(U^i, B^i) \right\} ||_2 + \epsilon_0 \right) \tag{4.13}$$

where ϵ_0 is set to 10^{-6}.

Starting with an initial solution $\{x_0\}$, the non-linear GMRES algorithm reads:

Non-Linear GMRES Algorithm:

1. Set *eps*. Compute $r_0 = b - Ax_0$, $\beta = ||r_0||_2$, $v_1 = r_0/\beta$
2. Define the $(m+1) \times m$ matrix $\overline{H}_m = \{h_{i,j}\}_{1 \le i \le m+1, 1 \le j \le m}$.
   Set $\overline{H}_m = 0$.
3. For $j = 1, 2, ..., m$ Do:

4. Compute $w_j = [F(x_0 + eps * w_j) - F(x_0)]/eps$
5. For $i = 1, ..., j$ Do:
6. $h_{ij} = (w_j, v_i)$
7. $w_j = w_j - h_{ij} v_i$
8. EndDo
9. $h_{j+1,j} = ||w_j||_2$. If $h_{j+1,j} = 0$ set $m = j$, goto 12
10. $v_{j+1} = w_j / h_{j+1,j}$
11. EndDo
12. Compute y_m the minimizer of $||\beta e_1 - \overline{H}_m y||_2$ and $x_m = x_0 + V_m y_m$.
13. If satisfied Stop, else set $x_0 = x_m$ goto 1.

Remark 5: It is possible to adjust *eps* at each iteration. For example, one can set $eps = eps_{mach}/||w_j||$ for each j, where eps_{mach} is the square root of the machine zero. However, one should be cautious regarding the influence of this choice on the convergence. Some numerical tests performed during this thesis have proven that setting ϵ to a constant makes the GMRES algorithm convergence much better than updating ϵ at each GMRES iteration.

4.3 Preconditioning of Linear Systems

While solving system (4.9), and like any other iterative method, the convergence of the non-linear GMRES method to the solution $\{x\}$ is known to depend, among other factors, on the spectral properties of the matrix $[A]$ (Saad [50]). In order to enhance the desired spectral properties of the matrix $[A]$, it is classical to introduce a preconditioning non-singular matrix $[M]$ and to solve the alternative system:

$$[M]^{-1}[A]x = [M]^{-1}b \tag{4.14}$$

By introducing this equivalent system, one hopes that the spectral properties of the new matrix $[M]^{-1}[A]$ will favor the convergence of the iterative method. A good preconditioning for the GMRES method should have the two following properties:

1. GMRES-like methods require, for a good convergence, that the eigenvalues be located in the smallest portion of the complex plane ([50]). Observing that the identity matrix $[I]$ presents the particularity of having all unit eigenvalues (all located in the same point); Constructing a preconditioning matrix that most closely approximates the original matrix $[A]$ should make the matrix product $[M]^{-1}[A]$ a good approximation of the identity matrix $[I]$. It is obvious that the more this property is satisfied, the more effective the preconditioner is. In the limit when $[M] = [A]$, the product matrix $[M]^{-1}[A]$ is equal to the identity matrix and one has the best possible preconditioner. However, the closer $[M]$ approximates $[A]$, the greater the computational requirements are.

2. The matrix $[M]$ should be easily "invertible", meaning that the system

$$[M]\{x\} = \{y\} \tag{4.15}$$

makes it easy to find:

$$\{x\} = [M]^{-1}\{y\} \tag{4.16}$$

It is obvious that the more this property is satisfied, the easier system (4.14) is solved with lower computational costs.

A good preconditioning matrix is thus a compromise between the above two contradictory properties.

As an extension to system (4.14), the system of equations is recast as:

$$[M_1]^{-1}[A][M_2]^{-1}[M_2]\{x\} = [M_1]^{-1}\{b\} \tag{4.17}$$

If $[M_1] = [I]$, the system is said to be right preconditioned and, if $[M_2] = [I]$, then it is left preconditioned. The right preconditioning form is mostly used in the literature mainly because the residual $\{b\}$ is the same for both the original system (4.9) and the preconditioned one (4.17). This property of right preconditioning thus allows a direct measure of the quality of the preconditioning and is most appropriate to study the influence of different preconditioning matrices on the convergence and the convergence rate.

4.3.1 Different Types of Right Preconditioning

A basic preconditioning that has been used is to choose $[M]$ as a diagonal matrix:

$$[M] = [D], \ d_{ii} = a_{ii} \text{ and } d_{ij} = 0, \ i \neq j \tag{4.18}$$

with d_{ij} and a_{ij} being, respectively, the coefficients of the matrices $[D]$ and $[A]$. This preconditioning has been applied successfully to the GMRES method (See reference [64]).

However, the diagonal preconditioning is not sufficiently robust in all cases. The work of Meijernick and Van Der Vorst [51], opened the way for the development of a new family of preconditionings which basically consist on an incomplete LU factorization of the matrix $[A]$, which is written as:

$$[M] = [L][U] = [A] + [E] \tag{4.19}$$

One can distinguish two classes of incomplete LU factorization preconditionings ([47]):

1. The zero-nonzero structure of $[L] + [U]$ is the same as the original matrix $[A]$, i.e., m_{ij} is a nonzero coefficient of $[L] + [U]$ if and only if a_{ij} itself is nonzero.

2. A certain amount of fill-in is allowed to take place in the structure of $[L] + [U]$. In the limit of large fill-in amount, $[M]$ becomes a complete LU factorization of $[A]$.

Among commonly used right preconditionings, ILU(0) is a representative of the first class ([50], [51]). More recently, Saad [52] developed the very promising ILUT method. The preconditioning matrix is obtained by constructing $[L]$ and $[U]$ subject to the restriction that for each row of both triangular matrices, only a controlled amount $lfil$ of non-zero coefficients are allowed in $[L]$ and $[U]$ during the Gauss elimination. Furthermore, coefficients of the matrix deemed to bring an insignificant contribution to the incomplete decomposition are dropped. Thus, two values characterize the ILUT method: an integer one, $lfil$, for the number of non-zero coefficients per row and a real one, tol, which is a criterion to measure the influence of a coefficient on the incomplete LU decomposition. Both $lfil$ and tol are to be set by the user.

For this thesis, the GMRES method has been associated with the ILUT($lfil, tol$) preconditioning for the solution of the fluid problem. The resulting non-linear right preconditioned GMRES/ILUT algorithm is written in the following form:

Non-Linear GMRES/ILUT Algorithm:

1. Set eps. Compute $r_0 = b - Ax_0$, $\beta = ||r_0||_2$, $v_1 = r_0/\beta$
2. Define the $(m+1) \times m$ matrix $\overline{H}_m = \{h_{i,j}\}_{1 \leq i \leq m+1, 1 \leq j \leq m}$.
   Set $\overline{H}_m = 0$.
3. For $j = 1, 2, ..., m$ Do:
4. Compute $w_j = M^{-1} v_j$
5. Compute $w_j = [F(x_0 + eps * w_j) - F(x_0)]/eps$
6. For $i = 1, ..., j$ Do:
7. $h_{ij} = (w_j, v_i)$
8. $w_j = w_j - h_{ij} v_i$
9. EndDo
10. $h_{j+1,j} = ||w_j||_2$. If $h_{j+1,j} = 0$ set $m = j$, goto 12
11. $v_{j+1} = w_j / h_{j+1,j}$
12. EndDo
13. Compute y_m the minimizer of $||\beta e_1 - \overline{H}_m y||_2$ and
    $x_m = x_0 + V_m y_m$.
14. If satisfied Stop, else set $x_0 = x_m$ goto 1.

4.4 The Magnetic Solver

Both the conservative formulation $(\mathbf{B}, q)$ and the vector potential formulation $(\mathbf{A}, \phi)$ (or the reduced vector potential $\hat{\mathbf{A}}$ formulation) give rise to a system of N equations which reads in the generic following form as:

$$[K'(U)] \ \{B\} = \{F'(B, U)\} \tag{4.20}$$

where $[K'(U)]$, $\{F'(B,U)\}$ and $\{B\}$ are, respectively, the global matrix, the global right-hand-side vector and the global nodal variables.

System (4.20) is linear, since the coefficients of the matrix $[K'(U)]$ do not depend on $(\mathbf{B}, q)$ (on $(\mathbf{A}, \phi)$ or on $\hat{\mathbf{A}}$); Indeed, they depend only on the velocity vector $\mathbf{u}$,

which, in this case, is a given data. For relatively large problems, it is preferable to use an iterative solver such as a linear GMRES solver. However, for our academic purposes and since the system is linear, a direct solver, based on the well-known Gauss elimination, is still a reasonable strategy for the resolution of system (4.20). The Gauss elimination proceeds by decomposing the matrix $[K'(U)]$ into two matrices (Dhatt and Touzot [53]):

$$[K'(U)] = [L]\ [U] \tag{4.21}$$

where $[L]$ is a lower triangular matrix with unity terms on its diagonal and $[U]$ is an upper triangular matrix obtained through the Gauss elimination process.

4.5 The Coupling Strategy

The fully-coupled problem which is described in its strong form by equations (2.70)-(2.73), or in its weak form by the variational statements (3.10), (3.11), and (3.26), can be recast as:

$$[K(U)]\{U\} = \{F(U,B)\} \tag{4.22}$$

and

$$[K'(U)]\{B\} = \{F'(B,U)\} \tag{4.23}$$

In equation (4.22), $[K(U)]$ is the global matrix, $\{U\}$ is the global nodal variables vector and $F(U,B)$ is the global right-hand-side vector, corresponding to the fluid problem. In (4.23), $[K'(U)]$ is the global matrix, $\{B\}$ is the global nodal variables vector and $F'(B,U)$ is the global right-hand-side vector, corresponding to magnetic problem.

4.5.1 Simultaneous Solution of the Coupled Problem

In order to approach the solution of (4.22) and (4.23), one can consider the simultaneous solution of these two systems. "Simultaneous", means the solution of both problems at the same time within the same global system:

$$[K_g(U,B)]\left\{\begin{array}{c} U \\ B \end{array}\right\} = \{F_g(U,B)\} \tag{4.24}$$

where $[K_g(U,B)]$ is the global matrix, $\{U,B\}^T$ is the simultaneous global nodal variables vector and $\{F_g(U,B)\}$ is the global right-hand-side vector, corresponding to the coupled problem.

Problem (4.24) is non-linear both in $\{U\}$ and $\{B\}$. The non-linearities are due to the presence of the advective terms within both the Navier-Stokes equations and the magnetic induction equation. These terms, depending on both the Reynolds number Re and the magnetic Reynolds number Re_m, could prove very strong, making the non-linearities very important. The solution of such systems requires an iterative method since the matrix $[K_g(U,B)]$ depends on the solution $\{U,B\}^T$ itself. Again a Newton-Raphson method could be used in order to linearize such a system and to solve it iteratively. If an initial guess is adequate within a certain *convergence radius*, then the convergence of the Newton algorithm is at least super-linear. While the simultaneous solution of the equations is the most robust technique, especially when associated with a Newton's-like algorithm, it is, however, the most expensive computationally especially for relatively large problems. At the elementary level, the matrix $[K_g]$ is an 32 by 32 square matrix, thus leading to a huge global system. Furthermore a Newton's method requires the re-computation of the matrix at each iteration. So the simultaneous method is not satisfactory from the point of view of efficiency, especially for 3D problems.

4.5.2 Segregated Methods

As an alternative to the simultaneous solution approach, one can use a segregated scheme. Two remarks hint for the justification of such approach.

- First, one can observe that for a given flow field (flow field means the three components of the velocity and the pressure), the magnetic field (the three components of the magnetic field and the scalar q) can be obtained directly without any other interference. The same thing can be said for the magnetic field.

- The second remark refers to the discussion in subsection (2.7.1). Actually, for MHD at the human level, we have underlined that the magnetic Reynolds number is small. The term small is relative and it does not in all cases exclude the existence of regions where "local" magnetic Reynolds numbers are more important. As seen in subsection (2.7.1), such moderate magnetic Reynolds numbers mean a moderate influence of the velocity field on the magnetic one. It suggests again for the use of a segregated method.

Segregated methods consist of a sequence of solutions of the two problems. The process is stopped when a certain convergence criterion is achieved during the iterative process. For time-dependent problems, coupling iterations are actually time steps and convergence is achieved when steady-state solution is obtained. In order to introduce the segregated algorithm, notice that solving systems (4.22) and (4.23) at each time step is equivalent to solving:

$$[K(U)]\left\{\Delta U^{i}\right\} = -\left\{R(U^{i-1}, B^{i-1})\right\} \tag{4.25}$$

$$[K'(U)]\left\{\Delta B^{i}\right\} = -\left\{R'(B^{i-1}, U^{i-1})\right\} \tag{4.26}$$

where, the residual vector of the fluid problem $\{R(U^{i-1}, B^{i-1})\}$ and the residual vector of the magnetic problem $\{R'(B^{i-1}, U^{i-1})\}$ are obtained by:

$$\left\{R(U^{i-1}, B^{i-1})\right\} = \{F(U, B)\} - [K(U)]\left\{U^{i-1}\right\} \tag{4.27}$$

$$\left\{R'(B^{i-1}, U^{i-1})\right\} = \{F(B, U)\} - [K'(U)]\left\{B^{i-1}\right\} \tag{4.28}$$

The generic form of the segregated algorithm could, then, be presented as:

Algorithm 1:Generic Form of the Segregated Algorithm

1- Choose initial solutions $\{U^0\}$ and $\{B^0\}$ and convergence criterion ϵ

2- Time Steps: For i=1,2,...,nsteps

-2.1. Solve the Magnetic Problem:

$$[K'(U^m)]\left\{\Delta B^i\right\} = -\left\{R'(B^{i-1}, U^{i-1})\right\}$$

-2.2. Update the Magnetic solution:

$$\left\{B^i\right\} = \left\{B^{i-1}\right\} + \left\{\Delta B^i\right\}$$

-2.3. Solve the Fluid Problem:

$$\left[K(U^i)\right]\left\{\Delta U^i\right\} = -\left\{R(U^{i-1}, B^n)\right\}$$

-2.4. Update the Fluid Solution:

$$\left\{U^i\right\} = \left\{U^{i-1}\right\} + \left\{\Delta U^i\right\}$$

-2.5. If $|| \{R(U^i, B^n)\} ||_2 \leq \epsilon$ Stop

3- End of Time Steps

4- End

Remark 6 In Algorithm (1), $\{U^m\}$ and $\{B^n\}$ are respectively the fluid and the magnetic solutions at certain previous *mth* and *nth* iterations.

Remark 7 This segregated algorithm is very interesting since the two, fluid and magnetic, problems are decoupled in the algorithmic sense while physically the effect of each of the fields on the other is still accounted for. Hence, by separately solving each of the problems, one can choose methods that are adapted to each type. Eventually, this permits the updating of each of the solvers in an independent fashion.

Remark 8 The convergence test is set for the fluid problem, since between the two problems the latter is more difficult to converge. As seen in section (4.4), the magnetic problem is solved with a direct solver, hence making the control of the convergence of the coupled problem an easy task.

4.5.3 The Simplest Segregated Algorithm

Since Algorithm (1) is a segregated one, then $m < i$ and $n \leq i$. Letting m take different values among $0, 1, ..., i$ and n take different values among $0, 1, 2, ..., i-1$, leads to a whole family of explicit schemes. For instance, setting $m = i - 1$ and $n = i$ gives the simplest segregated algorithm. "Simplest" means the most obvious algorithm, in the algorithmic sense. In such case, Algorithm (1) becomes:

Algorithm 2:Classical Segregated Algorithm

1- Choose initial solutions $\{U^0\}$ and $\{B^0\}$ and convergence criterion ϵ

2- Time Steps: For i=1,2,...,nsteps

-2.1. Solve the Magnetic Problem:

$$\left[K'(U^{i-1})\right]\left\{\Delta B^i\right\} = -\left\{R'(B^{i-1}, U^{i-1})\right\}$$

-2.2. Update the Magnetic solution:

$$\left\{B^i\right\} = \left\{B^{i-1}\right\} + \left\{\Delta B^i\right\}$$

-2.3. Solve the Fluid Problem:

$$\left[K(U^i)\right]\left\{\Delta U^i\right\} = -\left\{R(U^{i-1}, B^i)\right\}$$

-2.4. Update the Fluid Solution:

$$\left\{U^i\right\} = \left\{U^{i-1}\right\} + \left\{\Delta U^i\right\}$$

-2.5. Convergence Test: If $|| \{R(U^i, B^i)\} ||_2 \leq \epsilon$ Stop

3- End of Time Steps

4- End

Steps (2.1) and (2.2) in the algorithm (2), consist of solving and updating the magnetic solution. It was already seen that the direct solver chosen for the solution of the magnetic problem is still an acceptable strategy for our academic purposes and when the magnetic problem is decoupled from the fluid one. However, when the fluid and the magnetic problems are coupled, this strategy is no longer practical because

it would involve the complete LU decomposition of the magnetic matrix at each time step of the segregated algorithm. One should then look for another strategy which would imply on one hand, reasonable computational requirements and robustness of algorithm, on the other hand.

One way to satisfy these two requirements is to make m take other values than $i-1$. This amounts to freezing the magnetic matrix $[K'(U^m)]$ for a certain number l of time steps. This, however, lags the magnetic matrix behind the residual magnetic vector, thus, requiring the implementation of an inner iteration for the magnetic problem. This inner iteration could be seen as a fixed-point method or as a Modified Newton method for the linear magnetic problem. In such case, the segregated algorithm (2) becomes:

Algorithm 3:Segregated Algorithm with Inner Magnetic Iterations

1- Choose initial solutions $\{U^0\}$ and $\{B^0\}$ and convergence criterion ϵ

2- Compute the LU decomposition of the matrix $[K'(U^0)] = [L][U]$

3- Time Steps: For i=1,2,...,nsteps

-3.1. If $(i.mod.m) = 0$ and $m \neq 0$ compute $[L][U] = [K'(U^i)]$

-3.2. Set $\left\{B_0^{i-1}\right\} = \{B^{i-1}\}$

-3.3. Inner Magnetic Iterations: For j=1,...,niter

-3.3.1. Solve The Magnetic Problem:

$$[L][U]\left\{\Delta B_j^{i-1}\right\} = -\left\{R'(B_{j-1}^{i-1}, U^{i-1})\right\}$$

-3.3.2. Update The Inner magnetic Solution:

$$\left\{B_j^{i-1}\right\} = \left\{B_{j-1}^{i-1}\right\} + \left\{\Delta B_j^{i-1}\right\}$$

-3.3.3. If $|| \left\{R'(B_j^{i-1}, U^{i-1})\right\} ||_2 \leq \epsilon$ Stop

-3.4. End of Magnetic Iterations

-3.5. Update The Magnetic Field:

$$\left\{B^i\right\} = \left\{B_j^{i-1}\right\}$$

-3.6. Solve the Fluid Problem:

$$\left[K(U^i)\right]\left\{\Delta U^i\right\} = -\left\{R(U^{i-1}, B^i)\right\}$$

-3.7. Update the Fluid Solution:

$$\left\{U^i\right\} = \left\{U^{i-1}\right\} + \left\{\Delta U^i\right\}$$

-3.8. Convergence Test: If $|| \{R(U^i, B^i)\} ||_2 \leq \epsilon$

4- End of Time Steps

5- End

In algorithm (3), the updating of the magnetic matrix takes place only when needed. This property is highly desired in order to take into account both low and high magnetic Reynolds numbers Re_m. Actually and as discussed in section (2.7), when diffusion is the dominant mechanism by which the magnetic field is transported, a certain decoupling exists between the magnetic field and the fluid one. Setting $m = 0$ is sufficient for the convergence of the segregated algorithm while resulting in a once and for all decomposition of the magnetic matrix.

However, when the magnetic Reynolds number Re_m is high, the magnetic matrix must be updated more frequently. Actually, in such cases, the magnetic field is frozen in the velocity field (in the physical sense), and any change in the fluid field is immediately captured by the magnetic field. Thus freezing the magnetic matrix (with the initial velocity field) would certainly result in the divergence of the algorithm. Hence, m can no longer be set to zero. The choice of m, as an updating criterion, depends on the magnetic Reynolds number Re_m. The higher the magnetic Reynolds is, the more frequent the necessary updating of the matrix is required.

Remark 9: Algorithm (3), described above could be seen as a compromise between and as a mixture of, the modified Newton method where the matrix is decomposed once and for all, and a substitution (or Picard's) method where the matrix is updated at each iteration.

4.5.4 Tighter Segregated Algorithms

In algorithm (2) and (3), the index n has been set to i giving rise to classical segregated schemes. If tighter coupling is required between the magnetic and the fluid problems, one could relate n to inner iterations of the fluid problem (Newton or GMRES iterations), rather than to time steps outer iterations. For instance, if the updating of the magnetic solution is required at each Newton iteration, the resulting algorithm becomes:

Algorithm 4:

1- Choose Initial Solution $\{U^0\}$ and Convergence Criterion ϵ.

2- Solve for the Initial Magnetic Solution with $\{U^0\}$.

3- Time Steps: For i=1,2,...,nsteps

-3.3. Newton Iterations: For j=1,...,nNewton

-3.3.1. Solve the Fluid Problem:

$$\left[J(U^{j-1})\right]\left\{\Delta U^j\right\} = -\left\{R(U^{j-1}, B^{j-1})\right\}$$

-3.3.2. Update the Fluid Solution:

$$\left\{U^j\right\} = \left\{U^{j-1}\right\} + \left\{\Delta U^j\right\}$$

-3.3.3. Solve the Magnetic Problem.

-3.3.4. Update the Magnetic Solution:

$$\left\{B^j\right\} = \left\{B^{j-1}\right\} + \left\{\Delta B^j\right\}$$

-3.4. End of Newton Iterations.

-3.5. Convergence Test: If $|| \{R(U^i, B^i)\} ||_2 \leq \epsilon$ Stop.

4- End of Time Steps.

5- End.

If the magnetic problem is updated for each Krylov iteration during the solution of the fluid problem with the GMRES algorithm, then the algorithm becomes:

Algorithm 5:

1- Choose Initial Solutions $\{U^0\}$ and Convergence Criterion ϵ.

2- Solve for the Initial Magnetic Solution with $\{U^0\}$.

3- Time Steps: For i=1,2,...,nsteps

-3.1. Newton Iterations: For j=1,...,nNewton

-3.1.1. Krylov Iterations: For k=1,...,nKrylov

-3.1.1.1. Compute the *kth* Element of the Krylov Base.

-3.1.1.2. Solve the Magnetic Problem.

-3.1.1.3. Update the Magnetic Solution:

$$\left\{B^k\right\} = \left\{B^{k-1}\right\} + \left\{\Delta B^k\right\}$$

-3.1.2. End of the Krylov Iterations.

-3.2. End of the Newton Iterations.

-3.4. Convergence Test: If $|| \{R(U^i, B^i)\} ||_2 \leq \epsilon$ Stop

4- End of Time Steps.

5- End.

4.5.5 Conclusion

The algorithms, associated with the solution strategies outlined throughout this chapter, have been used to obtain the solutions of different numerical tests. These tests concern both the decoupled magnetic problem (with $(\mathbf{B}, q)$, $(\mathbf{A}, \phi)$ or $\hat{\mathbf{A}}$) and the coupled problem $(\mathbf{B}, q, \mathbf{u}, p)$. The next chapter is dedicated to the presentation of these numerical tests and their results.

Chapter 5

Numerical Results

5.1 Results for the $\mathbf{B}, q$ formulation

For the $\mathbf{B}, q$ formulation, numerical tests have been carried out in two steps. In the first one, the accuracy and the stability of the method have been studied. In particular, the convergence rates of the different methods obtained with the different combinations of the stabilization coefficient τ_1 and of the penalization factor τ_2 are computed. The performance of the conservative formulation, developed in this thesis is compared to that of the "Helmholtz" formulation in both cases of steady state and unsteady solutions.

Once the stability and the accuracy of the conservative formulation have been studied, some benchmark tests are carried out. These tests are well-known in the context of MHD and put into evidence two physical unique characteristics of MHD flows: The Hartmann layer and the Alfven waves. While being simple tests, they illustrate typical industrial configurations. The tests are presented as follows:

- The Hartmann-Poiseuille flow,
- The Hartmann-Poiseuille flow with external electric current,
- The Hartmann-Couette flow,
- The Hartmann-Rayleigh flow.

Finally a three-dimensional test case is shown. This test case illustrates the transition between two extreme situations occurring in the context of MHD flow: the

quasi-diffusion of the magnetic field, where the velocity field plays a negligible role, and the quasi-convection of the magnetic field by the velocity one. In the latter case, the magnetic field is said to be frozen in the velocity field.

5.1.1 Steady Case

In order to assess the stability and the quality of the finite element formulation (3.10)-(3.11), we study this problem in a cubic domain ($0 \leq x \leq 1, 0 \leq y \leq 1, 0 \leq z \leq 1$). The velocity vector is set to $\mathbf{u} = (1, 0, 0)^T$. The Dirichlet boundary conditions and the right-hand-side vector $\mathbf{f} = (2x - 2\eta, -2\eta, 2z)^T$ are imposed in such a way as to reproduce approximately an arbitrary solution of the continuous problem, namely $\mathbf{B} = (x^2, y^2, -2(x+y)z)^T$ and $q = 0$. The dissipation coefficient τ_1 can be given by one or the other of the two following expressions:

$$\tau_1 = \alpha \frac{h^2}{4\eta}, \tag{5.1}$$

$$\tau_1 = \alpha \left(\left(\frac{2||\mathbf{u}||}{h} \right)^2 + \left(\frac{4\eta}{h^2} \right)^2 \right)^{-1/2}. \tag{5.2}$$

The penalization factor τ_2 is set to either:

$$\tau_2 = 0, \tag{5.3}$$

which corresponds to the original physical model, or to:

$$\tau_2 = ||\mathbf{u}||h/2. \tag{5.4}$$

In the latter case, the coefficient $r = \tau_2 - \eta$ ends up to be:

$$r = \eta \left(1 - \frac{Re_{mh}}{2} \right), \tag{5.5}$$

where Re_{mh} is the local magnetic Reynolds number defined by:

$$Re_{mh} = \sigma\mu||\mathbf{u}||h. \tag{5.6}$$

Computations have been made for two different magnetic diffusion coefficients $\eta = 1.2 \times 10^{-1}$ and $\eta = 1.2 \times 10^{-3}$ representing, respectively, a highly diffusive case and a highly convective one, and for $\alpha = 0.1$, $1/3$ and 1.0. For each case, we calculated the mesh variation of the $L_2(\Omega)$-norms of the magnetic field divergence $||\nabla \cdot \mathbf{B}_h||$, the error $||\mathbf{B}_h - \mathbf{B}||$, the Lagrange multiplier $||q_h||$ and its gradient $||\nabla q_h||$.

Comments:

Highly Convective Case: When the magnetic convection is important ($\eta = 1.2 \times 10^{-3}$), the best solutions are obtained with $\tau_2 = ||\mathbf{u}||h/2$ and this is true regardless of the expression used for τ_1. Actually, the methods generated with $\tau_2 = ||\mathbf{u}||h/2$ are much more conservative and accurate than the "Helmholtz" formulation (Figure 5.1) and than the formulation obtained with $\tau_2 = 0$ (Figure 5.2). Results are shown with $\alpha = 0.1$ for the first comparison and with $\alpha = 1.0$ for the second comparison, using τ_1 as defined in Equation (5.2) in both cases. However, the trends are maintained in both cases with other α values and with τ_1 as in Equation (5.1).

However, it should be noticed that when $\tau_2 = ||\mathbf{u}||h/2$, the formulations obtained with τ_1 as given in Equation (5.2), which is of order $O(h)$ when the convection is dominant, gives optimal convergence rates for both $\mathbf{B}_h$ and q_h. In fact, for the Lagrange multiplier q and the magnetic field, convergence error rates are equal to 2. For the gradient of q_h and the divergence of $\mathbf{B}_h$, the rates are around unity (Figure 5.3). These rates are independent of the value assigned to α (Figure 5.4).

When τ_1 is expressed by Equation (5.1), which in the convective dominant case is of order $O(h^2)$, the convergence rates are still optimal for the magnetic induction field and for its divergence, while for the scalar q and its gradient the rates become sub-optimal. For q_h, the rate is around 1 and the gradient of q_h seems to be bounded by a constant (Figure 5.5). Figure (5.6) shows these convergence rates for $\alpha = 1/3$ and $\alpha = 1.0$. In contrast, the method generated by Equation (5.2) gives rise to better accuracy and magnetic conservation than the method generated by Equation (5.1). Overall, the two methods do not seem to be very sensitive to the value of the constant α, so $\alpha = 0.1$ seems a suitable value to be assigned for both methods.

If $\tau_2 = 0$ (Figure 5.7) and the convection is still dominant then the accuracy of the method is very poor and the error norms are very important especially when Equation (5.1) is used for τ_1. Moreover, and regardless of the expression used for τ_1, the method is very sensitive to the value of the constant α, showing signs of instabilities due to the effect of the convection. No general trend for the convergence rates could be drawn.

Thus, one should avoid using such a method.

Highly Diffusive Case When the diffusion is dominant ($\eta = 1.2 \times 10^{-1}$), then all the methods obtained by the different expressions for τ_1 and τ_2 are accurate, convergent and stable. When $\tau_2 = 0$, both expressions arising from Equations (5.1) and (5.2) for τ_1 give approximately the same results in terms of the magnetic field error and the magnetic divergence. This can be explained by the fact that since the magnetic diffusion is dominant, Equations (5.1) and (5.2) lead both to expressions of $O(h^2)$.

The convergence rates obtained for the two expressions for τ_1 are the same. We obtain convergence rates of 1 for the magnetic field divergence and for the scalar q. The convergence rate for the magnetic induction is of order 2 and the gradient of q is bounded by a constant (Figure 5.8). As expected, the linear interpolation on tetrahedral elements keeps the optimal convergence rates for the magnetic induction and its gradient, while q and its gradient converge at sub-optimal rates.

When $\tau_2 = ||\mathbf{u}||h/2$, we obtain the best results in terms of the error on $\mathbf{B}_h$ and on its divergence. However, the differences between these results and those obtained with $\tau_2 = 0$ are not very important. Again, the convergence rates are those expected: optimal for the magnetic field and sub-optimal for the scalar q (Figure 5.9). Once again, the results obtained are quite independent of τ_1 and of the constant α.

5.1.2 Unsteady Case

In order to highlight the advantages of using the conservative stable formulation (3.10)-(3.11) rather than a formulation derived from the "Helmholtz" formulation, one should look at the behavior of the solutions obtained with the two methods, for an unsteady problem, and compare them in terms of the norm of the divergence of the magnetic field. In the same manner as in section (5.1.1), the velocity vector $\mathbf{u} = (1, 0, 0)^T$, the right-hand-side vector $\mathbf{f} = (2x - 2\eta + 1, -2\eta, 2z)^T$ and the Dirichlet boundary conditions are imposed in such a way as to reproduce approximately an arbitrary unsteady solution of the continuous problem $\mathbf{B} = (x^2 + t, y^2, -2(x + y)z)^T$

and $q = 0$. Computations have been made with the following coefficients: $\tau_1 = 1.0h^2/4\eta$, $\tau_2 = ||\mathbf{u}||h/2\ \eta = 1.2 \times 10^{-1}$ and $\Delta t = 0.1$ and starting from a zero initial solution.

Figure (5.10) shows the evolution of the divergence of the magnetic field as a function of time. In the top figure, the solutions during the first 50 time steps are highlighted, while in the bottom part, the solutions are shown over 1000 time steps. It is seen that the conservative formulation performs much better than the "Helmholtz" formulation. The magnetic divergence reaches an "optimal" value after 50 time steps, then keeps on that same divergence, which is non-zero as a result of the linear interpolation of a quadratic function. With the "Helmholtz" formulation, the divergence first increases then is reduced to a constant plateau that is approximatively five times higher than the one obtained with the conservative formulation.

5.1.3 The Hartmann-Poiseuille Flow

The Hartmann flow is one of the cornerstone examples of MHD flows (Moreau [54]). The validation of any MHD code should use this flow as a benchmark test. The Hartmann-Poiseuille problem consists of a liquid metal flowing under the influence of a pressure gradient, in the x-direction, through a rectangular cross section duct infinitely long in the z-direction. A uniform external magnetic field $\mathbf{B_0}$ is applied along the y-direction (Figure 5.11). The liquid flow induces a perturbation of the imposed magnetic field $\mathbf{B_0}$, that is in the same x-direction as the flow. Assuming that the walls are at $y = \pm h$ and are perfectly insulating, using the non-slip boundary conditions for the velocity and imposing the perturbation of the magnetic field to be zero at these walls, the problem has an analytical solution for the velocity and the magnetic field, that can be put in the following form([54]):

$$u_x = -\frac{\rho G Ha}{\sigma B_0^2}\left(\frac{\cosh(Ha) - \cosh(yHa/h)}{\sinh(Ha)}\right) \tag{5.7}$$

$$B_x = -\frac{B_0 Re_m}{Ha}\left(\frac{\sinh(yHa/h) - (y/h)\sinh(Ha)}{\cosh(Ha) - 1}\right) \tag{5.8}$$

where B_x and u_x are, respectively, the x components of the magnetic and the velocity fields, ρG the pressure gradient keeping the fluid in motion (ρ being the density)

and Re_m and Ha are the magnetic Reynolds number and the Hartmann number, respectively, defined as:

$$Re_m = \sigma \mu u h \tag{5.9}$$

$$Ha = B_0 h \left(\frac{\sigma}{\rho \nu} \right)^{1/2} \tag{5.10}$$

The square of the Hartmann number is the ratio between the electromagnetic forces and the viscous forces. In Equation (5.9), u is the velocity u_x at $y = 0$ and in Equation (5.10) ν is the kinematic viscosity of the liquid metal.

The Hartmann flow, with the velocity field given as input data, has been computed for the following physical parameters: $\sigma = 7.14 \times 10^5 (\Omega \cdot m)^{-1}$, $\eta = 1.2 \times 10^{-1} m^2 \cdot s^{-1}$, $\rho\nu = 1.5 \times 10^{-4} Kg \cdot m^{-1} \cdot s^{-1}$, $\rho G = 4.85 \times 10^{-5} Pa \cdot m^{-1}$, $h = 0.5m$, $B_0 = 1.4494 \times 10^{-4} Tesla$ ([19]). The unstructured nearly uniform mesh consists of 4446 elements and 1600 nodes. We compare the results for B_x obtained from the analytical solution with the results from the numerical computations. The agreement between the two is quite good (Figure 5.12). Then, a parametric study is made using the Hartmann number as a parameter ($Ha = 1, 2, 5, 10, 20$) (Figure 5.12). This parametric study shows a very good agreement with the analytical solution. Furthermore, this study puts into evidence the building of the Hartmann layer.

Figure (5.13) shows the analytical solution for the velocity ($Ha = 1, 2, 5, 10, 20$). It is seen that the intensity of the applied transversal magnetic field influences the velocity field. From a Poiseuille profile when the magnetic field is zero ($Ha = 0$), the velocity profile is flattened and becomes nearly constant in the core region of the duct, with the gradient of the velocity concentrated in two boundary layers (Hartmann layer) near the walls, when the magnetic field is strong ($Ha \gg 1$). The flattening of the velocity profile is due to the magnetic braking of the flow. In Figure (5.12), one can see the magnetic signature of this boundary layer. As the Hartmann number is increased from 1 to 20, one can see a boundary layer type behavior developing for the induced magnetic field. This behavior can be put into evidence because the walls are perfectly insulating which allows the use of the Dirichlet conditions for the

magnetic field. If the walls were perfectly conducting, then the boundary conditions should be set to the Neumann type conditions and hence the magnetic signature of the Hartmann layer would disappear.

5.1.4 Circuit with an External Electric Current

For the Hartmann-Poiseuille problem described in the previous section, analytical considerations show that the only non-zero component of the electric current density, j_z is given by([54]):

$$\frac{j_z}{\sigma B_0 V} = \frac{E}{B_0 V} + 1 - \frac{\cosh(\frac{y\,Ha}{h})}{\cosh Ha} \tag{5.11}$$

and that the electric current mean value, J, becomes:

$$J = \frac{1}{2h}\int_{-h}^{h} j_z\, dy = \sigma B_0 U + \sigma E \tag{5.12}$$

where:

$$U = \frac{1}{2h}\int_{-h}^{h} u\, dy = V\left(1 - \frac{\tanh(Ha)}{Ha}\right) \tag{5.13}$$

$$V = \frac{\rho G}{\sigma {B_0}^2} - \frac{E}{B_0} \tag{5.14}$$

$$E = \frac{\rho G}{\sigma B_0}\left(1 - \frac{Ha}{\tanh Ha}\right) \tag{5.15}$$

Suppose, now, that the channel extent in the z direction is not anymore infinite but has a length L. Consider, however, that it is still long enough that no variations occur in that direction. Suppose also that the walls in the z direction are carrying an electric current I provided by an external source (Figure 5.14); then, if $I \neq 0$, the operation of the duct could be interpreted in terms of energy conversion (Figure 5.15). Actually, when $0 < I < 2hL\rho G/B_0$, the system is a generator of electric current. A part of its mechanical energy is converted into electrical power supplied to the external circuit. When $I < 0$, the system operates as an electromagnetic pump. When $I > 2hL\rho G/B_0$, it operates as an electromagnetic brake under the influence of the Lorentz forces and, when these forces are strong enough, they can reverse the direction of the flow. With $I \neq 0$, analytical solutions (Moreau [54])) are written as

follows:

$$\frac{u_x}{V} = 1 - \frac{\cosh(Hay/h)}{\cosh Ha} \tag{5.16}$$

$$\frac{B_x}{Re_m B_0} = \frac{1}{Ha}\frac{\sinh(Hay/h)}{\cosh Ha} - \left(1 + \frac{E}{B_0 V}\right) \tag{5.17}$$

with E and V being in this case:

$$E = \left(-\frac{\rho G}{\sigma B_0}\left(1 - \frac{\tanh Ha}{Ha}\right) + \frac{I}{2\sigma Lh}\right)\frac{Ha}{\tanh Ha} \tag{5.18}$$

$$V = \left(\frac{\rho G}{\sigma {B_0}^2} - \frac{I}{2\sigma B_0 Lh}\right)\frac{Ha}{\tanh Ha} \tag{5.19}$$

Numerical solutions have been computed for $I = 450A$, $I = 50A$ and $I = -100A$ for $Ha = 2$ and $Ha = 10$. The mesh is the same one used in the Hartmann-Poiseuille flow test case. The computed solutions show good agreement with the analytical ones (Figure (5.16)). Figure (5.17) shows, for $Ha = 10$ and $Ha = 2$, the analytical solution of the $x-$ component of the velocity field. The possibility of flow reversal is illustrated in the case when $I > 2hL\rho G/B_0$.

5.1.5 The Hartmann-Couette Flow

The Hartmann-Couette flow is the MHD counterpart of the known hydrodynamic Couette flow and it is studied using the same geometry as the Hartmann-Poiseuille flow, with the difference that the walls are no longer at $y = \pm h$, but rather at $y = 0$ and $y = h$ (Figure (5.18)). Moreover, in this case no driving pressure gradient is applied; the imposed sliding movement U_0 of the wall $y = h$, in the direction perpendicular to the applied magnetic field $\mathbf{B_0}$, drives the flow between the two walls. The flow velocity analytical solution is written as([54]):

$$u = U_0\frac{\sinh(Hay/h)}{\sinh Ha} + \frac{E}{B_0}R_1 \tag{5.20}$$

where R_1 is given by the expression:

$$R_1 = \left(\frac{\sinh(Hay/h)}{\sinh Ha}(1 - \cosh Ha) + \cosh(Hay/h) - 1\right) \tag{5.21}$$

This velocity field induces a magnetic perturbation B_x, which analytical expression is:

$$B_x = B_0 \frac{Re_m}{Ha} \frac{\cosh(Hay/h)}{\sinh Ha} - \frac{\mu\sigma E h}{Ha} R_2 \tag{5.22}$$

where R_2 is:

$$R_2 = \left(\frac{\cosh(Hay/h)}{\sinh Ha}(1 - \cosh Ha) + \sinh(Hay/h) \right) \tag{5.23}$$

These solutions satisfy the hydrodynamic boundary condition of no-slip velocity at walls $u(y = 0) = 0$ and $u(y = h) = U_0$. It can be shown that the mean value of the electric density is given by:

$$J = \frac{1}{h} \int_h j_z dy = \sigma B_0 U_0 \left(1 + \frac{2\,E}{B_0 U_0} \right) \frac{1 - coshHa}{sinhHa} \tag{5.24}$$

Since the boundaries are insulating, the electric current has to close up in the fluid which means that the mean value J is null. The expression of J requires, then, that:

$$E = -B_0 U_0 / 2 \tag{5.25}$$

The magnetic aspects of the Hartmann-Couette flow, with the velocity field given as an input data, have been computed for the same physical parameters and with same mesh as for the Hartmann-Poiseuille problem (See Section 5.1.3). The boundary conditions are imposed on the walls through the exact solution (5.22). Results have been obtained for different Hartmann numbers ($Ha = 2, 5, 10$) and have been compared with the corresponding analytical solution obtained by equations (5.20) and (5.22). The comparison (Figure 5.19) shows good agreement between the computed and the analytical induced magnetic field.

5.1.6 The MHD Rayleigh Flow

Suppose an infinite plane plate is at rest in a semi-infinite domain which is electrically conducting. Let B_0 be an applied magnetic field along y, the coordinate normal to the plate. Suppose the plate is suddenly set into motion at $t = 0$, with a constant velocity U (Figure 5.20). Then, the motion propagates within the fluid domain as a wave. Ahead of this diffusive wave front, the fluid is still at rest; behind the front,

the fluid is in motion. Within the moving fluid, one can distinguish two regions: The Hartmann layer in the vicinity of the plane plate, which has a characteristic thickness $\delta = \left(\frac{\rho\nu}{\sigma}\right)^{1/2}/B_0$, and a second region which is essentially a uniform plateau where the velocity is maximum and constant. The development of such a velocity field induces a perturbation in the imposed magnetic field. This perturbation propagates as a plane wave. This wave is called the Alfven wave and travels within the fluid domain with a constant velocity $A_0 = B_0/(\mu\rho)^{1/2}$. When the kinematic viscosity of the fluid is equal to its magnetic diffusivity, then the magnetic Prandtl number is equal to one ($P_m = \nu/\eta$), and an analytical solution exists for the MHD Rayleigh problem (Moreau [54]).

This analytical solution is written in the following form:

$$u = \frac{U}{4}\left(2 - (erf\lambda_+ + erf\lambda_-) + e^{-A_0 y/d}(1 - erf\lambda_-) + e^{A_0 y/d}(1 - erf\lambda_+)\right) \tag{5.26}$$

$$a = \frac{U}{4}\left(erf\lambda_- - erf\lambda_+) + e^{-A_0 y/d}(1 - erf\lambda_-) - e^{A_0 y/d}(1 - erf\lambda_+)\right) \tag{5.27}$$

where:

$$\lambda_\pm = \frac{y \pm A_0 t}{2(dt)^{1/2}} \tag{5.28}$$

$$d = \nu = \eta \tag{5.29}$$

$$a = \frac{b}{(\mu\rho)^{1/2}} \tag{5.30}$$

and u and b are the x components of respectively the velocity field and the induced magnetic field. This MHD Rayleigh problem, with the velocity space field given as an input data, has been computed with the following physical parameters:$\sigma = (10^7/(4\pi))\,(\Omega \cdot m)^{-1}$, $\eta = 1.0m^2 \cdot s^{-1}$, $\rho = 0.4 \times 10^{-4} kg \cdot m^{-1} \cdot s^{-1}$, $B_0 = 1.4494 \times 10^{-4} Tesla$, $\Delta t = 0.01$, $t \leq 0.08s$ and with the same mesh as for the Hartmann-Poiseuille flow. The homogeneous Dirichlet conditions are imposed for the magnetic field on the plate. We compare the results obtained from the analytical solution and the numerical computations. The agreement between the two is quite good (Figure

5.21). The three regions (Hartmann layer, the magnetic plateau and the wave front) are clearly distinguished.

5.1.7 Lid-Driven Cavity Problem

Let the domain of study be a cubic unity domain ($0 \leq x \leq 1, 0 \leq y \leq 1, 0 \leq z \leq 1$). Suppose the hydrodynamic solution of the classical lid-driven cavity problem at a certain Reynolds number Re, where the $x-$ component of the velocity is imposed to u_0 in the plane $y = 1$, is given as input data. Suppose, then, that a transverse uniform magnetic field $\mathbf{B_0}$, is imposed in the y direction (Figure 5.22). The three-dimensional velocity field will convect the magnetic field through its lines.

The capacity of the velocity field of convecting the magnetic field through its own lines depends on the magnetic Reynolds number, Re_m. When Re_m is low, the magnetic field is transported in a quasi-pure diffusive manner. The convection of the magnetic field by the velocity could hence be neglected. As the magnetic Reynolds number increases, the convection of the magnetic field becomes more important. When Re_m is high enough, the convection of the magnetic field becomes the dominant regime of the transport mechanism and the magnetic field is said to be "frozen" in the velocity field.

Computations have been carried out in the above described geometry for different magnetic Reynolds numbers ($Re_m = 0.1, 1, 10, 100, 400, 1000$). The unstructured mesh consists of 41873 elements and 8147 nodes. In each case, we seek the steady-state solution. The velocity field given as input data represents the hydrodynamic solution for $Re = 400$. The choice of this Reynolds number is somewhat arbitrary since the purpose of the test is to show the effect of different values of the Re_m number on the magnetic field transport. Dirichlet boundary conditions are imposed, thus, representing the non-perturbation of the external magnetic field by the internal induced one. The computed solutions show the gradual evolution of the magnetic field transport from a quasi-diffusive regime to a quasi-convective one. In Figures (5.23) to (5.26), the magnetic field in the mid-plane $z = 0.5$ is shown for $Re_m = 0.1, 100, 400, 1000$ and the gradual evolution from diffusive transport to convective transport is put into

evidence. In Figures (5.27) and (5.28), the magnetic field norm and the y-component of the magnetic field are shown respectively along the medians $y = 0.5$ and $x = 0.5$. The convective transport is again put into evidence as the Re_m grows from 0.1 to 1000. In Figure (5.29), we show the velocity field (given as an input data for this case test) norm and the y-component of the velocity along the median $y = 0.5$. Comparing the qualitative behaviors of the velocity (Figure (5.29)) and of the magnetic field (Figure (5.28)) gives the ultimate explanation for the statement :*the magnetic field freezing in the velocity field.*

5.2 Results for the $\mathbf{A}, \phi$ Formulation

In this section, the test cases that are carried out for the $\mathbf{A}, \phi$ formulation are presented. In the same fashion as for the $\mathbf{B}, \mathbf{q}$ formulation, we first study the stability and the convergence of the finite element formulation (3.33)-(3.34). Once this first step is done, two other numerical tests are presented:

- A 1-D test, where an external magnetic field is applied on a unidirectional fluid flow.
- A 2-D test, where the rotation of a solid cylinder convects the constant imposed magnetic field.

5.2.1 Stability of the Formulation

In order to assess the stability and the quality of the finite element formulation (3.33)-(3.34), we study this problem in a cubic domain ($0 \leq x \leq 1, 0 \leq y \leq 1, 0 \leq z \leq 1$). The velocity vector is fixed to $\mathbf{u} = (1, 1, 1)^T$. The Dirichlet boundary conditions and the right-hand-side vector $\mathbf{f} = (2z - 2\eta + 1, 2z - 2\eta + 1, 1 - 4z, 4)^T$ are imposed in such a way as to reproduce approximately an arbitrary solution of the continuous problem, namely $\mathbf{A} = (x^2, y^2, -2(x + y)z)^T$ and $\phi = x + y + z$. Computations have been performed with $\eta = 0.1$. In the same manner as in section (5.1), we compute the mesh variation of the $L_2(\Omega)$-norms of the magnetic vector potential divergence $||\nabla \cdot \mathbf{A}_h||$, the vector potential error $||\mathbf{A}_h - \mathbf{A}||$, the electric scalar potential $||\phi_h||$ and

its gradient $||\nabla\phi_h||$. Figure (5.30) shows the variation of these norms. The method is stable. The convergence rates (slopes) have been computed for the vector potential. The slopes are around unity for the divergence of the vector potential and around 2 for the vector potential itself.

5.2.2 Uniform Flow under a Magnetic Field

Suppose an electrically conducting fluid domain Ω has an uniform $y-$component velocity V. An external alternative magnetic field $\mathbf{B}$ with frequency ω, is applied on the fluid domain. Suppose further that $\mathbf{B}$ has only one component along the x direction with B_x being only a function of y: $\mathbf{B} = (B_x(y), 0, 0)$. Then, if one uses the reduced vector potential $\mathbf{A}^*$ formulation, the magnetic field condition $\mathbf{B} = (B_x(y), 0, 0)$ becomes in terms of the new reduced potential, $\mathbf{A}^* = (0, 0, A_z{}^*(y))$. The described problem has an analytical solution (Trophime [33]) in terms of the reduced vector potential $\mathbf{A}^*$ which can be written, when the frequency ω is null, as (for simplicity of notation A^* stands for $A_z{}^*$):

$$A^*(y) = \frac{A_0\left(e^{Re_m} - 1\right) + (A_1 - A_0)\left(e^{Re_m y/L} - 1\right)}{e^{Re_m} - 1} \tag{5.31}$$

with the boundary conditions being:

$$A^*(0) = A_0 \tag{5.32}$$

$$A^*(L) = A_1 \tag{5.33}$$

Numerical solutions have been computed for different magnetic Reynolds numbers ($Re_m = 1, 5, 10, 20, 40, 50$). The results show a quite good agreement between computed and analytical solutions (Figure 5.31).

5.2.3 Convection of a Magnetic Field by a Rotating Velocity Field

A very long cylinder of radius r_0 with a conductivity σ is rotating in the xy plane with an angular velocity ω_0. Suppose, then that the cylinder is immersed in an uniform magnetic field $\mathbf{B}$ directed along the x axis (Figure 5.32). The magnetic field lines are

then convected by the velocity of the cylinder. The effect of convection is proportional to the magnetic Reynolds number ($Re_m = \mu\sigma\omega_0 {r_0}^2$). In the limit of infinite Re_m, the magnetic field is expulsed out of the cylinder. Assuming the cylinder to be infinite along the z axis and steady state conditions ($\frac{\partial}{\partial t} = 0$), the vector potential has only one non trivial component A_z which is a function of x and y. The vector potential problem consists then on finding A_z such that:

$$\nabla^2 A_z - (\mathbf{u} \times \nabla \times \mathbf{A})_z = 0 \qquad r > r_0 \tag{5.34}$$

$$\nabla^2 A_z = 0 \qquad r \leq r_0 \tag{5.35}$$

The problem has an analytical solution which has been developed by Moffat [55] and is written as:

$$A_z = Im[Bf(r)e^{i\theta}] \tag{5.36}$$

where:

$$f(r) = r + \frac{C}{r} \qquad r > r_0 \tag{5.37}$$

$$f(r) = DJ_1(pr) \qquad r \leq r_0 \tag{5.38}$$

with:

$$p = \frac{(1-i)k_0}{\sqrt{2}} \tag{5.39}$$

$${k_0}^2 = \frac{Re_m}{{r_0}^2} \tag{5.40}$$

The constants C and D are:

$$C = \frac{r_0[2J_1(pr_0) - pr_0 J_0(pr_0)]}{pJ_0(pr_0)} \tag{5.41}$$

$$D = \frac{2}{pJ_0(pr_0)} \tag{5.42}$$

The boundary conditions are imposed as in Figure (5.32). Numerical solutions have been computed for different magnetic Reynolds number ($Re_m = 0, 6, 12, 24, 48$). The unstructured nearly uniform mesh consists of 4446 elements and 1600 nodes. Figures (5.33) and (5.34) show the effect of increasing the angular velocity ω_0 on the convection of the magnetic field. These results are in good agreement with the analytical solution.

On the other hand, the beginning of the expulsion of the magnetic field is showed in Figure (5.35). One can see that as the magnetic Reynolds number Re_m increases, the vector potential goes to lower values in the vicinity of the cylinder. In these computations, the radius of the cylinder is set to $r_0 = 0.2m$.

5.3 Results for the $(\mathbf{u}, p, \mathbf{B}, q)$ Coupled Formulation

For the coupled problem, results are obtained for the lid-driven cavity problem under a constant transversal magnetic field B_0. When the external imposed magnetic field is zero, the problem becomes the classical hydrodynamic lid-driven cavity problem. The cavity is a cubic domain with $(0 \leq x \leq 1, 0 \leq y \leq 1, 0 \leq z \leq 1)$. The fluid movement in the cavity is induced by the imposed boundary condition $u = u_0$ of the plane $y = 1$ (Figure 5.22). The velocity field induces a perturbation of the magnetic field in the fluid domain. Moreover, the interaction between the velocity and the magnetic fields creates the electromagnetic Lorentz forces. These new body forces are responsible for the change of the structure of the flow. The hydrodynamic Reynolds number Re is set to $Re = 10^3$ and a parametric study of the magnetic Reynolds number Re_m and the Hartmann number Ha has been conducted. The unstructured nearly uniform mesh consists of 41873 elements and 8147 nodes. The parameters of the solution algorithm are set to the following:

- Time step $\Delta t = 5.0$.
- Number of time steps $N = 100$.
- For the ILUT algorithm $lfil = 15$ and $tol = 10^{-09}$.
- For the GMRES algorithm, the number of Krylov basis vectors $m = 8$.
- For the Newton iterations, $niter = 5$.

The Dirichlet boundary conditions are imposed for both the velocity field and the magnetic field, thus expressing the non-slip property at solid walls and the non-perturbation of the external magnetic field by the induced one.

5.3.1 Low Magnetic Reynolds Numbers

First, we investigate the influence of the Hartmann number Ha at a low magnetic Reynolds number where the magnetic diffusion dominates the magnetic convection. To do so, we set the magnetic Reynolds number to $Re_m = 1$. The Hartmann number is set successively to $Ha = 1, 2, 5, 7, 10, 20, 30$. Two algorithms are tested. In Algorithm (3), the magnetic matrix is computed and decomposed during the first time step, and kept constant during all the other time steps. The magnetic problem is solved once at each time step. In algorithm (5), the magnetic matrix is again decomposed once at the first time step, but the magnetic problem is solved at each GMRES iteration of the fluid problem.

Surprisingly, the segregated algorithm (3) performs much better than the tighter algorithm (5). In Figure (5.36), the performances of both algorithms in terms of the residual norm are compared. In Figure (5.37), The CPU time performances of both algorithms are compared together. Obviously, the segregated algorithm is the fittest algorithm.

Figures (5.38) to (5.40) show the evolution of the velocity field at the mid-plane $z = 0.5$ from $Ha = 0$ to $Ha = 20$. One can observe the dramatic change of the structure of the vortices. When no external magnetic field is applied ($Ha = 0$), there are two vortices: a large central one in the core region (clockwise rotation) and a smaller one in the right bottom corner (counter clockwise rotation). As the Hartmann number Ha becomes greater, the large central vortex becomes more horizontal and eventually breaks into many vortices. The small vortex in the right bottom corner becomes larger. These changes in the vortices structure are due to the increasing effect of the electromagnetic forces. These forces weaken the vortices strength, leading to the breaking of vortices. An analogy exists with the Rayleigh-Benard cell problem under a magnetic field. Seungsoo [17] showed numerical results confirming the multiplication of initial bouancy vortices under the effect of a transversal magnetic field.

High Hartmann numbers When the Hartmann number becomes greater ($Ha > 20$), marching the problem in time does not yield a steady-state solution. The convergence of the algorithm (in terms of time steps) reaches a stagnant plateau; however, the algorithm converges pretty well within a time step (the residual is reduced by 6 to 7 orders of magnitude). In Figure (5.41), a typical behavior of the residual evolution is shown. This can be a sign of the absence of a steady solution under such conditions and the fluid keeps on exhibiting an unsteady behavior as time is increased. In order to show this, we study the behavior of the fluid properties (essentially the different components of the velocity) in terms of time steps, under the following conditions:

- Time step $\Delta t = 0.1$.
- Number of time steps $N = 1900$.
- The Hartmann number $Ha = 30$.

Figure (5.42) shows the time evolution of the velocity norm for five nodes located in different locations of the domain (Figure 5.43). One can see that no steady state is obtained and that the solution continues to oscillate in time. This behavior can be the signature of instabilities developing in the fluid domain due to the effect of the electromagnetic forces which, in this case, are of the same order of magnitude as the convective forces. The absence of predominant forces prevents the development of a pattern of flow leading to a steady state solution. The study of the stability of the flow is beyond the scope of this thesis; however, a parametric study with the Ha number is thought to be necessary for the study of these instabilities that develop within the fluid and for the study of the eventual bifurcations that could be generated.

5.3.2 Moderate and High Magnetic Reynolds Numbers

When Re_m is greater than one, the convection of the magnetic field by the velocity one is no longer negligible compared to its diffusion. In such cases, the updating of the magnetic matrix should take place more than once during the time marching process. If the matrix is updated only once, then the algorithm diverges. However,

the frequency of the updating depends on the intensity of the Reynolds magnetic number Re_m. Actually, when $Re_m = 10$, it is still possible to converge the algorithm to the machine zero with the magnetic matrix computed and decomposed only at the beginning of the iterative process. When $Re_m = 100$, the matrix is updated every 10 time steps. When $Re_m = 200$, the updating takes place every 5 time steps. For each of the magnetic Reynolds numbers, the computed velocity and the magnetic fields are given in the plane $z = 0.5$ (Figures (5.44) to (5.46)).

Again, for these numerical tests, two algorithms are used: Segregated Algorithm (3) and Tighter Algorithm (5). Again, the performance of Algorithm (3) is better than the performance of Algorithm (5), both in terms of convergence residual and CPU time (Figures (5.47) and (5.48)). Such results suggest that as the magnetic Reynolds number Re_m increases, it is the quality of the updating of the magnetic solution that is more critical than the frequency of such updating. It is more beneficial for the convergence of the method to update the magnetic matrix while keeping the algorithm segregated, than to use a tighter algorithm with the magnetic matrix frozen at the first iteration.

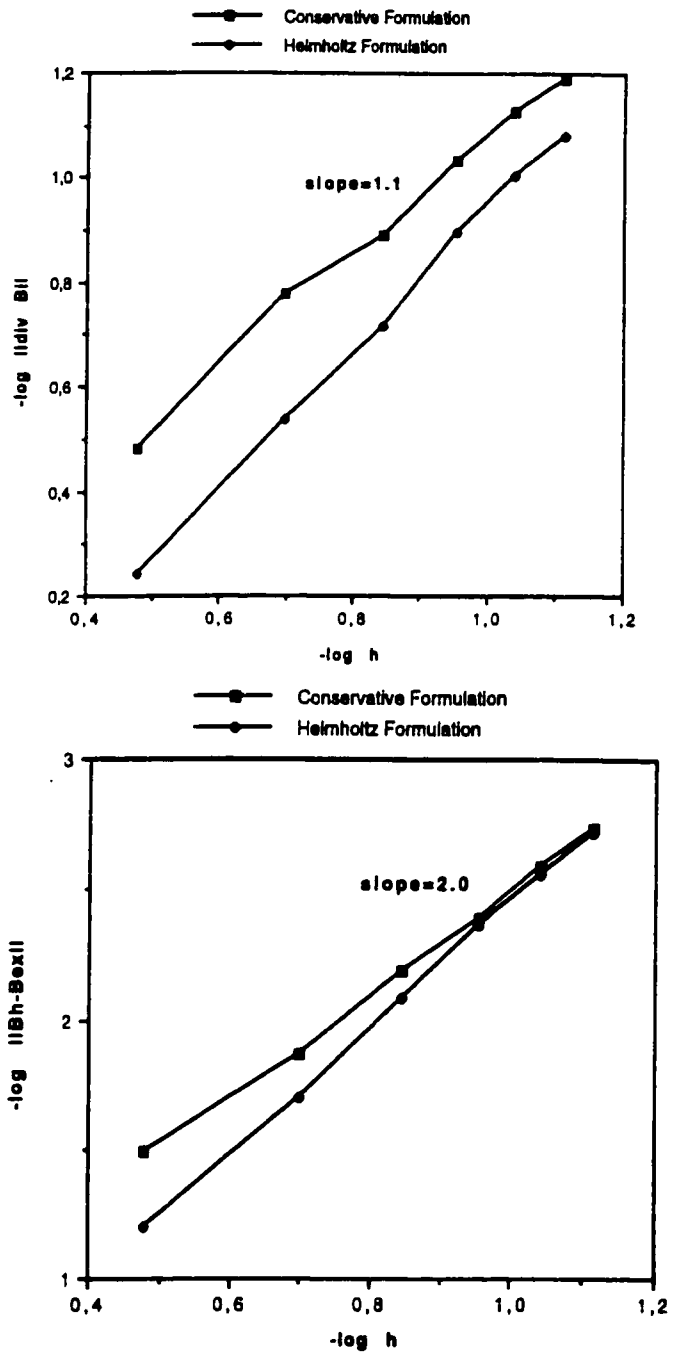

Figure 5.1: Above: L_2 norm of the magnetic field divergence vs the mesh size; Bottom: L_2 norm of the magnetic field error vs the mesh size. $\tau_1 = 0.1\left(\left(\frac{2||\mathbf{u}||}{h}\right)^2 + \left(\frac{4\eta}{h^2}\right)^2\right)^{-1/2}$; $\tau_2 = ||\mathbf{u}||h/2$; $\eta = 1.2 \times 10^{-3}$.

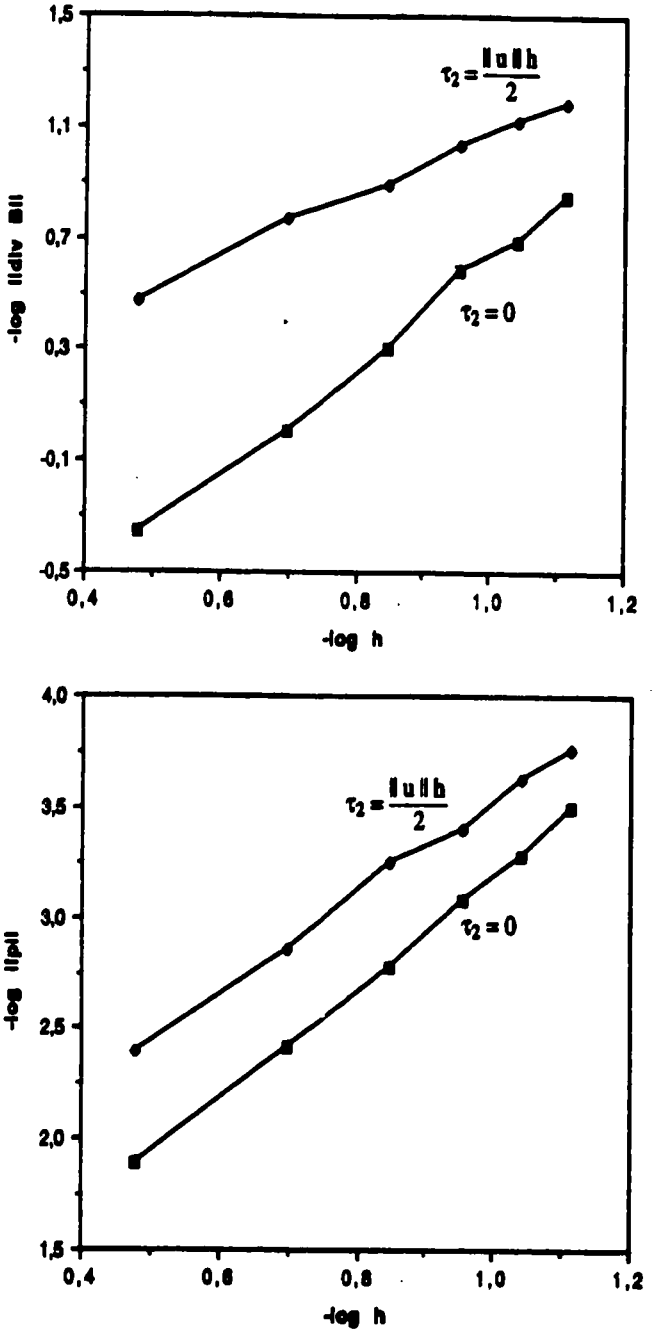

Figure 5.2: Above: L_2 norm of the magnetic field divergence vs the mesh size; Bottom: L_2 norm of the scalar q. $\tau_1 = 1.0 \left(\left(\frac{2\|u\|}{h} \right)^2 + \left(\frac{4\eta}{h^2} \right)^2 \right)^{-1/2}$.

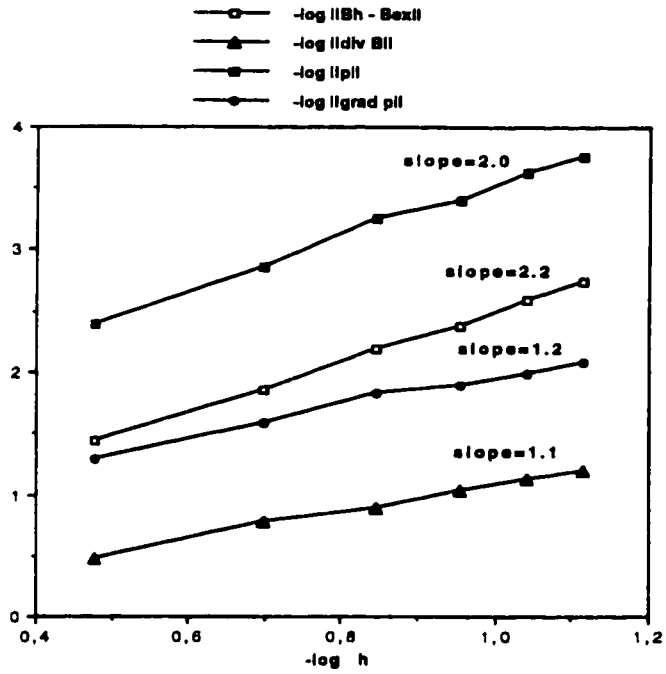

Figure 5.3: Different L_2 norms vs the mesh size with $\alpha = 1.0$.

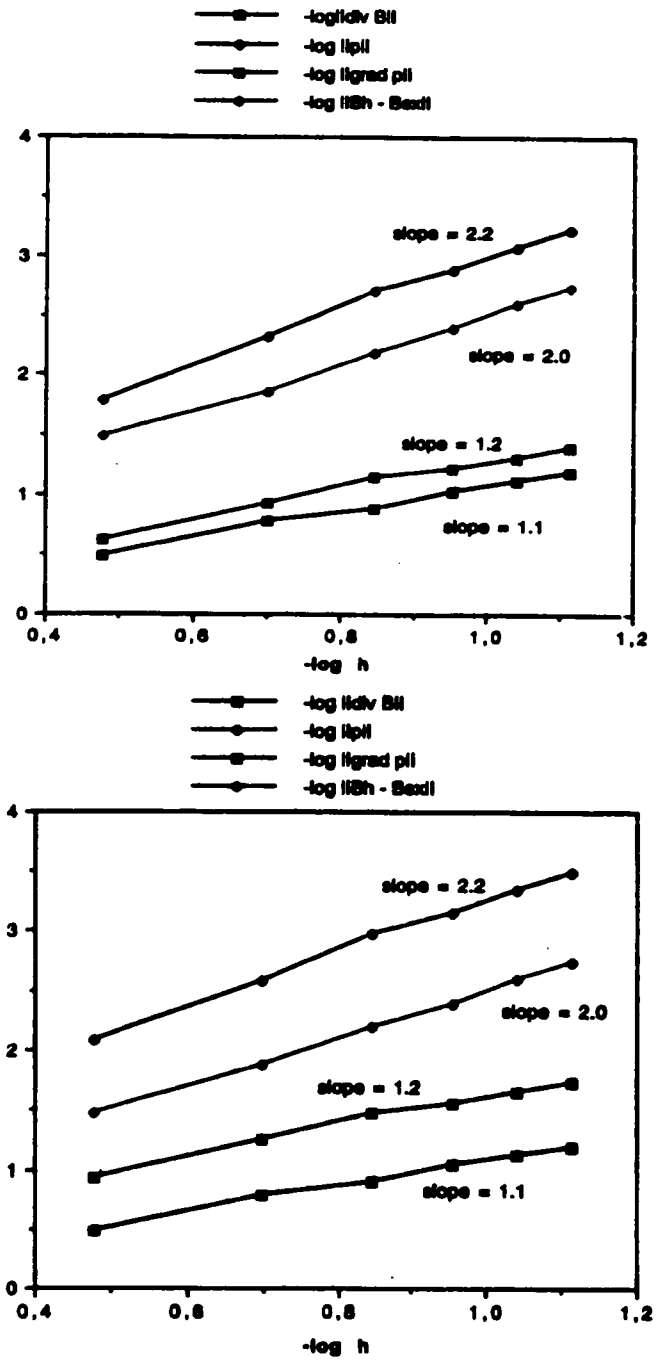

Figure 5.4: Different L_2 norms vs the mesh size; Above: $\alpha = 0.1$, Bottom: $\alpha = 1/3$. $\tau_1 = \alpha \left(\left(\frac{2||\mathbf{u}||}{h} \right)^2 + \left(\frac{4\eta}{h^2} \right)^2 \right)^{-1/2}$; $\tau_2 = ||\mathbf{u}||h/2$; $\eta = 1.2 \times 10^{-3}$.

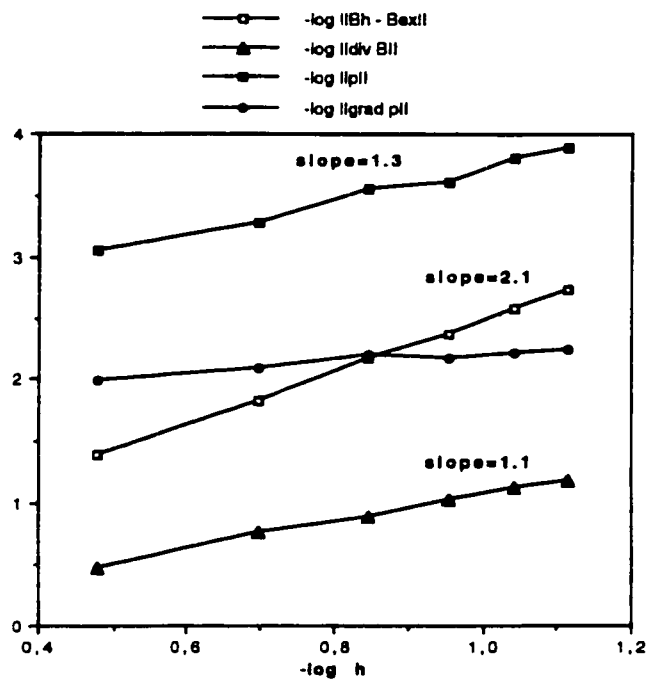

Figure 5.5: Different L_2 norms vs the mesh size with α=0.1. $\tau_1 = \alpha\frac{h^2}{4\eta}$; $\tau_2 = ||\mathbf{u}||h/2$; $\eta = 1.2 \times 10^{-3}$.

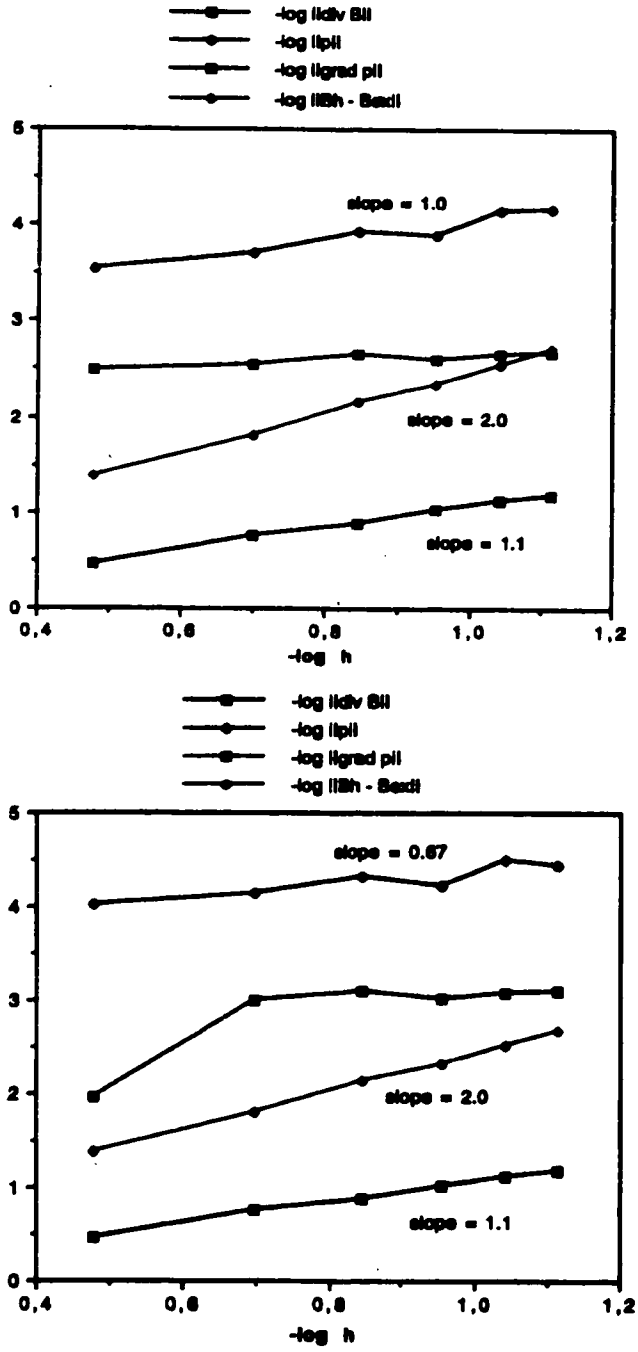

Figure 5.6: Different L_2 norms vs the mesh size; Above: $\alpha = 1/3$, Bottom: $\alpha = 1.0$. $\tau_1 = \alpha\frac{h^2}{4\eta}$; $\tau_2 = ||\mathbf{u}||h/2$; $\eta = 1.2 \times 10^{-3}$.

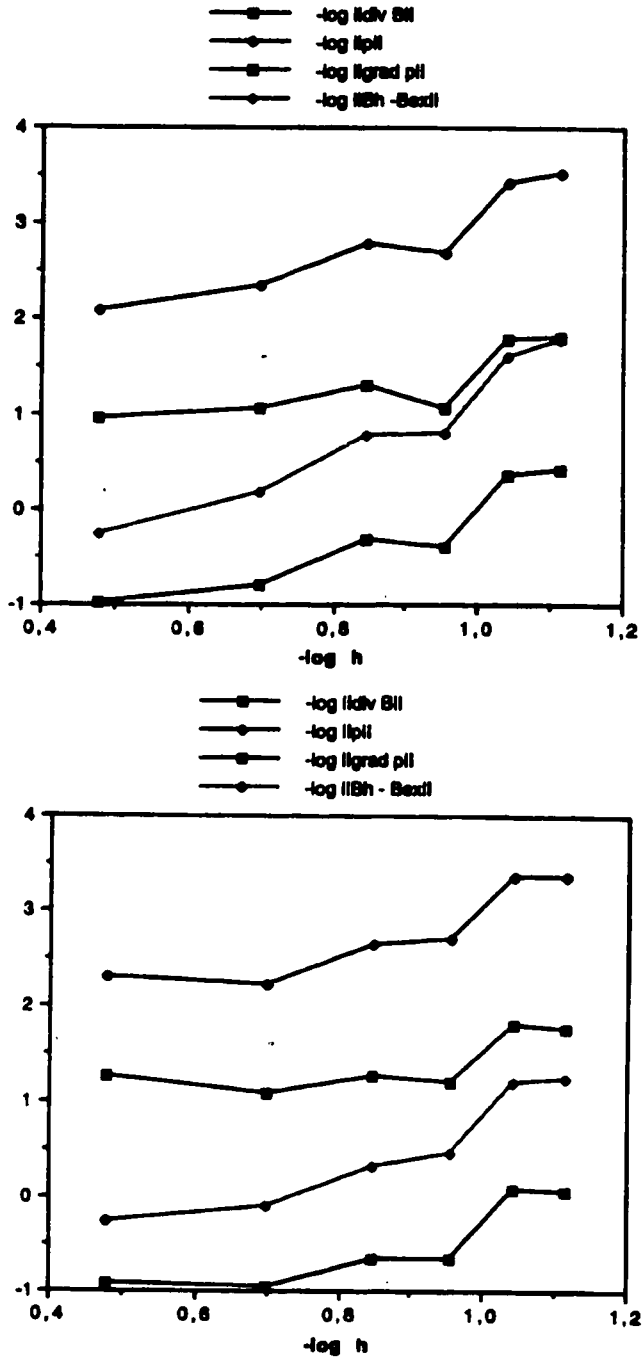

Figure 5.7: Different L_2 norms vs the mesh size; Above: $\alpha = 1/3$, Bottom: $\alpha = 1.0$. $\tau_1 = \alpha\frac{h^2}{4\eta}$; $\tau_2 = 0$; $\eta = 1.2 \times 10^{-3}$.

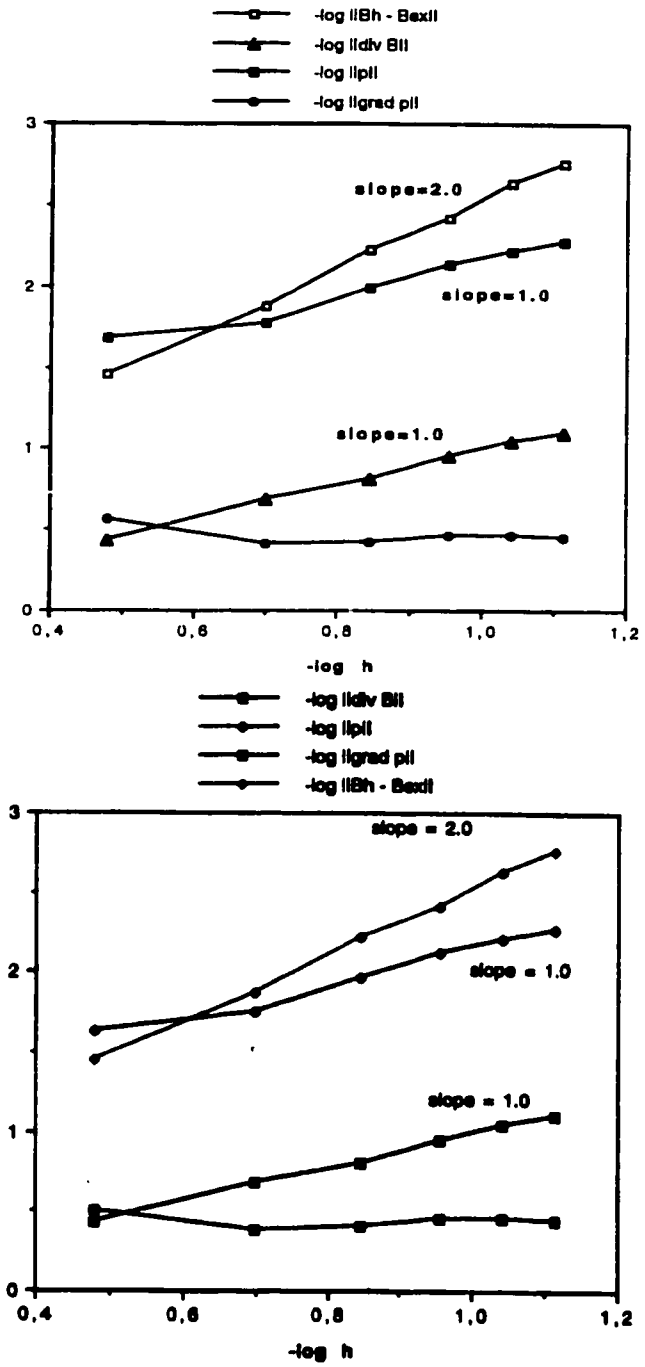

Figure 5.8: Different L_2 norms vs the mesh size with $\alpha = 0.1$, $\tau_2 = 0$ and $\eta = 1.2 \times 10^{-1}$; Above: $\tau_1 = \alpha \frac{h^2}{4\eta}$, Bottom: $\tau_1 = \alpha \left(\left(\frac{2\|\mathbf{u}\|}{h} \right)^2 + \left(\frac{4\eta}{h^2} \right)^2 \right)^{-1/2}$.

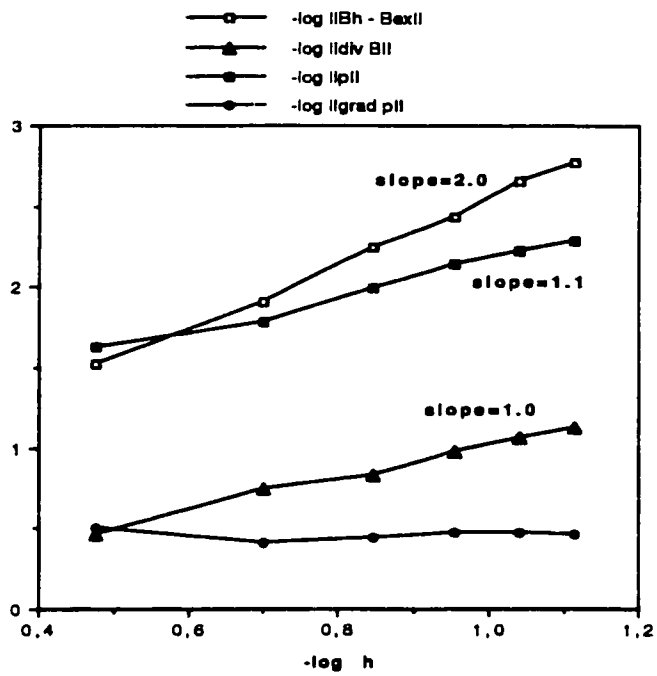

Figure 5.9: Different L_2 norms vs the mesh size; Conservative Formulation with: $\tau_1 = 0.1\frac{h^2}{4\eta}$; $\tau_2 = ||\mathbf{u}||h/2$; $\eta = 1.2 \times 10^{-1}$.

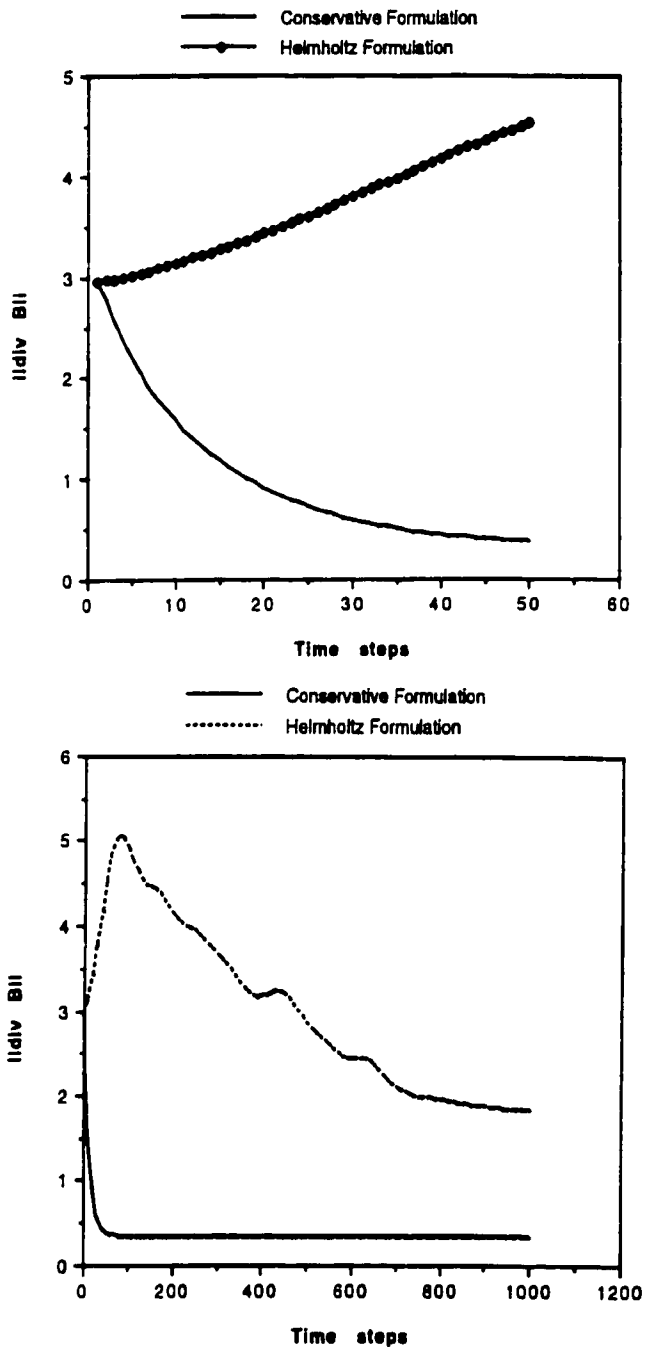

Figure 5.10: L_2 norm of the magnetic divergence vs time steps; Above: The first 50 steps, Bottom: The first 1000 steps. $\tau_1 = 1.0\ \frac{h^2}{4\eta}$; $\tau_2 = ||\mathbf{u}||h/2$; $\eta = 1.2 \times 10^{-1}$.

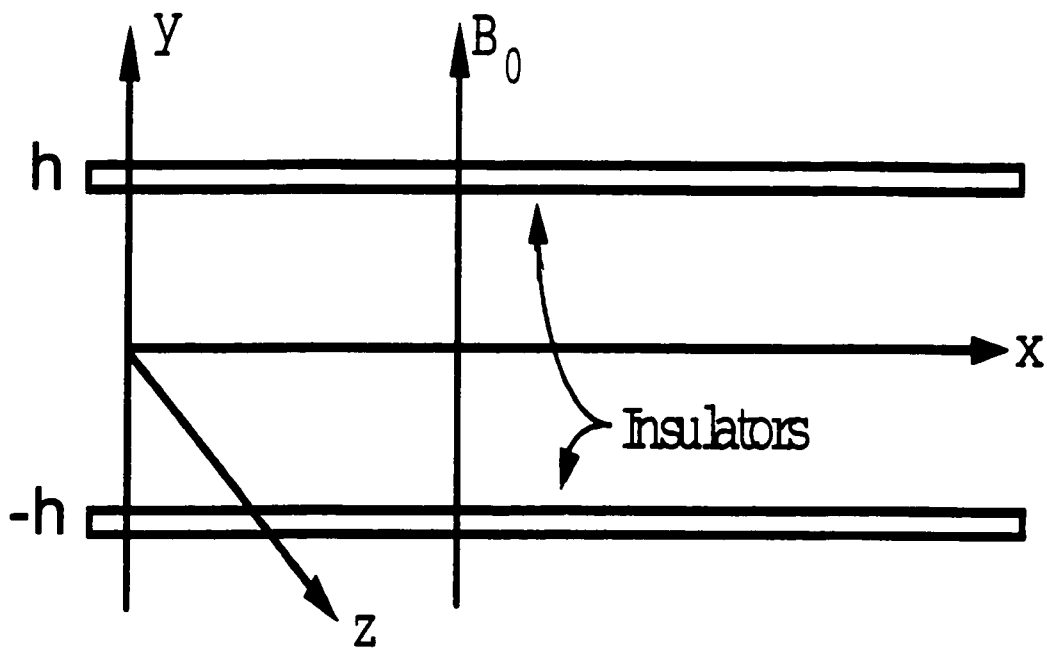

Figure 5.11: Geometry of the duct for the Hartmann-Poiseuille flow

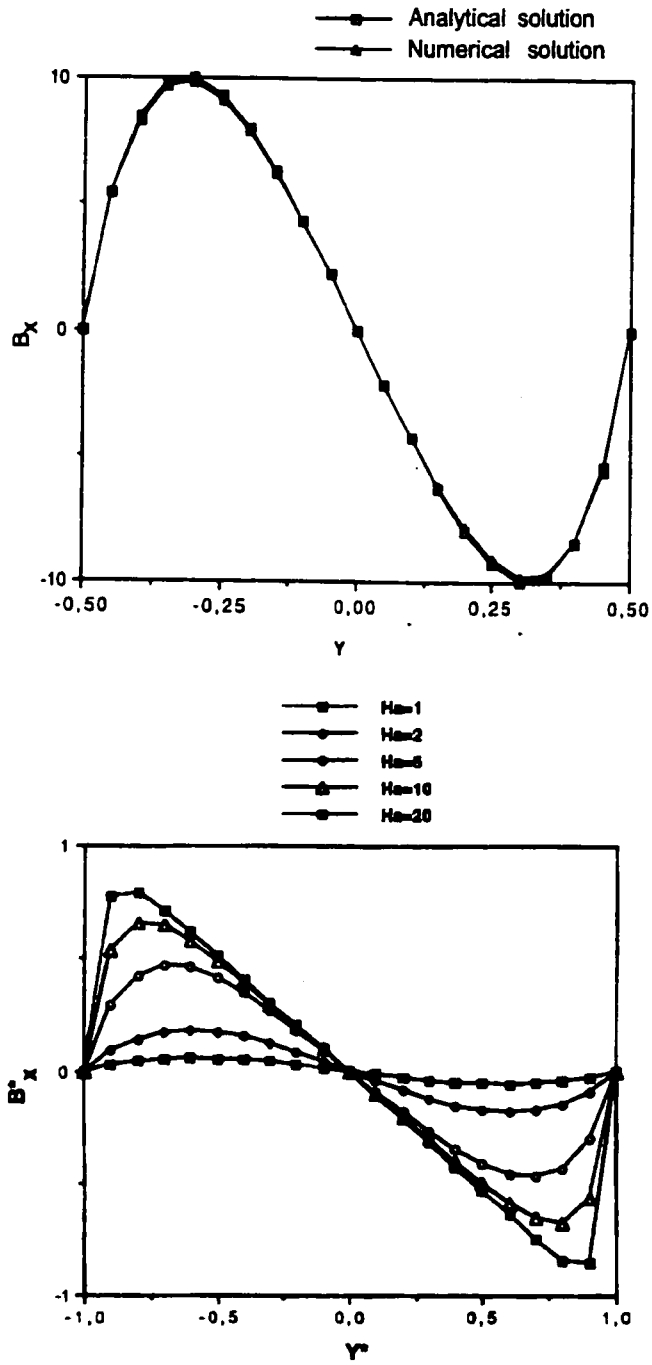

Figure 5.12: Above: Induced magnetic field B_x ($10^{-7}Tesla$) along the y-axis (m), $Ha = 3.45$, Comparison between numerical and analytical solutions; Bottom: Non-dimensional induced magnetic filed B^*_x vs the non-dimensional coordinate y^* for different Ha numbers.

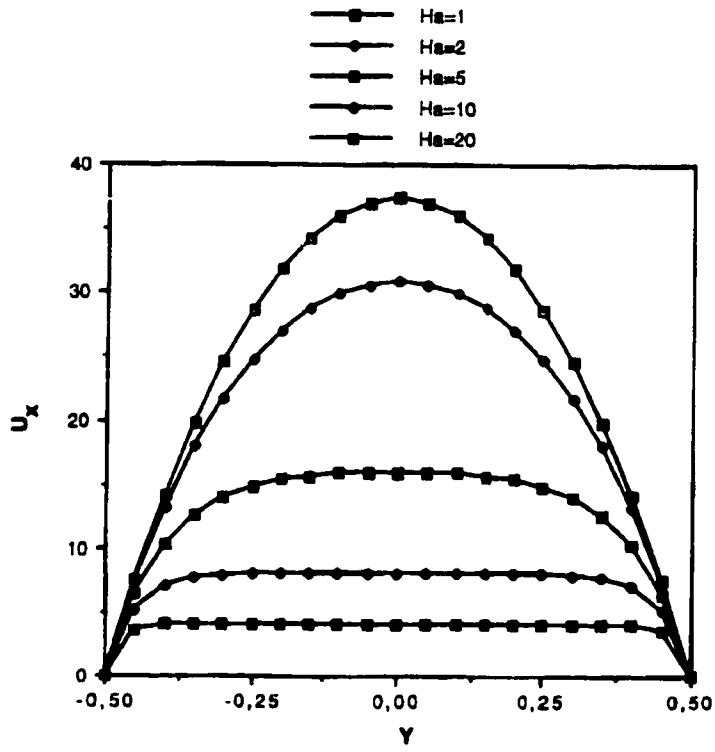

Figure 5.13: The x-component of the velocity ($10^{-3}\ m.s^{-1}$) along the y-axis (m) for different Ha numbers: Analytical solution given as an input data for the Hartmann-Poiseuille test case.

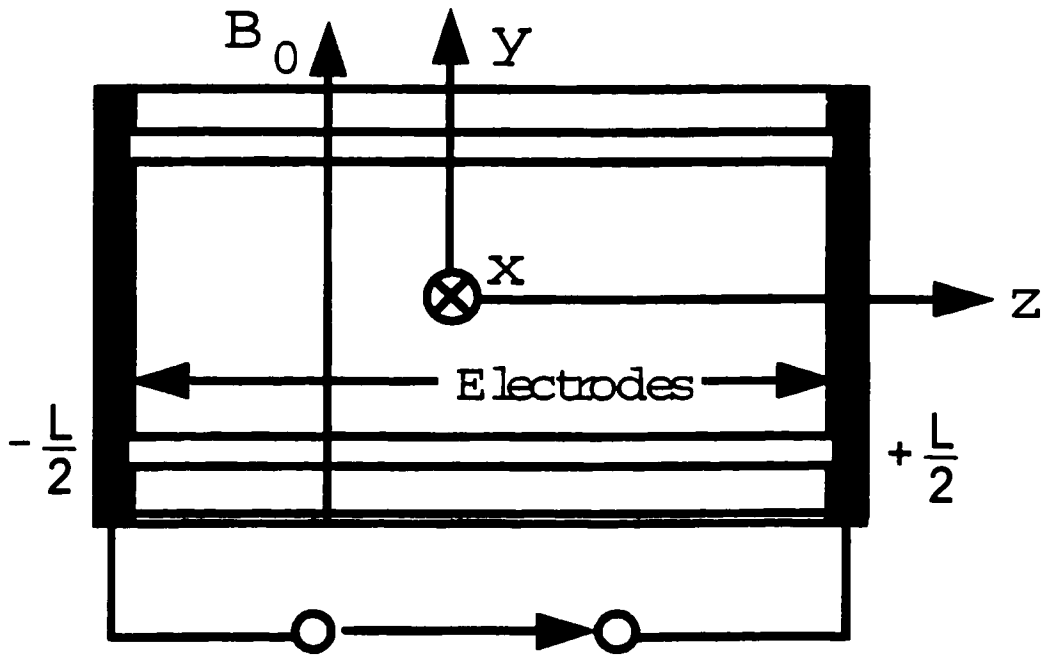

Figure 5.14: Geometry of the duct for the Hartmann-Poiseuille flow carrying an external electric current

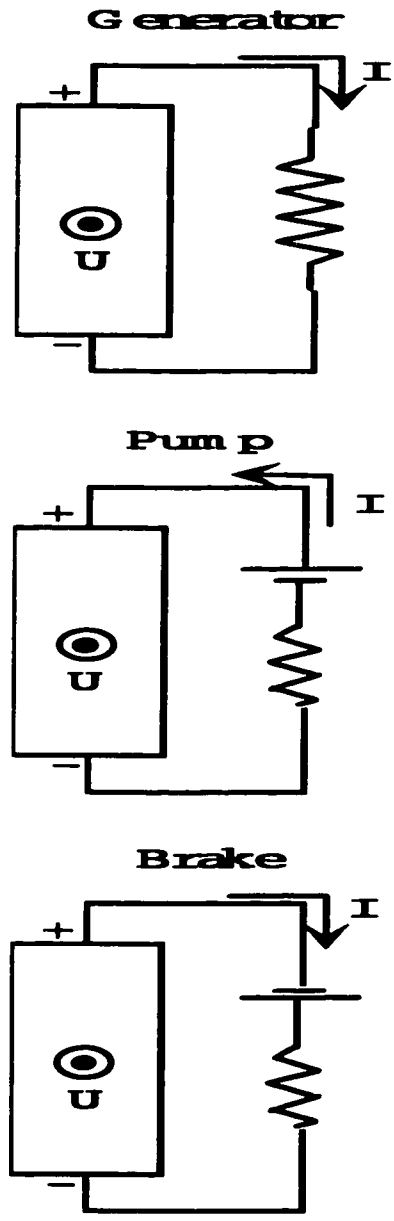

Figure 5.15: Different interpretations of the Hartmann duct.

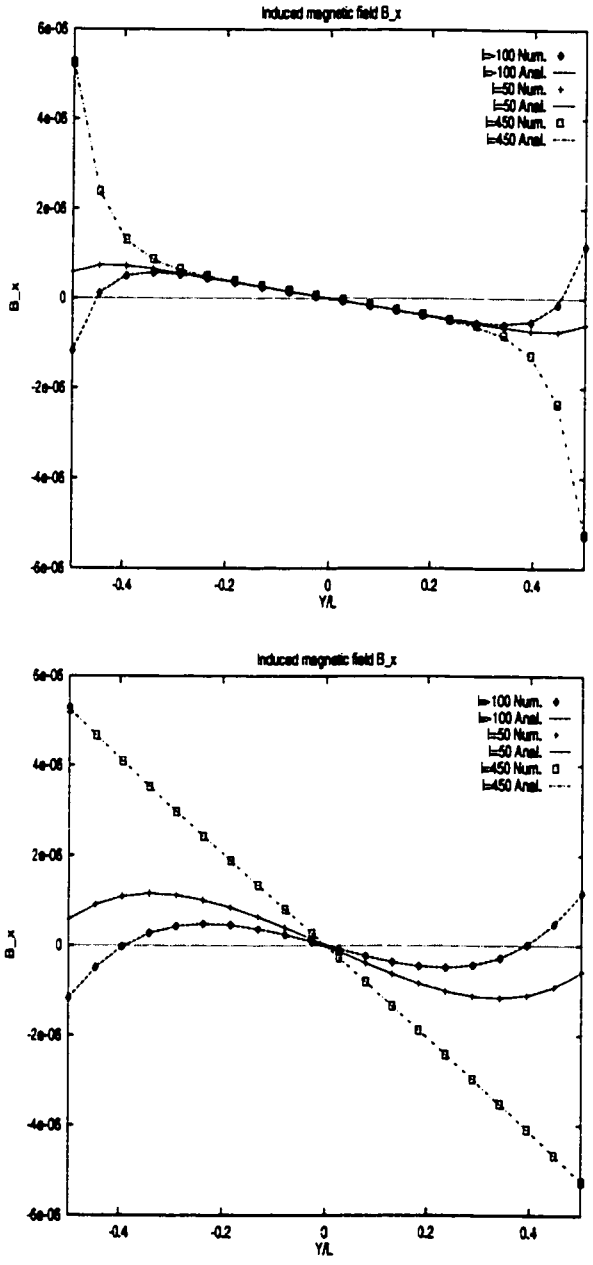

Figure 5.16: Induced magnetic field along the y-axis for different values of I, Comparison between analytical and numerical solutions; Above: Ha=10; Bottom: Ha=2.

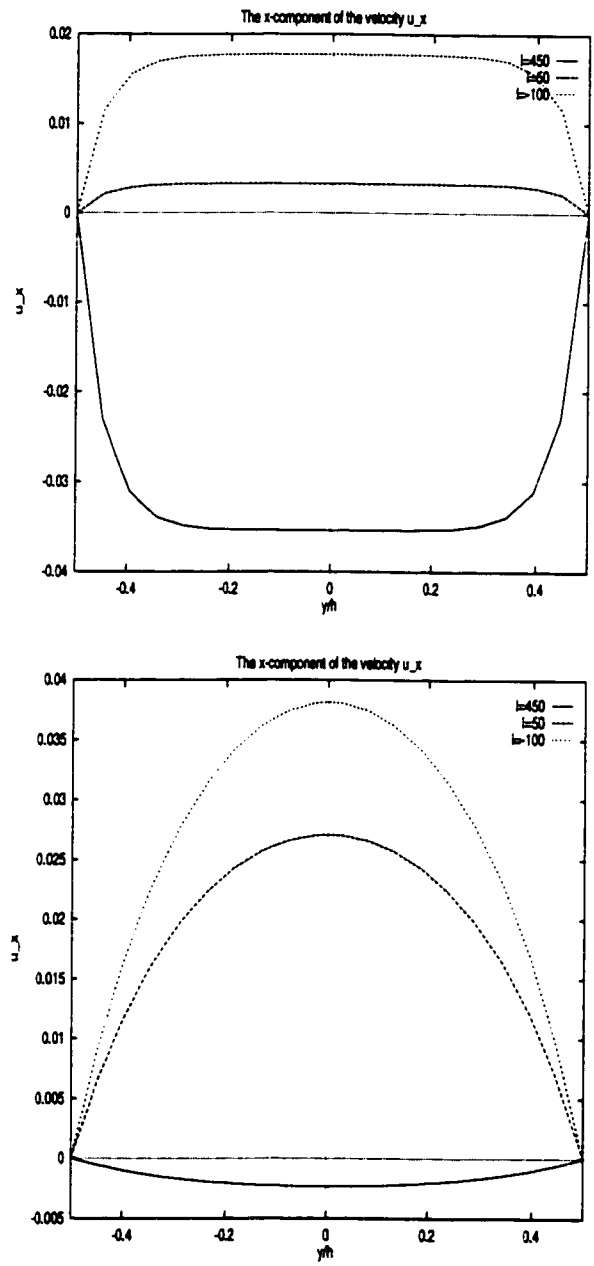

Figure 5.17: The x-component of the velocity field along the y-axis ; Above: Ha=10; Bottom: Ha=2.

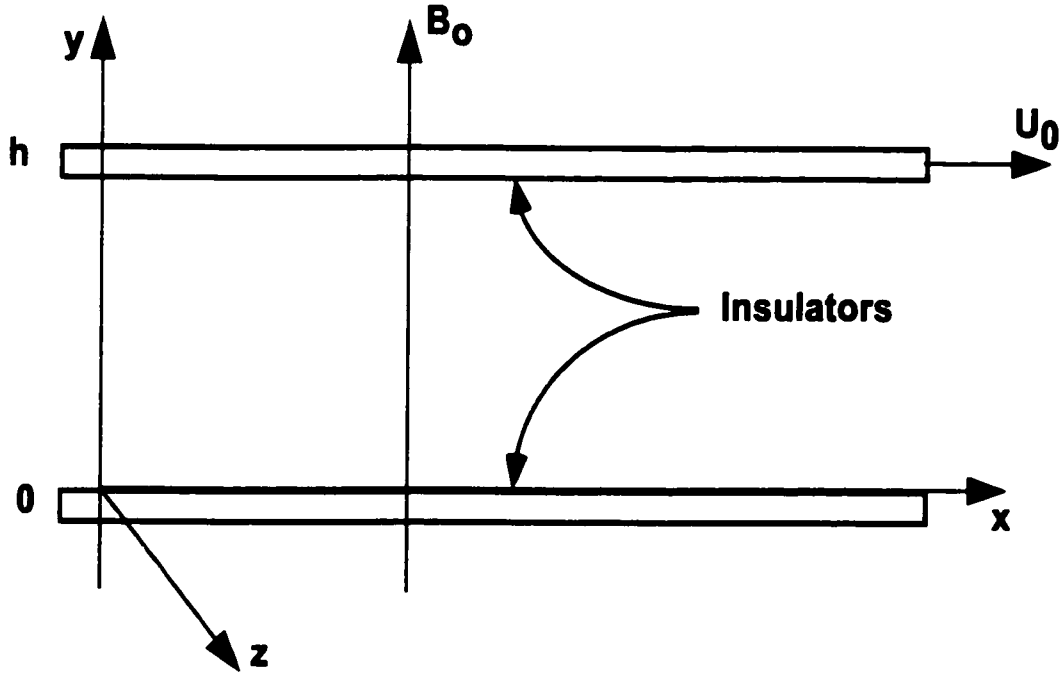

Figure 5.18: Geometry of the duct for the Hartmann-Couette flow .

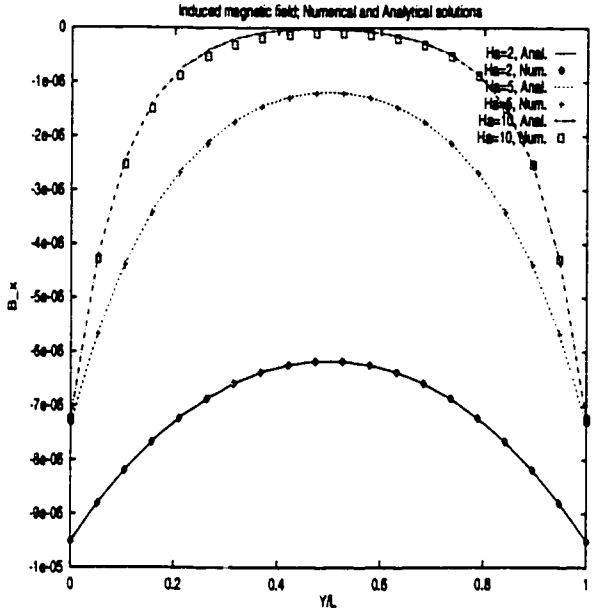

Figure 5.19: Induced magnetic field along the y-axis for different values of Ha, Comparison between analytical and numerical solutions for Hartmann-Couette flow.

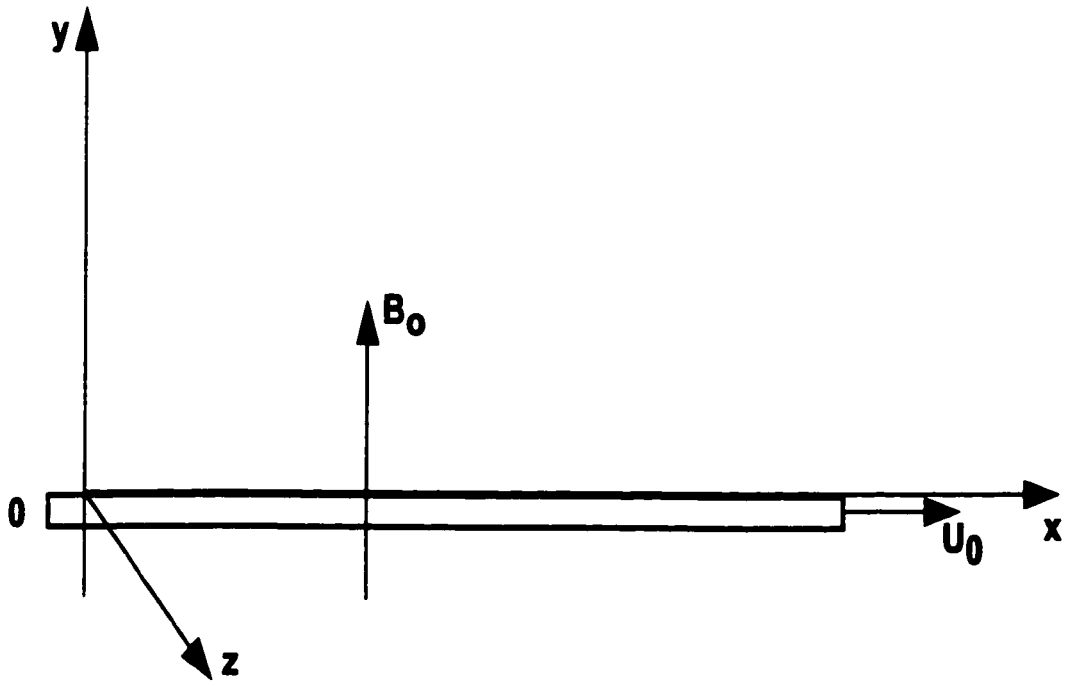

Figure 5.20: Geometry of the duct for the Hartmann-Rayleigh flow .

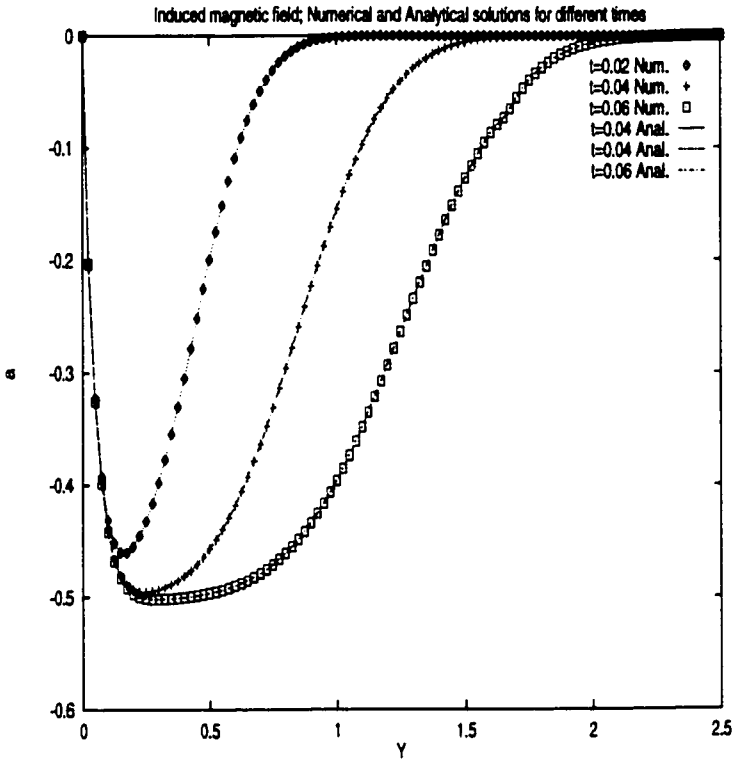

Figure 5.21: Induced magnetic field along the y-axis for different times, Comparison between analytical and numerical solutions for MHD Rayleigh flow.

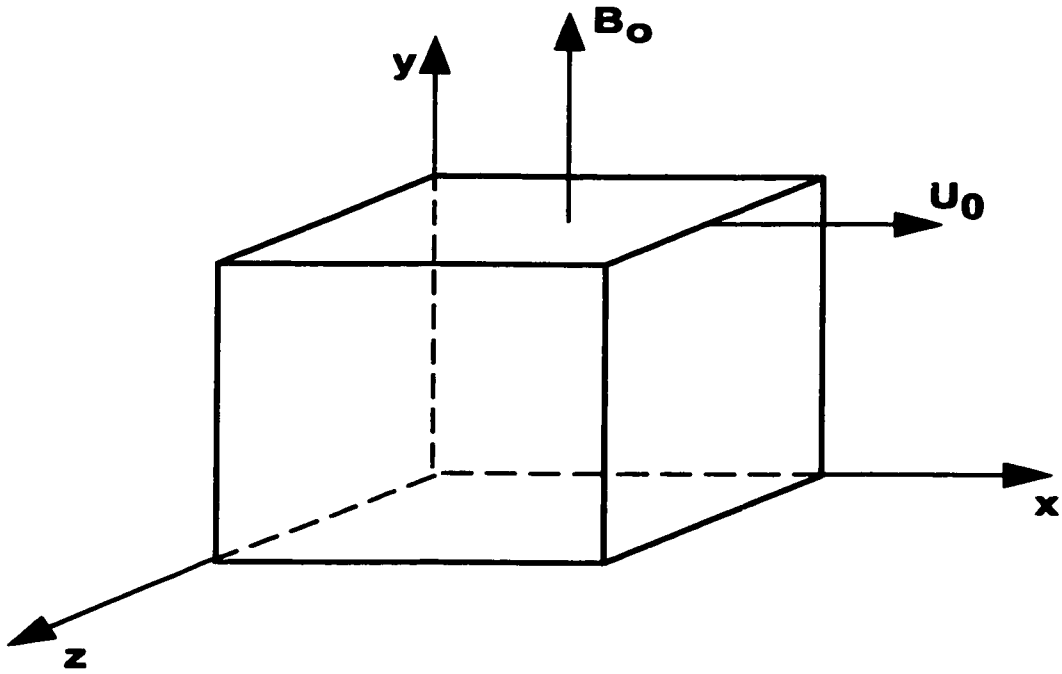

Figure 5.22: Geometry for the Cavity-driven problem .

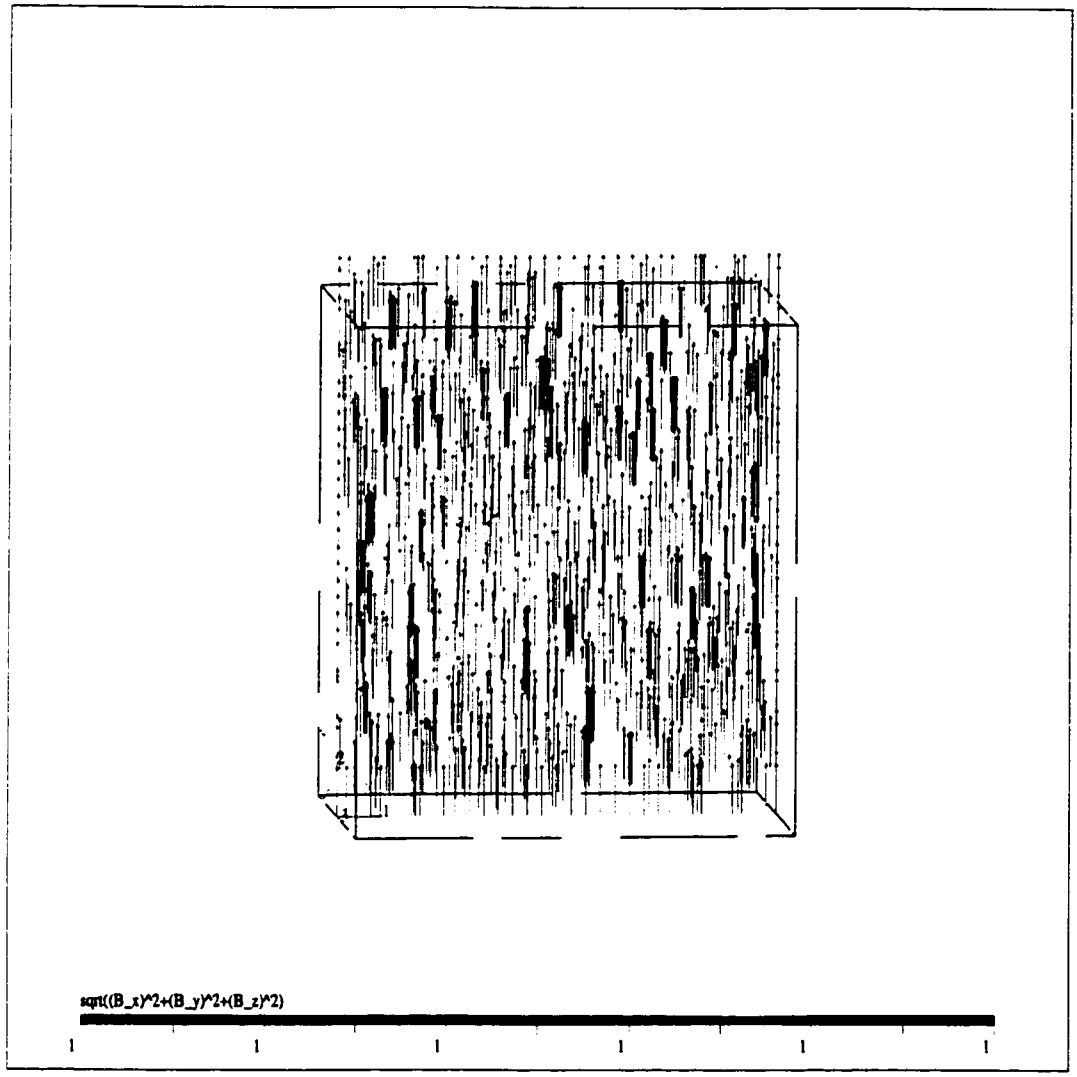

Figure 5.23: Magnetic field at the mid-plane z=0.5; $Re_m = 0.1$.

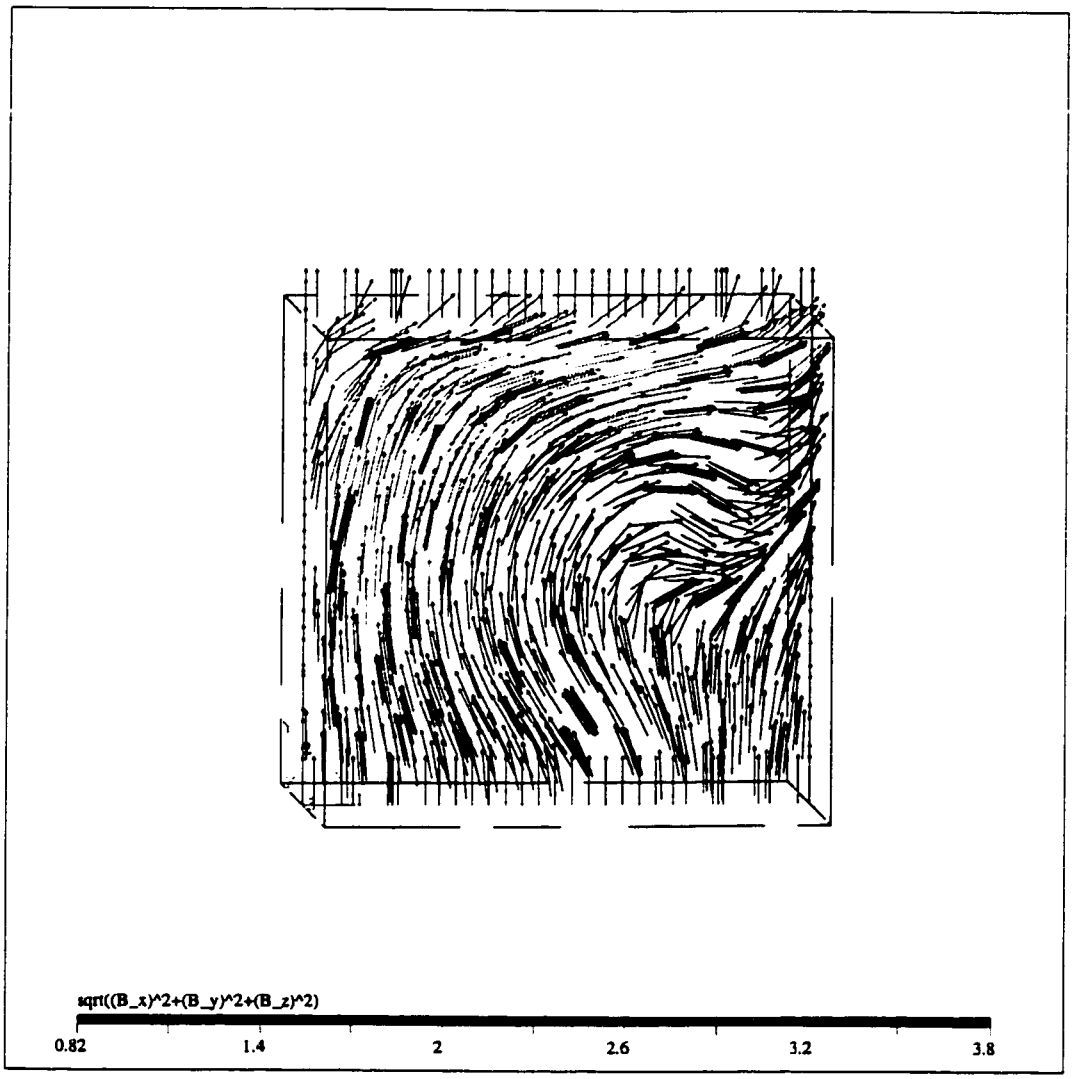

Figure 5.24: Magnetic field at the mid-plane z=0.5; $Re_m = 100$.

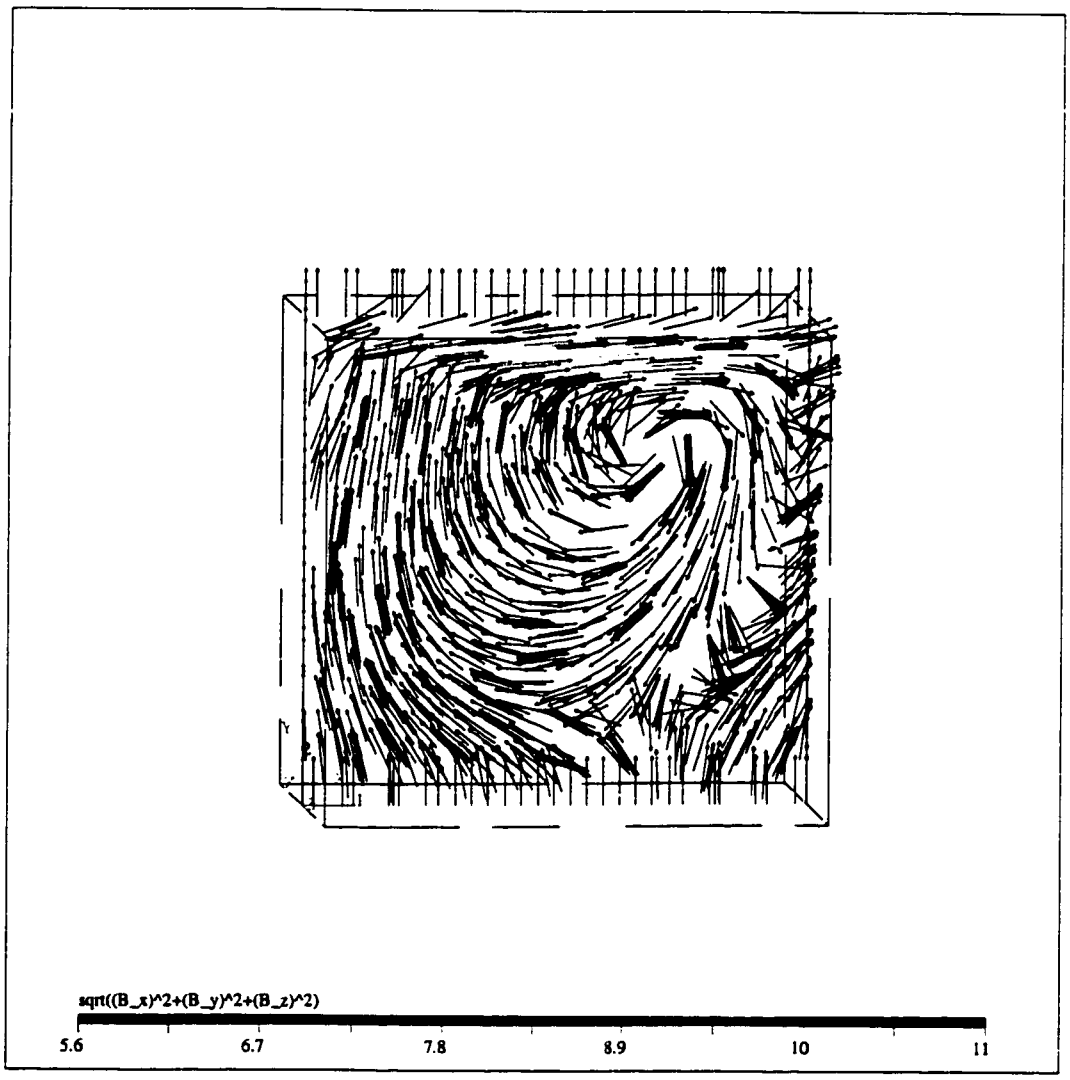

Figure 5.25: Magnetic field at the mid-plane z=0.5; $Re_m = 400$.

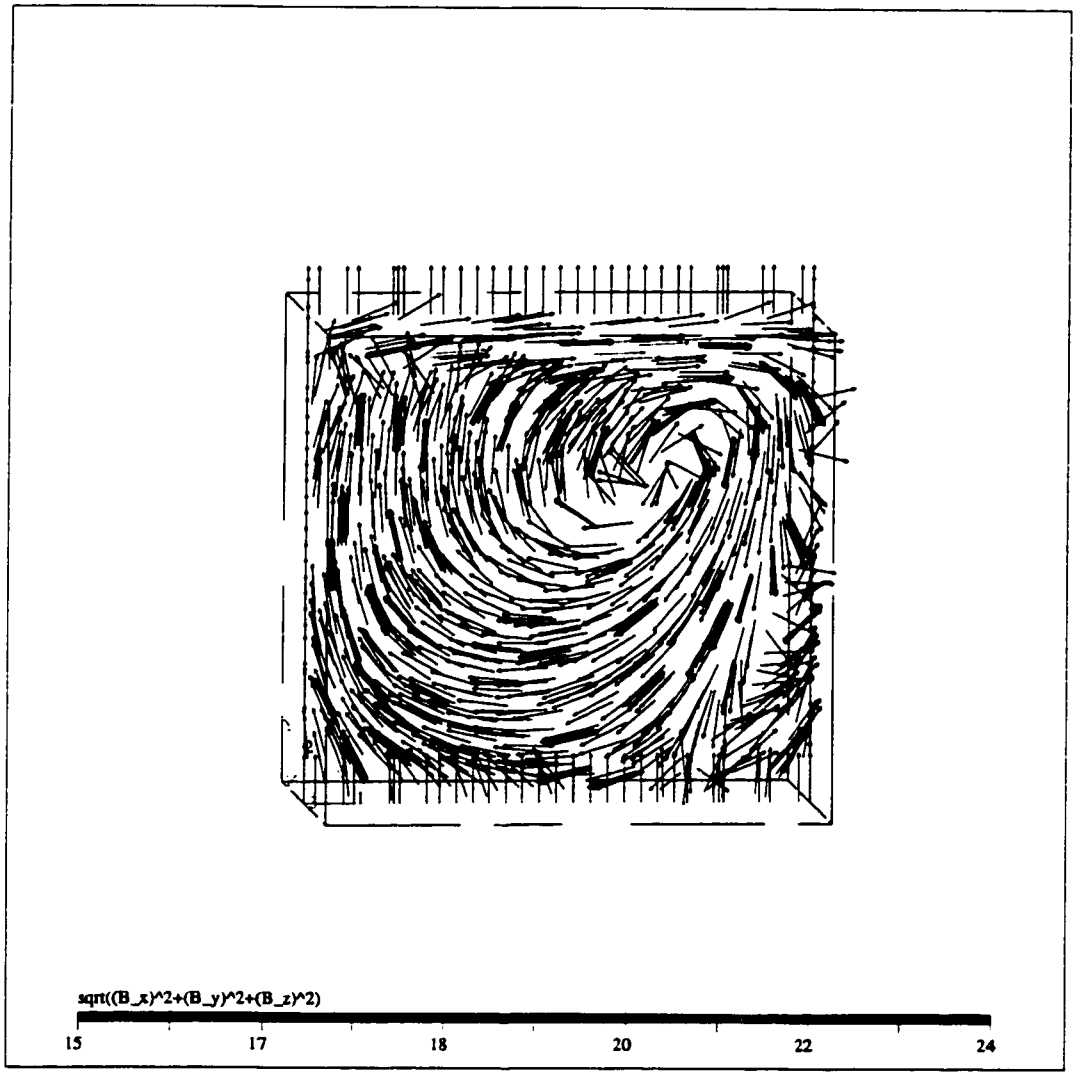

Figure 5.26: Magnetic field at the mid-plane z=0.5; $Re_m = 1000$.

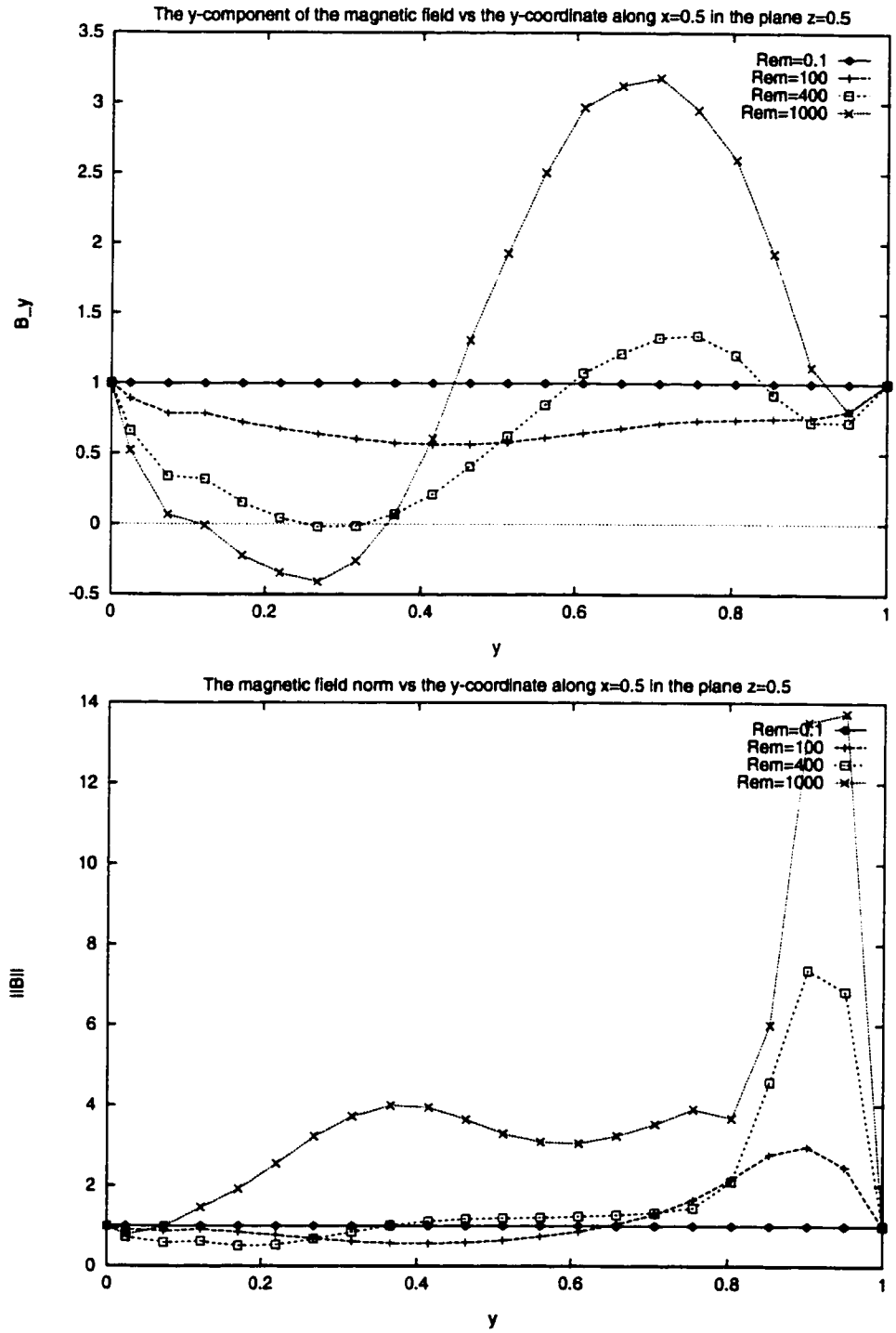

Figure 5.27: The magnetic field along the median x=0.5; Above: The y-component of the magnetic field, Bottom: The magnetic vector norm.

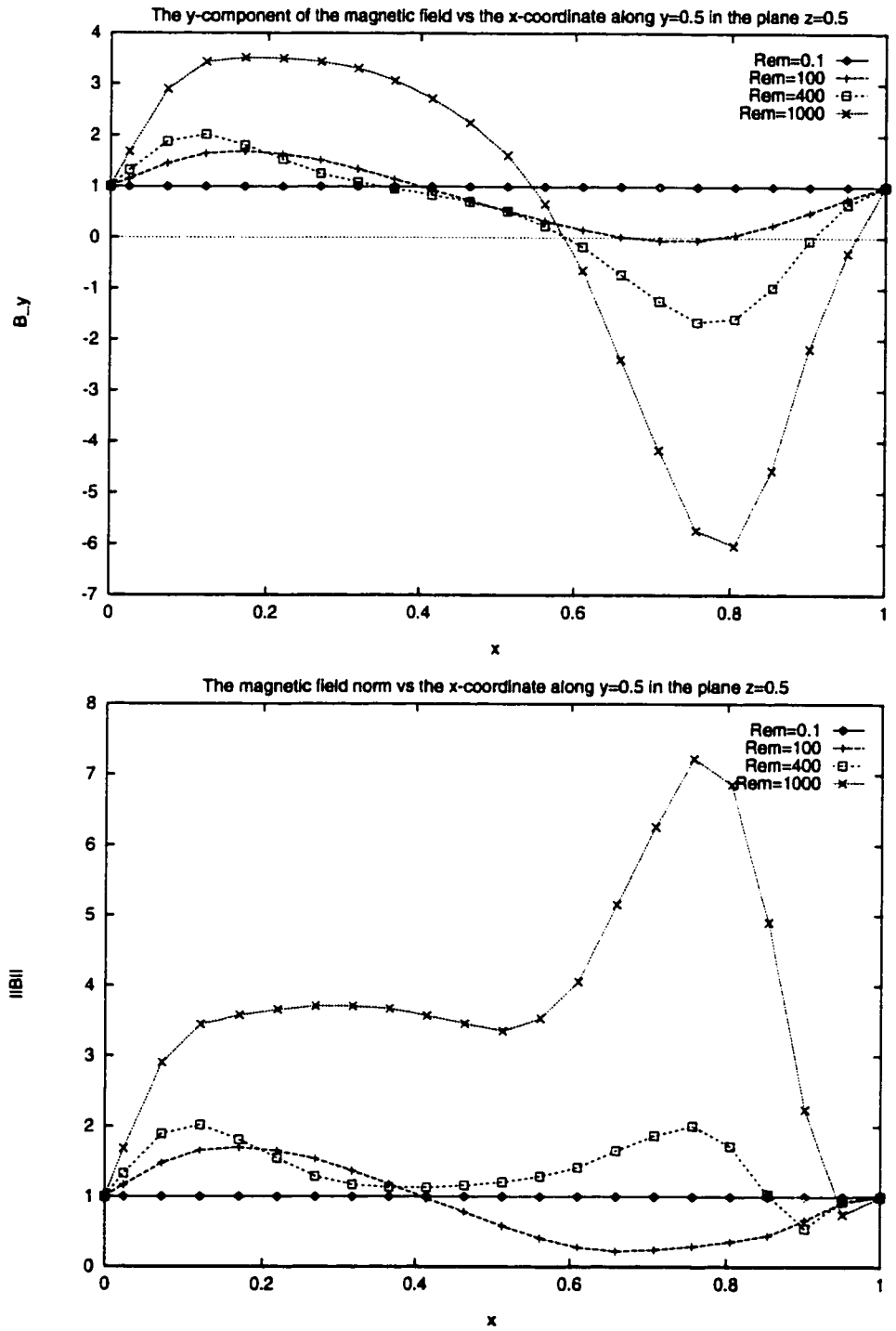

Figure 5.28: The magnetic field along the median y=0.5; Above: The y-component of the magnetic field, Bottom: The magnetic vector norm.

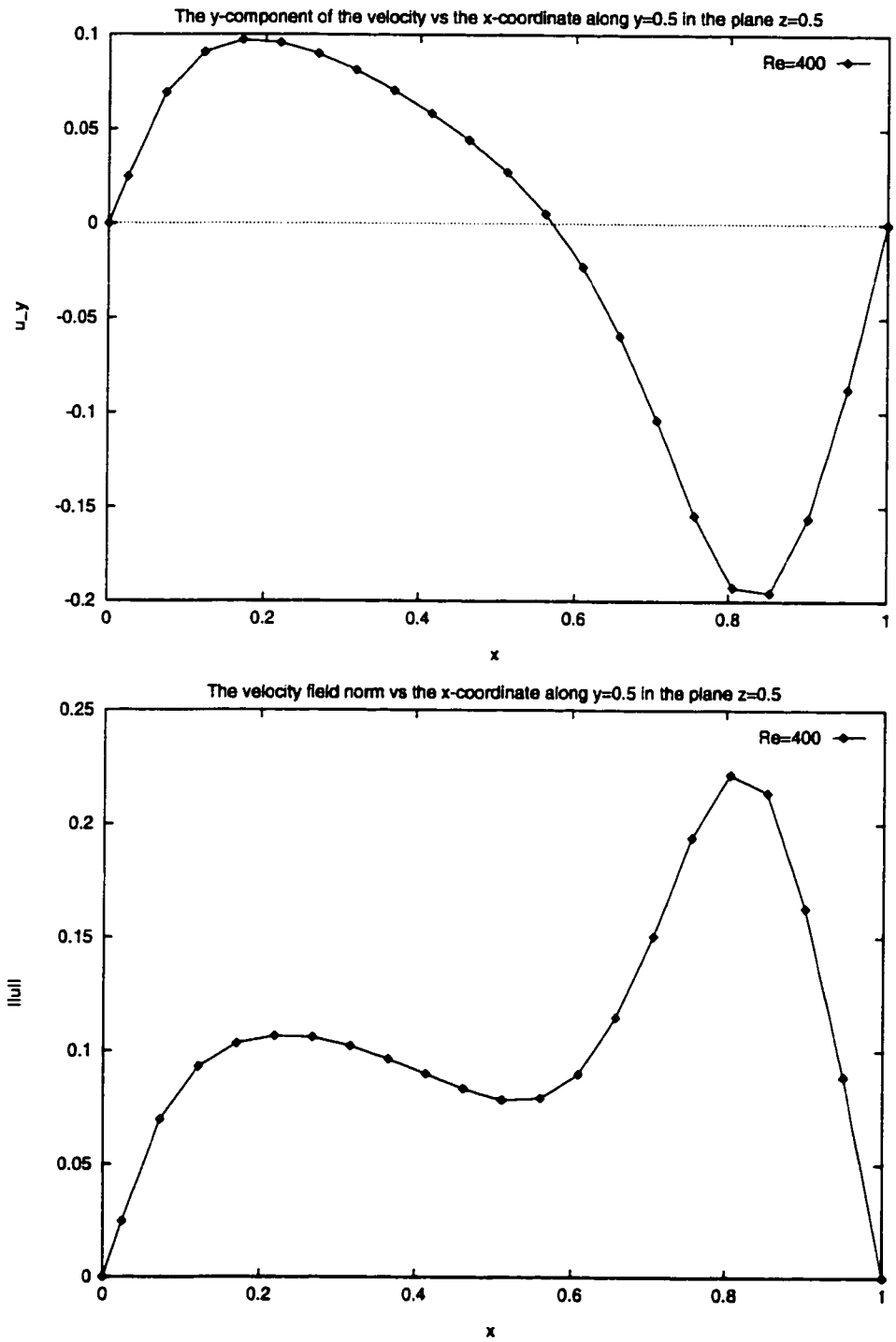

Figure 5.29: The velocity field along the median y=0.5; Above: The y-component of the velocity, Bottom: The velocity vector norm.

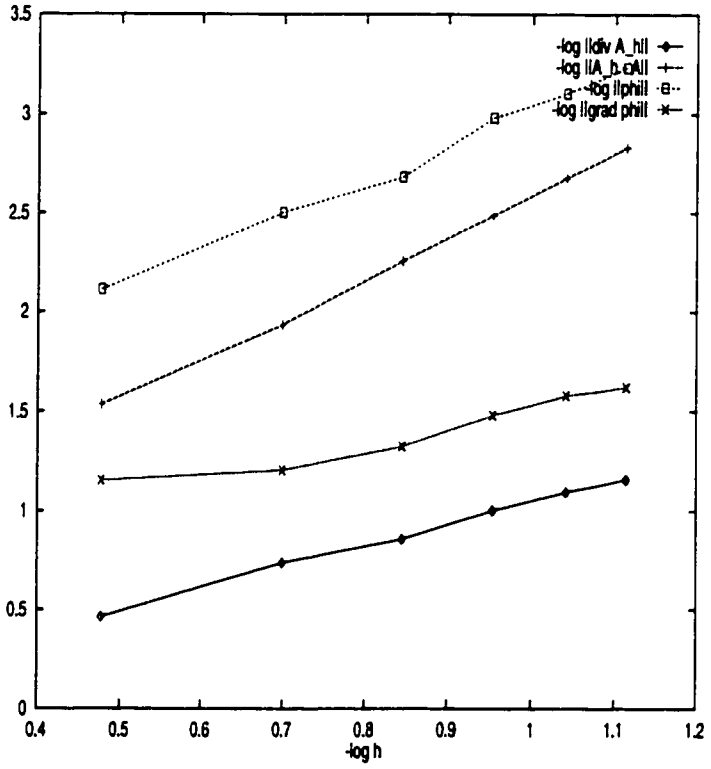

Figure 5.30: Different L_2 norms vs the mesh size.

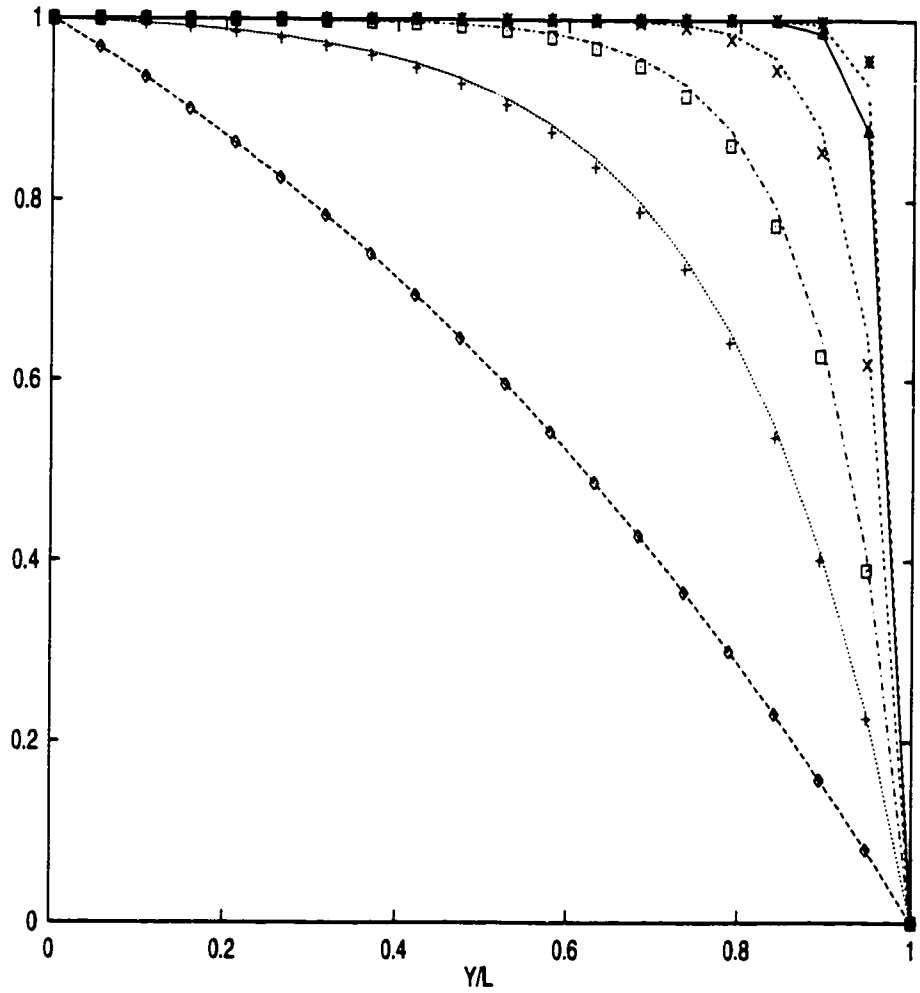

Figure 5.31: The reduced potential along the y-axis, Comparison between analytical and numerical solutions for $Re_m = 1, 5, 10, 20, 40, 50$ (from bottom to above).

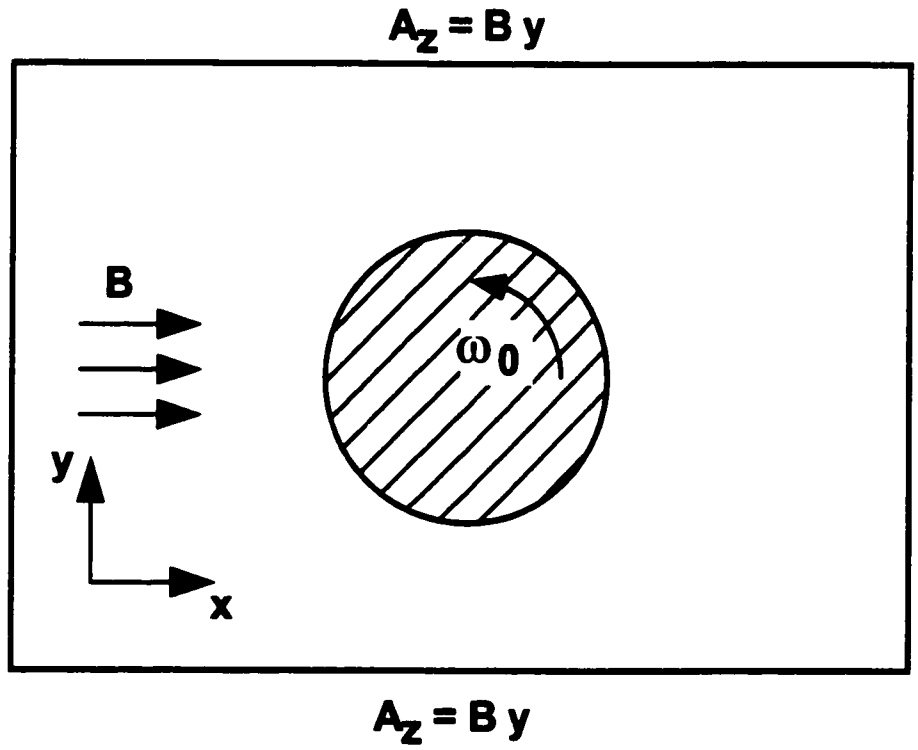

Figure 5.32: Geometry for the magnetic field convection by a rotating cylinder .

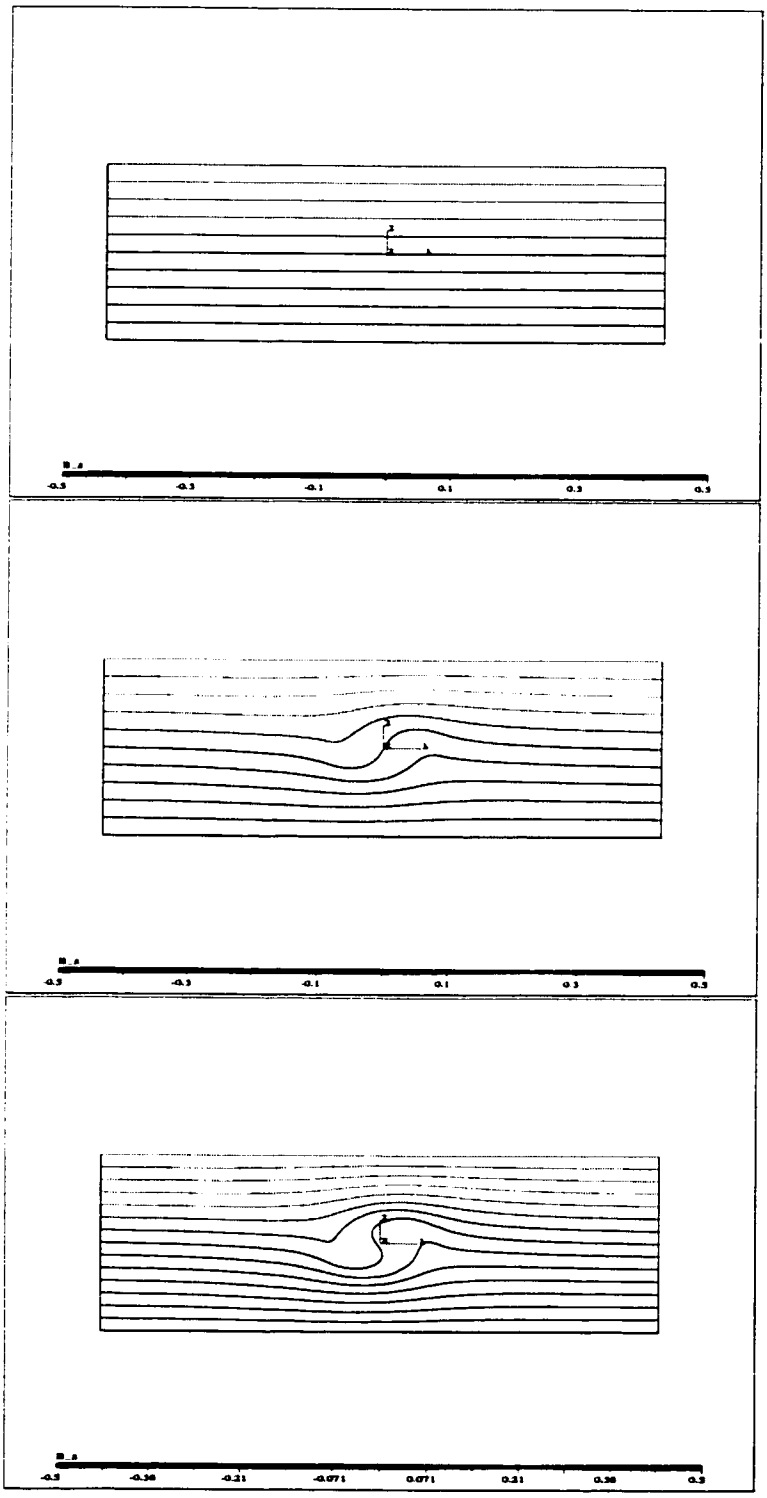

Figure 5.33: The isolines of the vector potential $A_z(x, y)$, numerical solutions for $Re_m = 0, 6, 12$ (from above to bottom).

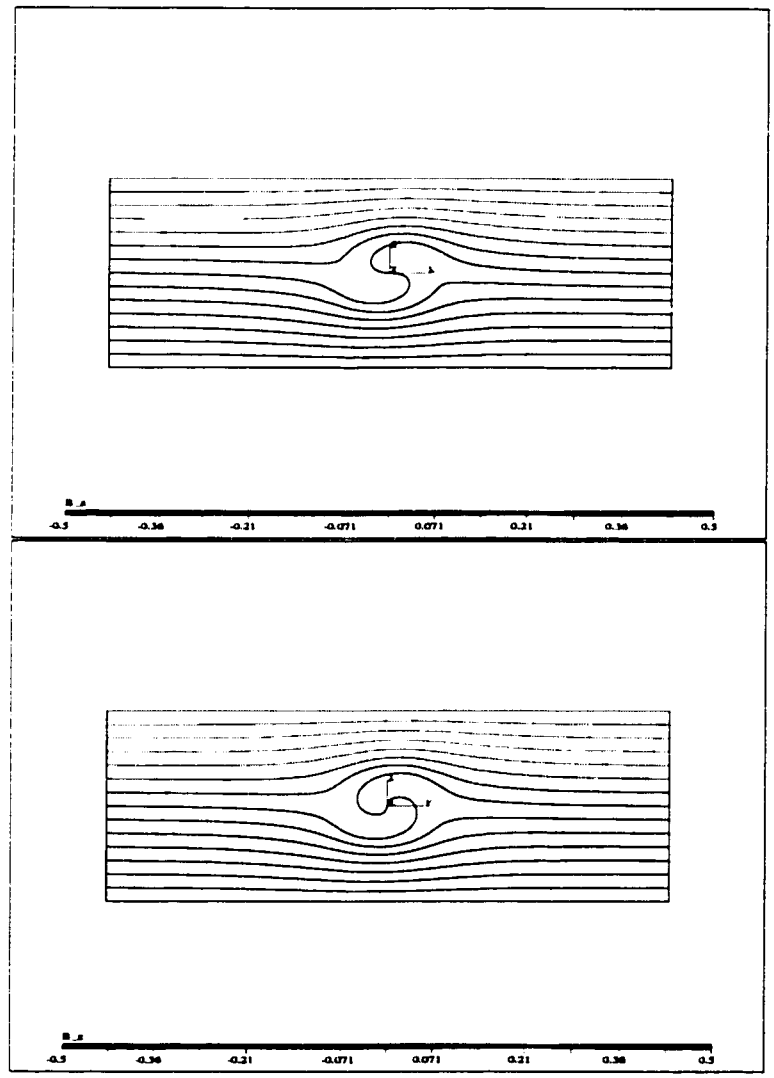

Figure 5.34: The isolines of the vector potential $A_z(x, y)$, numerical solutions for $Re_m = 24, 48$ (from above to bottom).

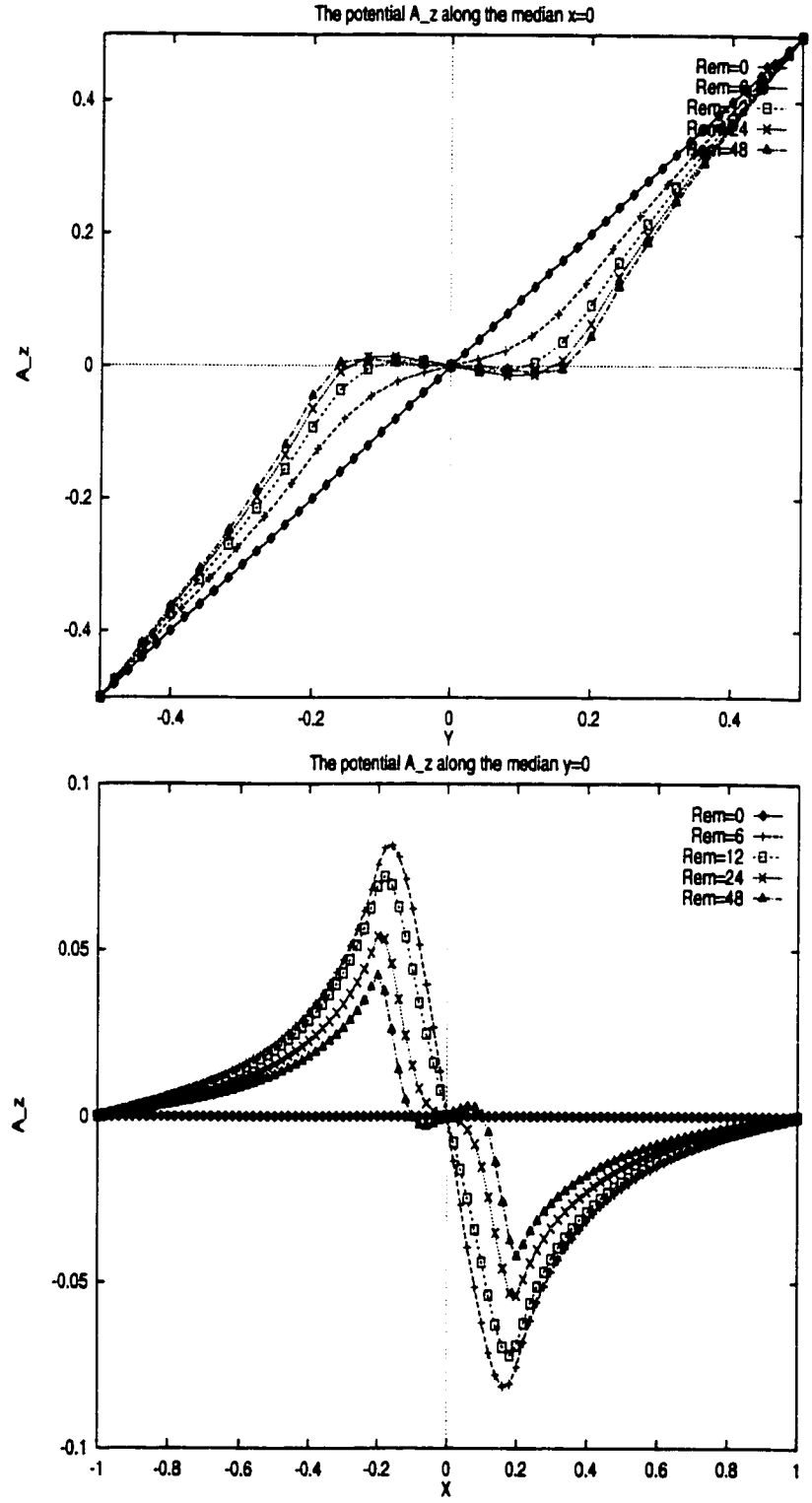

Figure 5.35: The vector potential $A_z(x, y)$ for different Re_m numbers, Above: Along the median $x = 0$, Bottom: Along the median $y = 0$.

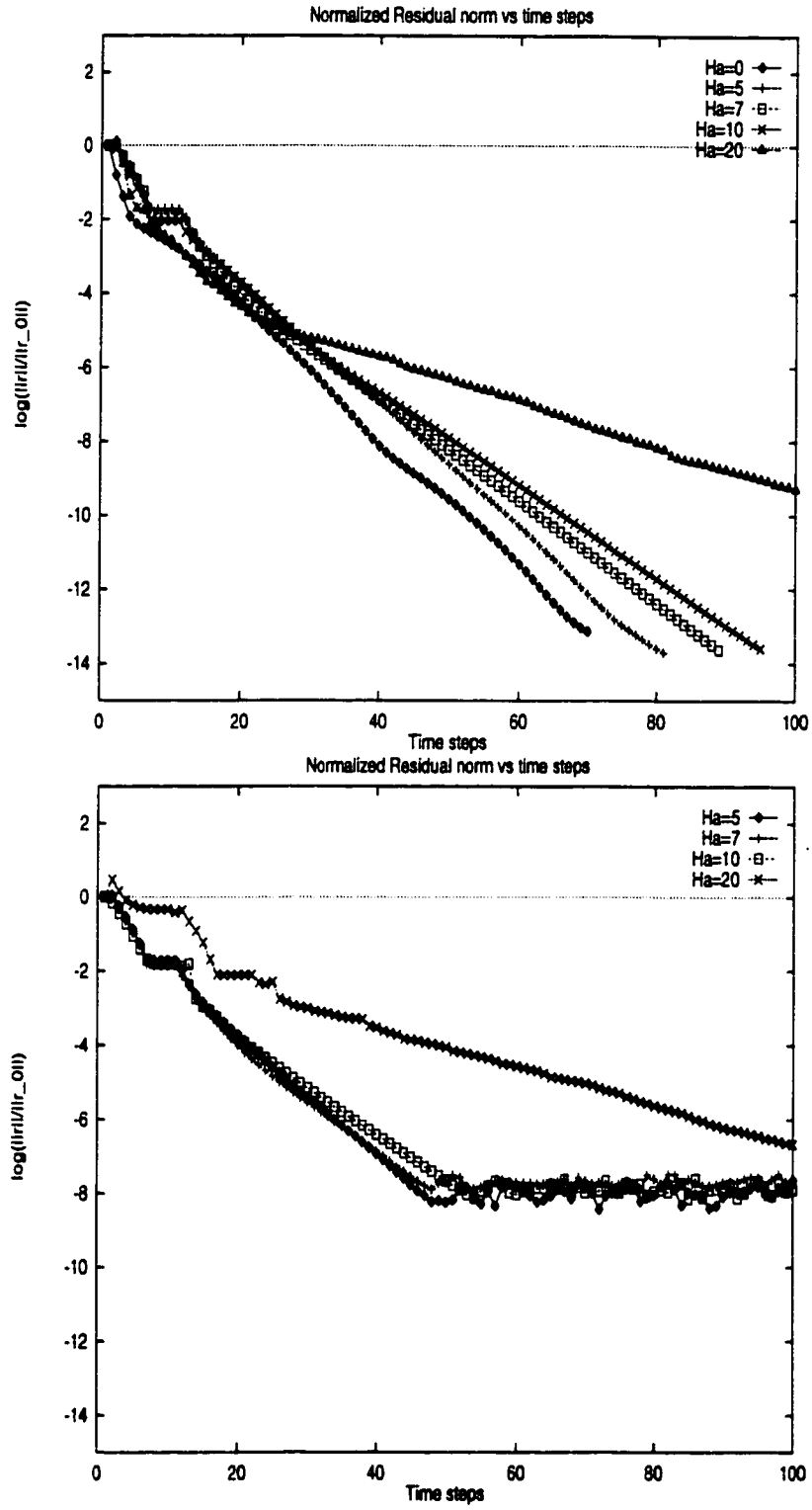

Figure 5.36: The convergence history; Above: The segregated algorithm (3), Bottom: The tighter algorithm (5) .

	CPU for Algorithm (5)	CPU for Algorithm (3)
Ha = 1	96080.6	15979.1
Ha = 2	101312	15619.4
Ha = 5	113945	31509.2
Ha = 7	121312	34002.9
Ha = 10	105845	34820.7
Ha = 20	126808	18346.3

Figure 5.37: Table for the comparison in terms of CPU time of algorithms (3) and (5), for different values of the Hartmann number .

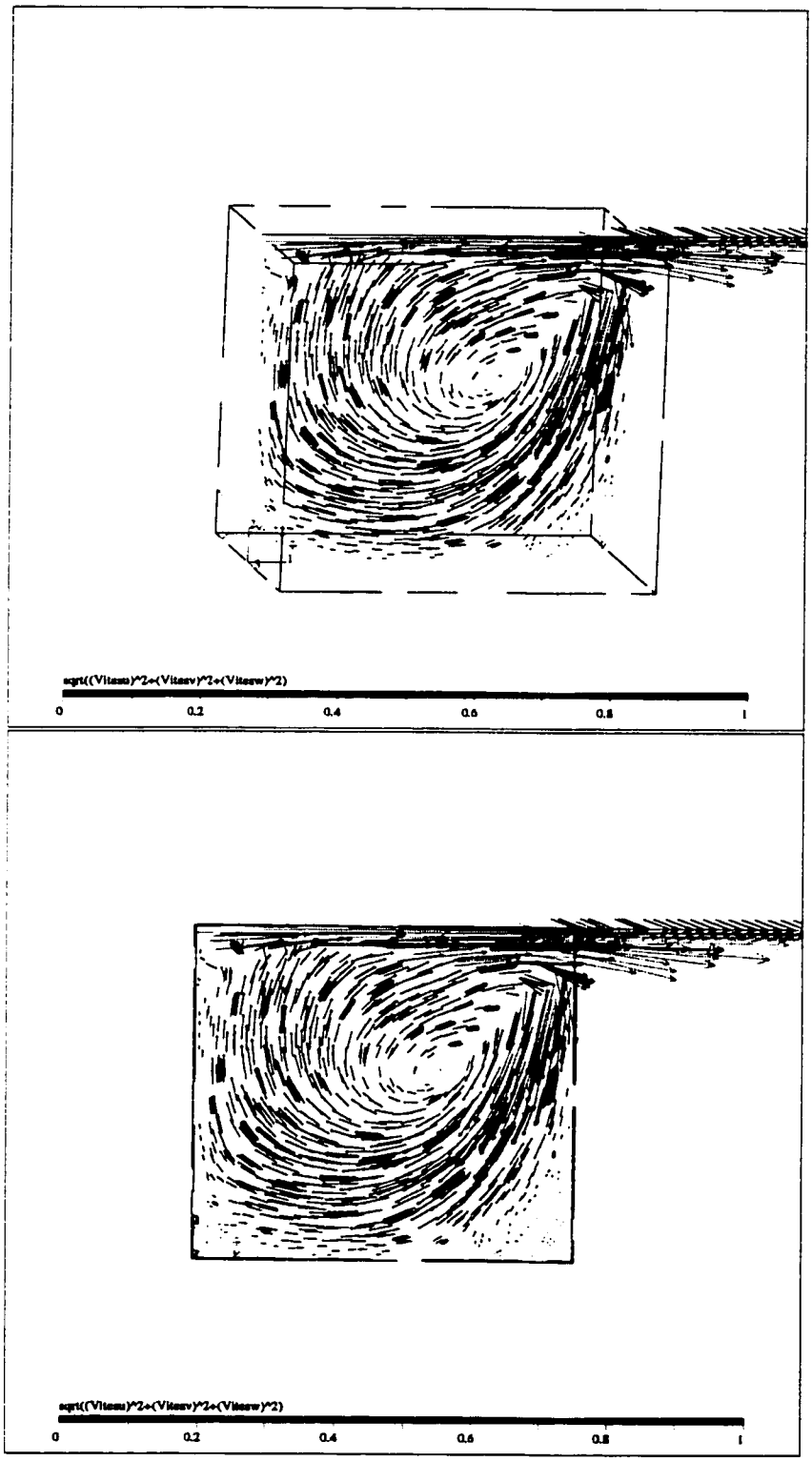

Figure 5.38: The velocity field at the mid-plane $z = 0.5$ with $Re = 10^3$ and $Re_m = 1$, Above: $Ha = 0$, Bottom: $Ha = 2$.

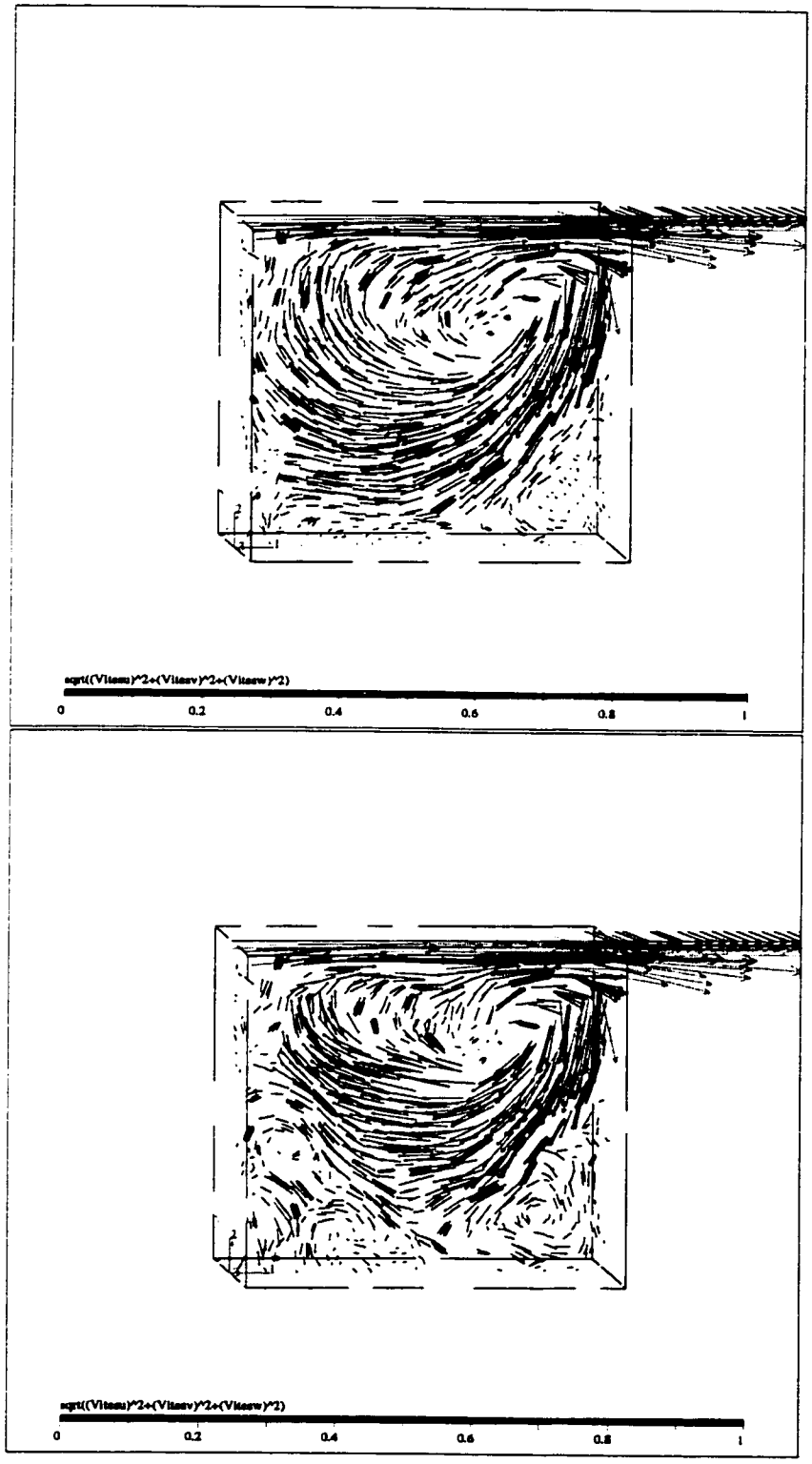

Figure 5.39: The velocity field at the mid-plane $z = 0.5$ with $Re = 10^3$ and $Re_m = 1$, Above: $Ha = 5$, Bottom: $Ha = 7$.

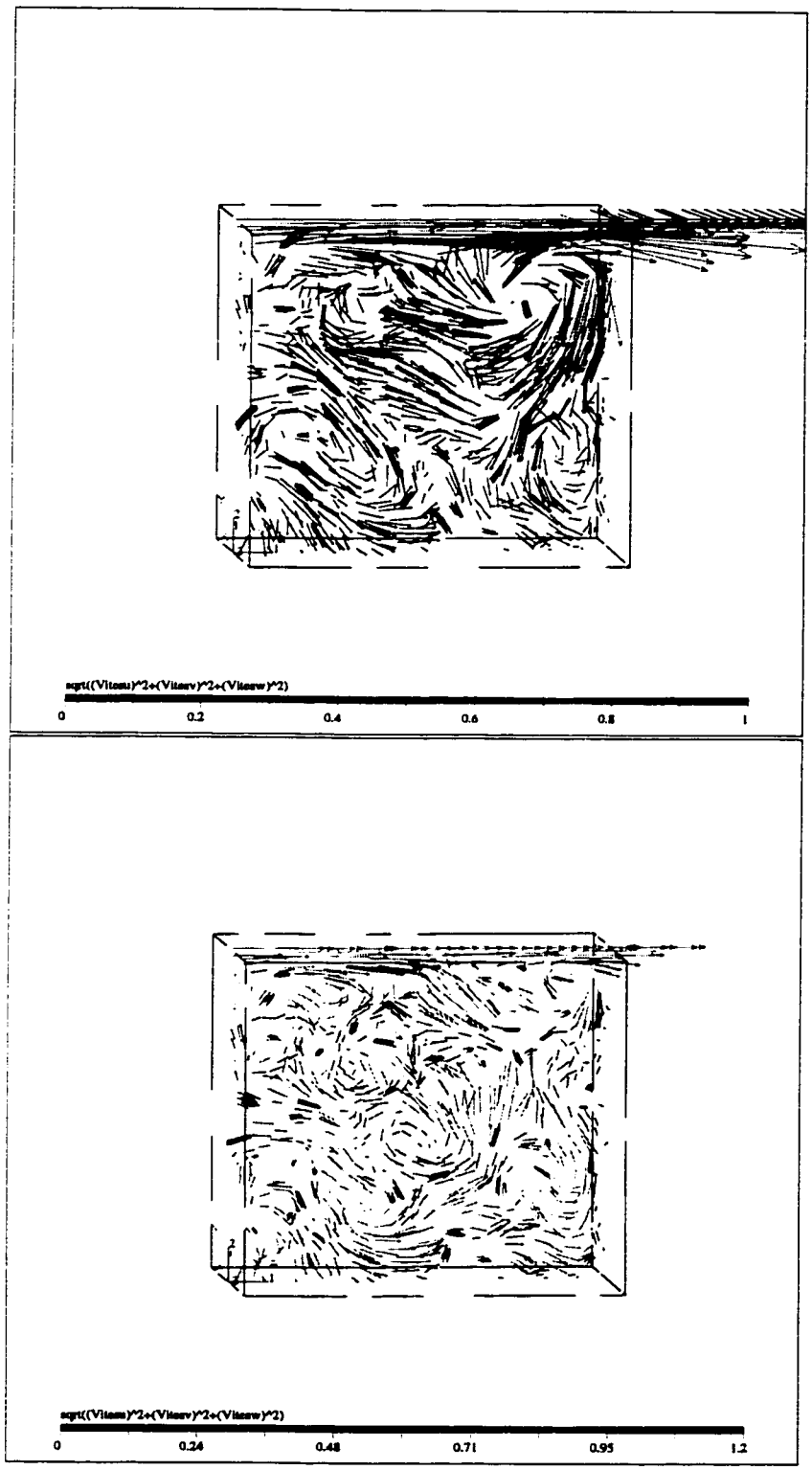

Figure 5.40: The velocity field at the mid-plane $z = 0.5$ with $Re = 10^3$ and $Re_m = 1$, Above: $Ha = 10$, Bottom: $Ha = 20$.

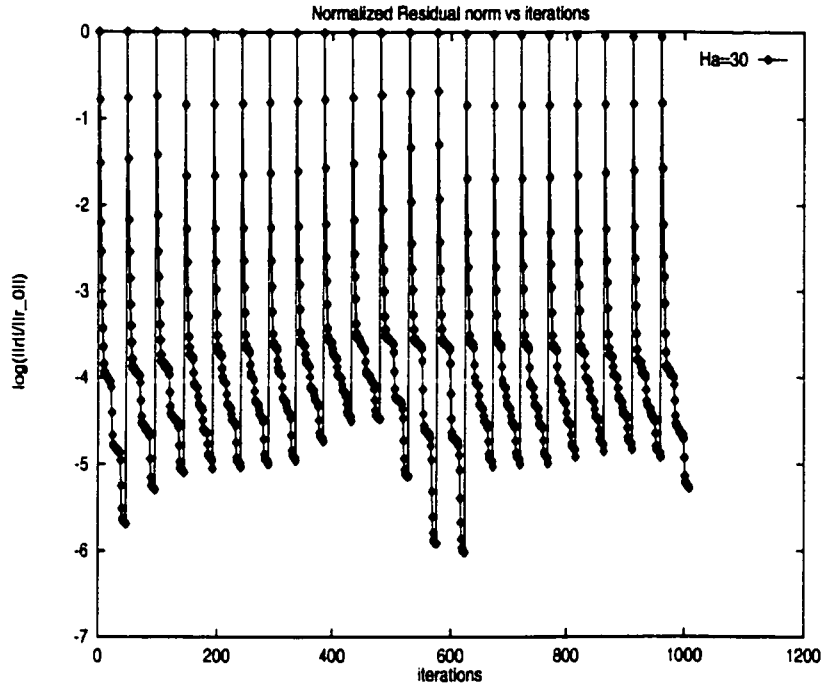

Figure 5.41: Typical convergence history for $Re = 10^3$,$Re_m = 1$ and $Ha = 30$.

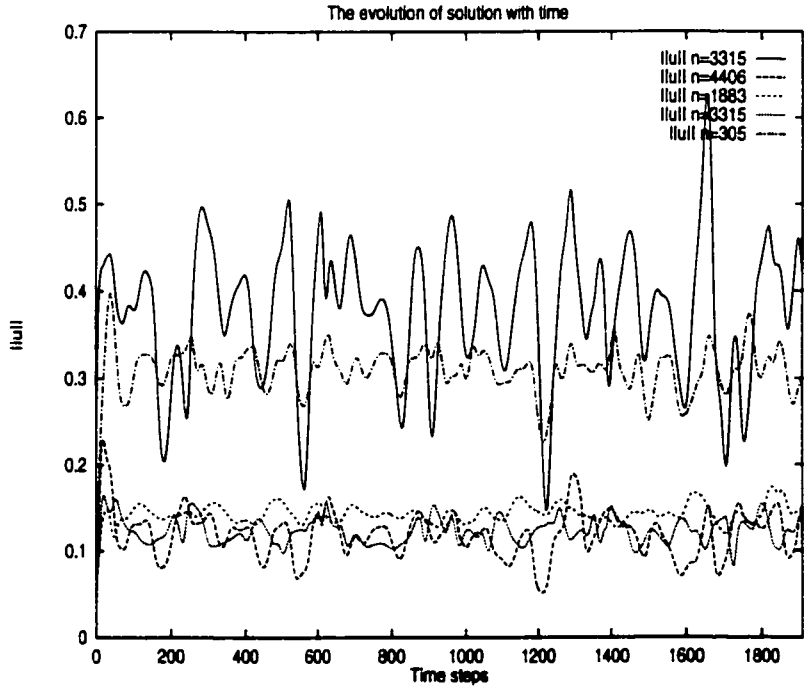

Figure 5.42: Transient solution at five different nodes, $Re = 10^3$, $Re_m = 1$ and $Ha = 30$.

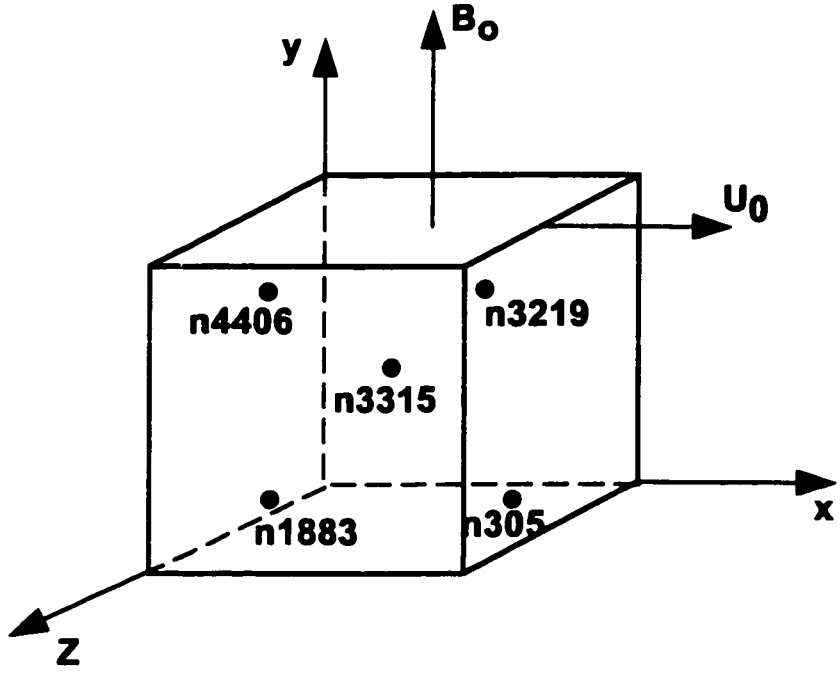

	x coordinate	y coordinate	z coordinate
Node 305	0.88	0.10	0.46
Node 1883	0.15	0.10	0.48
Node 3219	0.85	0.89	0.53
Node 3315	0.50	0.50	0.50
Node 4406	0.18	0.72	0.49

Figure 5.43: The nodes considered for the stability; Above: Location of the nodes on the domain, Bottom: Coordinates and numbers of the nodes .

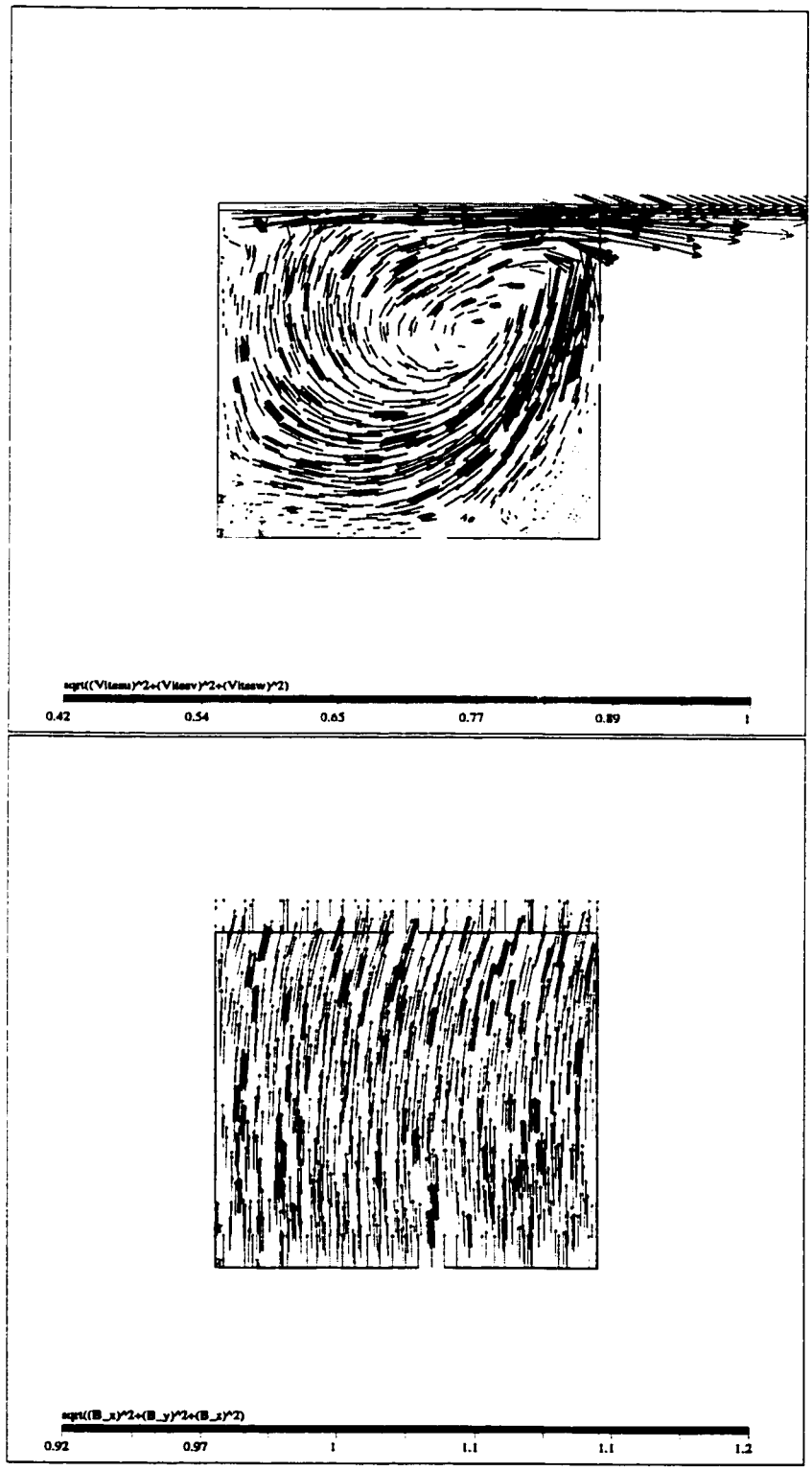

Figure 5.44: Results at the mid-plane $z = 0.5$ with $Re = 10^3$, $Re_m = 10$ and $Ha = 10$. Above: The velocity field, Bottom: The magnetic field.

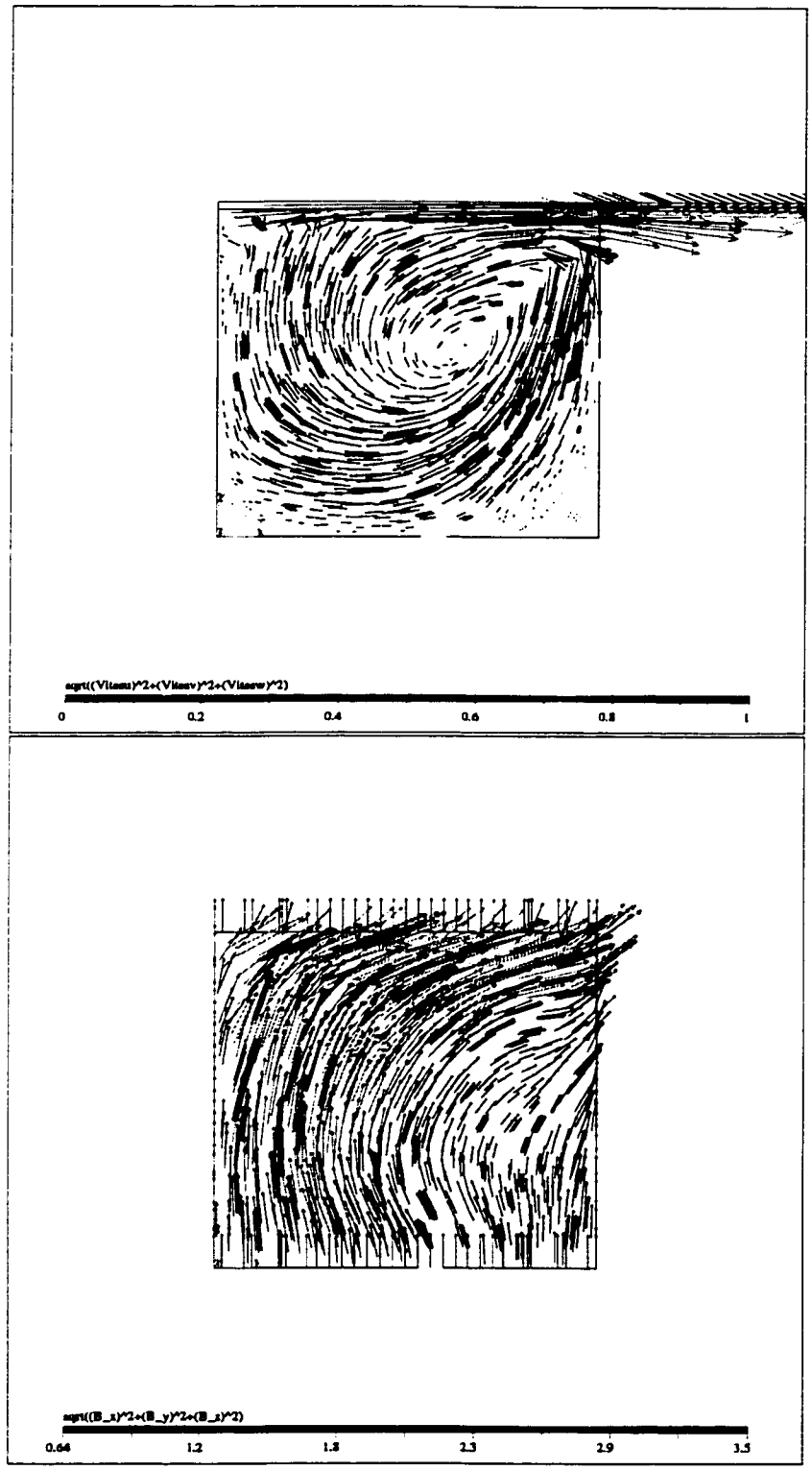

Figure 5.45: Results at the mid-plane $z = 0.5$ with $Re = 10^3$, $Re_m = 100$ and $Ha = 10$. Above: The velocity field, Bottom: The magnetic field.

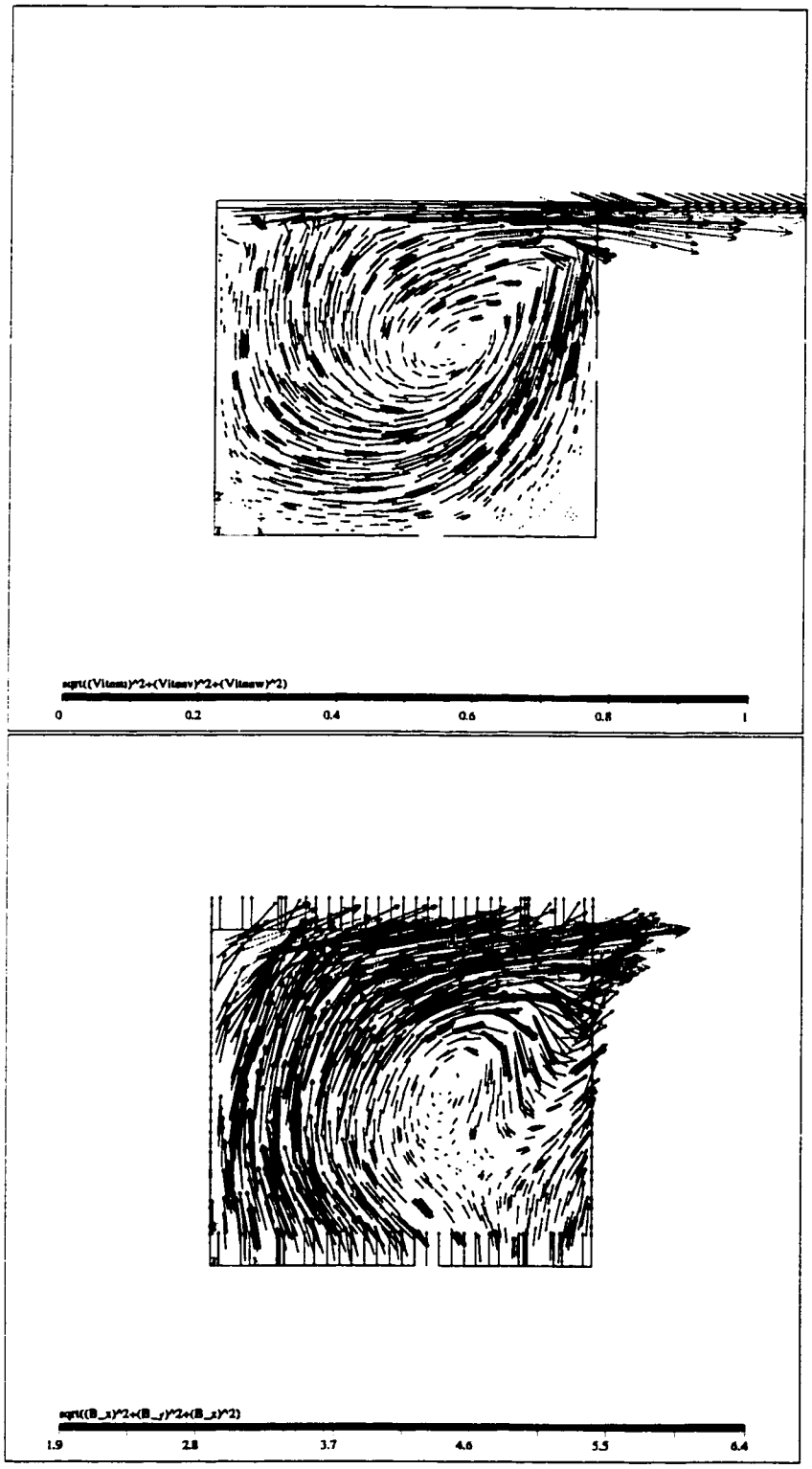

Figure 5.46: Results at the mid-plane $z = 0.5$ with $Re = 10^3$, $Re_m = 200$ and $Ha = 10$. Above: The velocity field, Bottom: The magnetic field.

	CPU for Algorithm (5)	CPU for Algorithm (3)
$Re_m = 10$	174913	16277.2
$Re_m = 100$	197423	52694.2
$Re_m = 200$	208255	99444.8

Figure 5.47: Table for the comparison in terms of CPU time of algorithms (3) and (5), for different values of Re_m the magnetic Reynolds number.

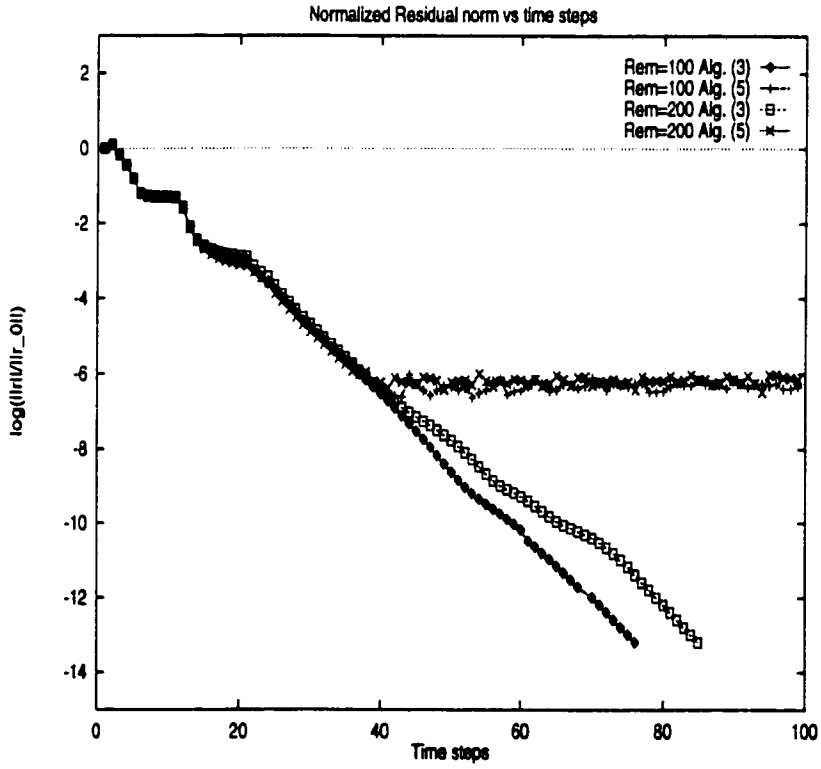

Figure 5.48: Convergence history of algorithms (3) and (5) for different Re_m magnetic Reynolds numbers .

Chapter 6

Conclusions and Future Work

A finite element method has been developed in this thesis for the solution of 3D magnetohydrodynamic (MHD) equations. This method has been developed in two main steps: In the first step, we focused on the appropriate formulation that has to be used to determine the magnetic aspects of MHD flows. This formulation is a conservative one, meaning that the local conservation of the magnetic field is accounted for. This formulation is stabilized, thus permitting the use of equal interpolation for all the variables.

Here, we insist that the conservative formulation is the appropriate way of formulating the MHD flow problem. The appropriate way does not mean that the alternative formulations are inadequate or inefficient. However, there should be only one way to formulate any MHD flow, with the magnetic field as the main electromagnetic quantity, and we believe that the conservative formulation is that way.

The second step has been selecting a strong and robust algorithm for the solution of the coupled problem. This algorithm is based on a segregated algorithm which is valid for both the high and low Re_m numbers. Surprisingly, this algorithm performs very well, even in the context of high magnetic Reynolds Re_m numbers. The non-linear GMRES algorithm associated with ILUT preconditioning proves to be a very robust and efficient algorithm. Numerical results have been obtained for many validation test cases, in steady and unsteady regimes, ranging from 1D to 3D for the decoupled $\mathbf{B}, q$ and $\mathbf{A}, \phi$ formulations, as well as for the coupled formulation $\mathbf{B}, q, \mathbf{u}, p$.

When the magnetic Reynolds number is low, the magnetic matrix can be computed

once and for all. All subsequent updates of the magnetic variables can be done using the initial decomposition of the magnetic matrix without affecting the convergence rates. When the magnetic Reynolds number is high, the matrix has to be updated and decomposed more frequently to guarantee convergence. This frequency depends mainly on the value of Re_m.

Eventually, future work should concentrate on some key points which, in our opinion, will lead to the maturation of the finite element MHD code. First, it is easy and straightforward to replace the direct solver for the magnetic problem with a linear GMRES algorithm. This will substantially reduce the time and storage requirements whenever the magnetic matrix has to be updated during the iterative process, which is important for 3D applications since memory is limited.

Of considerable importance is the extension of the vector potential formulation solver to account for a quasi-steady regime under the assumption of a low frequency source. This will enhance the capabilities of the MHD package developed in this thesis. After that, the coupling between the Navier-Stokes solver and the vector potential solver should be performed. Another possible future improvement would be to take account for the electric scalar potential within the magnetic field formulation. This will make it possible to impose an electric potential difference as a source term, while still solving for the magnetic field. For the Navier-Stokes solver, an extension to account for the turbulence within the fluid domain is certainly an obvious eventual future work.

Finally, we would like to comment on the somewhat inadequate way we handle the magnetic boundary conditions for the high Re_m cases. Actually, when Re_m is high, there is no reason to suppose that the external magnetic field is not affected by the induced magnetic field. The appropriate way to solve such a problem is to solve the MHD equations in two domains. The first domain is the conducting fluid, where the MHD equations are written as shown in chapter 2. The second domain, surrounding the conducting domain, is non-conducting by definition and is large enough to suppose that the induced magnetic field at its boundaries is null. The MHD equations in this domain are written without the convective term, since the velocity is nil. At the

boundaries between the two domains, and since in MHD the permeability is constant, the magnetic field is continuous over the interface and no boundary conditions have to be specified.

The few points listed in this chapter represent some directions of future improvement of the MHD finite element method developed and presented in this thesis.

References

[1]- Shercliff, J.A. (1965): A Textbook of Magnetohydrodynamics, Pergamon.

[2]- Cowling, T.G. (1934): Solar Dynamo Theory; Mon. Not. Roy. Astr. Soc., Vol. 94, No. 39.

[3]- Ferraro, V.C.A. (1937): Behavior of Magnetic Field in rotating Star; Mon. Not. Roy. Astr. Soc., Vol. 97, No. 458.

[4]- Hartmann, J. (1937): Flow in Pipes under Transverse Magnetic Field; Math.-fys. Medd., Vol. 15, No. 6 and 7.

[5]- Alfvèn, H. (1942): Discovery of Alfven Waves; Nature, Vol. 76, No. 194.

[6]- Berton R. (1991): Magnétohydrodynamique, Masson.

[7]- Alemany A. (1995): La magnétohydrodynamique: présentation générale; L'Onde Électrique, Vol. 75, No. 2, pp. 14-18.

[8]- Motora, S.; Imaichi, K.; Nakato, M. and Takesawa S. (1991): An outline of the R. and D. Project on Superconducting MHD Ship Propulsion; Proceedings MHDS 91, pp. 53-68, Japan, October 1991.

[9]- Roe, P.L. and Balsara D.S. (1996): Notes on the Eigensystem of Magnetohydrodynamics; SIAM J. on Appl. Math., Vol. 56, No. 1, pp. 57-67.

[10]- Powell, K.G. (1996): Solution of Euler and Magnetohydrodynamic Equations on Solution-Adaptative Cartesian Grids; Von Karman Institute for Fluid Dynamics, Lecture Series 1996-06 Computational Fluid Dynamics, Concordia University, Montreal, Canada.

[11]- Walker, J.S. (1986): Laminar Duct Flows in Strong Magnetic Fields; Liquid-Metal Flows and Magnetohydrodynamics, H. Branover, P.S. Likoudis and M. Moon (Eds), American Institute of Aeronautics and Astronautics (new-York), 1986, Vol. 2, pp 3-16.

[12]- Hua, T.Q. and Walker J.S. (1995): MHD Flow in Rectangular Ducts with Inclined Non-Uniform Transverse Magnetic Field; Fusion Eng. and Design, Vol. 27, pp. 703-710.

[13]- Cuevas, S.; Picologlou, B.F.; Walker, J.S. and Talmage G. (1997): Liquid-Metal MHD Flow in Rectangular Ducts with Thin Conducting or Insulating Walls: Laminar and Turbulent Solutions; Int. J. Engng. Sci., Vol. 35, No. 5, pp. 485-503.

[14]- Ramos, J.I. and Winowich N.S. (1990): Finite Difference and Finite Element Methods for MHD Channel Flows; Int. J. for Numerical Methods in Fluids, Vol. 11, pp. 907-934.

[15]- Scandiuzzi, R. and Schrefler B.A. (1990): F.E.M. in Steady MHD Duct Flow Problems; Int. J. for Numerical Methods in Eng., Vol. 30, pp. 647-659.

[16]- Sterl, A. (1990): Numerical Simulation of Liquid-Metal MHD Flows in Rectangular Ducts; J. of Fluid Mech., Vol. 216, pp. 161-191.

[17]- Seungsoo, L. and Dulikravich G.S. (1991): Magnetohydrodynamic Steady Flow Computations in Three Dimensions; Int. J. for Numerical Methods in Fuids, Vol. 13, pp. 917-936.

[18]- Dulikravich G.S., Ahuja, V. and Seungsoo L. (1994): Three-Dimensional Control of Crystal Growth Using Magnetic Fields; Proceedings of SPIE- The international Society for Optical Engineering Proceedings of Smart Structures and Materials, Vol. 1916, Feb. 1994.

[19]- Sazhin, S.S. and Makhlouf M. (1995): Solution of Magnetohydrodynamic Problems Based on a Conventional Computational Fluid Dynamics Code; Int. J. for Numerical Methods in Fuids, Vol. 21, pp. 433-442.

[20]- Peterson, J.S. (1988): On the Finite Element Approximation of Incompressible Flows of an Electrically Conducting Fluid; Numerical Methods for Partial Differential Equations, Vol. 4, pp. 57-68.

[21]- Gardner, L. T. R. and Gardner G. A. (1995): A Two-dimensional Bi-Cubic and B-Spline Finite Element: Used in a Study of MHD Duct Flow; Comp. Meths Appl. Mech. Engrg. Vol. 124, pp. 365-375.

[22]- Gyimesi, M. and Lavers J. D. (1992): Generalized Potential Formulations for Magnetostatic Problems; IEEE Trans. on Magnetics, Vol. 28, No. 4, pp. 1924-1929.

[23]- Zienkiewicz, O. C.; Lyness J. and Owen D. R. J. (1977): Three-Dimensional Magnetic Field Determination Using a Scalar Potential, A Finite Element Solution; IEEE Trans. on Magnetics, Vol. 13, No. 5, pp. 1649-1656.

[24]- Garg, V. K. and Weiss J. (1986): Finite Element Solution of Transient Eddy Current Problems in Multiply Exited Magnetic Systems; IEEE Trans. on Magnetics, Vol. 22, No. 5, pp. 1257-1259.

[25]- Tandon, S. C. and Chari V. K. (1981): Transient Solution of the Diffusion Equation by the Finite Element Method; J. Appl. Phys., Vol. 52, No. 3, pp. 2431-2432.

[26]- Biro, O. and Preis K. (1989): On the Use of Magnetic Vector Potential in the Finite Element Analysis of Three-Dimensional Eddy Currents; IEEE Trans. on Magnetics, Vol. 25, No. 4, pp. 3145-3159.

[27]- Fautrelle Y. R. (1981): Analytical and Numerical Aspects of Electromagnetic Stirring Induced by Alternating Magnetic Fields; J. Fluid Mech., Vol. 102, pp. 405-430.

[28]- Mestel, A. J. (1982): Magnetic Levitation of Liquid Metals; J. Fluid Mechs., Vol. 117, pp. 27-43.

[29]- Lympany, S. D.; Evans J. W. and Moreau R. (1984): Magnetohydrodynamic Effects in Aluminium Reduction Cells; Metallurgical Applications of Magnetohydrodynamics, Proceedings of a Symposium of the International Union of The Theoritical and Applied Mechanics, Cambridge, U.K. (Sep. 6-10, 1982), H. K. Moffat and M. R.

E. Proctor (Eds), The Metals Society, London, 1984, pp. 15-23.

[30]- Besson, O.; Bourgeois J.; Chevalier P. A.; Rappaz J. and Touzani R. (1991): Numerical Modelling of Electromagnetic Casting Processes; J. Comp. Phys., Vol. 92, pp. 482-507.

[31]- Conraths, H. J. (1996): Eddy Current and Temperature Simulation in Thin Moving Metal Strips; Int. J. for Numerical Methods in Eng., Vol. 39, pp. 141-163.

[32]- Masse, P.; Fautrelle, Y. and Gagnoud A. (1992): Coupled Methods for 3D Coupled Problems, 10 years of Experiments in MHD; IEEE Trans. on Magnetics, Vol. 28, pp. 1275-1278.

[33]- Trophime C. (1995): Modélisation Numérique du Couplage Magnétohydrodynamique (M.H.D.) fort. Application à la Propulsion M.H.D. Navale, Thèse de Doctorat à l'Institut National Polytechnique de Grenoble, France.

[34]- Tanahashi, T. and Oki Y. (1995): Numerical Analysis of Natural Convection of Thermo-electrically Conducting Fluids in a Square Cavity Under a Uniform Magnetic Field; JSME International Journal, Vol. 38, No. 3, pp. 374-381.

[35]- Tanahashi, T. and Oki Y. (1996): Numerical Analysis of Natural Convection of Thermo-electrically Conducting Fluids in a Square Cavity Under a Uniform Magnetic Field (Calculated Results, Frequency Characteristics); JSME International Journal, Vol. 39, No. 3, pp. 508-516.

[36]- Ben Salah, N.; Soulaimani A.; Habashi W. G. and Fortin M. (1997): A Conservative Stabilized Finite Element Method for the Magnetohydrodynamic Equations; Advances in Computational Engineering Science, International Computational Engineering and Science 97, S. N. Atluri and G. Yagawa (Eds), Tech Science Press (Forsyth, Georgia), 1997, pp. 269-276.

[37]- Ben Salah, N.; Soulaimani A.; Habashi W.G. and Fortin M. (1999): A Conservative Stabilized Finite Element Method for the Magneto-Hydrodynamic Equations;

Int. J. for Numerical Methods in Fluids, Vol. 29, pp. 535-554.

[38]- Bossavit, A.; Emson, J. and Mayergoyz (1991): Méthodes Numériques en Électromagnétisme: Géométrie Différentielle, Élements Finis, Méthodes d'Hysteresis.

[39]- Emson, C. and Simkin J. (1983): An Optimal Method for 3D Eddy Currents; IEEE Trans. on Magnetics, Vol. 19, pp. 2450-2452.

[40]- Jiang, B.; Wu J. and Povinelli L.A. (1995): The Origin of Spurious Solutions in Computational Electromagnetics; NASA-TM-106921, E-9633, ICOMP-95-8.

[41]- Brezis, H. (1983): Analyse Fonctionnelle, Théorie et Applications; Collection Mathématiques Appliquées pour la Maîtrise sous la Direction de P. G. Ciarlet et J. L. Lions; Masson.

[42]- Brezzi, F. and Fortin M. (1991): Mixed and Hybrid Finite Element Methods, Springer Series in Computational Mathematics; 15, Springer-Verlag.

[43]- Hugues, T.; Franca L. and Ballestra M. (1986): A New Finite Element Formulation for Computational Fluid Dynamics: V. Circumventing the Babuska-Brezzi Condition: A Stable Petrov Galerkin Formulation of the Stokes Problem Accommodating Equal Order Interpolations; Comp. Meths Appl. Mech. Engrg. Vol. 59, pp. 85-99.

[44]- Brezzi, F. and Pitkaranta J. (1984): On the Stabilization of Finite Element Approximations of the Stokes Problem, in: W. Hackbusch ed., Efficient Solutions of Elliptic Systems; Notes on Numerical Fluid Mechanics, Vol. 10 (Viewig, Wiesbaden) pp. 11-19.

[45]- Baruzzi, G. S.; Habashi W.G and Hafez M.M. (1995): A Second Order Finite Element Method for the Solution of the Transonic Euler and Navier-Stokes Equations; Int. J. for Numerical Methods in Fluids, Vol. 20, pp. 671-693.

[46]- Hugues, T.; Franca L. and Hulbert G.M. (1989): A New Finite Element Formu-

lation for Computational Fluid Dynamics: VIII. The Galerkin/Least Squares Method for Advective-Diffusive Equations; Comp. Meths Appl. Mech. Engrg. Vol. 73, pp. 173-189.

[47]- Dutto L.C. (1993): On the Iterative Methods for Solving Linear Systems of Equations; Revue Européenne des Élements Finis, Vol. 2, No. 4, pp. 423-448.

[48]- Saad, Y. and Schultz M.H. (1986): GMRES: a Generalized Minimal Residual Algorithm for Solving Non-Symmetric Linear Systems; SIAM J. Sci. Stat. Comput., Vol. 7, pp. 856-869.

[49]- Brown, P. (1987): A Local Convergence Theory for Combined Inexact Newton/Finite Difference Projection Methods; SIAM J. of Numerical Anal., Vol. 24, pp 407-434.

[50]- Saad, Y. (1996): Iterative Methods for Sparse Linear Systems; PWS Publishing CO, Boston.

[51]- Meijerink, J.A. and Van Der Vorst H.A. (1977): An Iterative Solution Method for Linear Systems of Which the Coefficient Matrix is a Symmetric M-Matrix; Math. Comput., Vol. 31, pp. 148-162.

[52]- Saad, Y. (1994): ILUT: A Dual Treshold Incomplete ILU Factorization; Numer. Linear Algebra Appl., Vol. 1, pp 387-402.

[53]- Dhatt, G. and Touzot G. (1981): Une Présentation de la Méthode des Éléments Finis; Les Presses de l'Université Laval.

[54]- Moreau, R. (1990): Magnetohydrodynamics; Kluwer Academic Publishers.

[55]- Moffat, H. K. (1983): Magnetic Field Generation in Electrically Conducting Fluids; Cambridge University Press.

[56]- Ben Salah, N.; Soulaimani A. and Habashi W.G. (1999): A Fully-Coupled Finite Element Method for the Solution of the 3D MHD Equations with a GMRES-Based

Algorithm; AIAA Paper 99-3322.